Chapter 3

RESULTS

3.1. Preparation and Characterization of Ligands

3.1.1. Preparation of ligands

The procedure was an adaptation of synthesis of azpy. 2-(4'-*N,N*-Dimethyl aminophenylazo)pyridine (dmazpy) ligand was synthesized by condensing *N,N*-dimethyl-4-nitrosoaniline with 2-aminopyridine in the presence of sodium hydroxide and toluene under refluxing conditions. In the preparation of 2-(4'-*N,N*-diethylaminophenylazo)pyridine (deazpy) ligand, *N,N*-diethyl-4-nitrosoaniline was used instead of *N,N*-dimethyl-4-nitrosoaniline. The yields of ligands gave low percentage because there were side reactions in the preparation method. Both ligands were very soluble in all solvents excepted water. In addition, ligands could be soluble in 0.1 M HCl and 0.1 M NH_4OH. Some of the physical properties of ligands are shown in Table 1.

Table 1 The physical properties of ligands.

Ligand	Physical properties		
	Appearance	Color	Melting point (^{o}C)
dmazpy	Cubic	Red	104-105
deazpy	Cubic	Red	109-110

3.1.2. Characterization of ligands

The chemistry of dmazpy and deazpy ligands were determined by using these techniques:

- Elemental analysis
- Electrospray mass spectrometry
- UV-Visible absorption spectroscopy
- Infrared spectroscopy
- Proton Nuclear Magnetic Resonance spectroscopy (^{1}H NMR)
- Cyclic Voltammetry
- X-ray Diffractometer

3.1.2.1 Elemental analysis

Elemental analysis is a principle method to study composition of elements in the ligands. Therefore, the elements in the ligands are confirmed by this method.

Table 2 Elemental analysis data of dmazpy and deazpy ligands.

Ligand	% C		% N		% H	
	Calc.	Found	Calc.	Found	Calc.	Found
dmazpy	69.00	69.85	24.76	23.81	6.23	6.34
deazpy	70.76	70.06	21.91	21.85	7.63	6.80

3.1.2.2. Electrospray mass spectrometry

The electrospray mass spectra of dmazpy and deazpy ligands are shown in Figure 2 and 3, respectively. From the data, the maximum peaks, which gave 100% relative abundance, were one protonation at m/z 227.1 and 255.3 for dmazpy and deazpy ligands, respectively. So the expected structure will be confirmed by this methods.

Table 3 Electrospray mass spectroscopic data of dmazpy ligand.

m/z	Unit	Equivalent species	Rel. Abun.
227.1	$[dmazpy+H]^+$	$[L+H]^+$	100

L ; dmazpy, MW = 226.28 g/mol

Table 4 Electrospray mass spectroscopic data of deazpy ligand.

m/z	Unit	Equivalent species	Rel. Abun.
255.3	$[deazpy+H^+]$	$[L+H]^+$	100
256.2	$[deazpy+2H]^+$	$[L+2H]^+$	35

L ; deazpy, MW = 254.34 g/mol

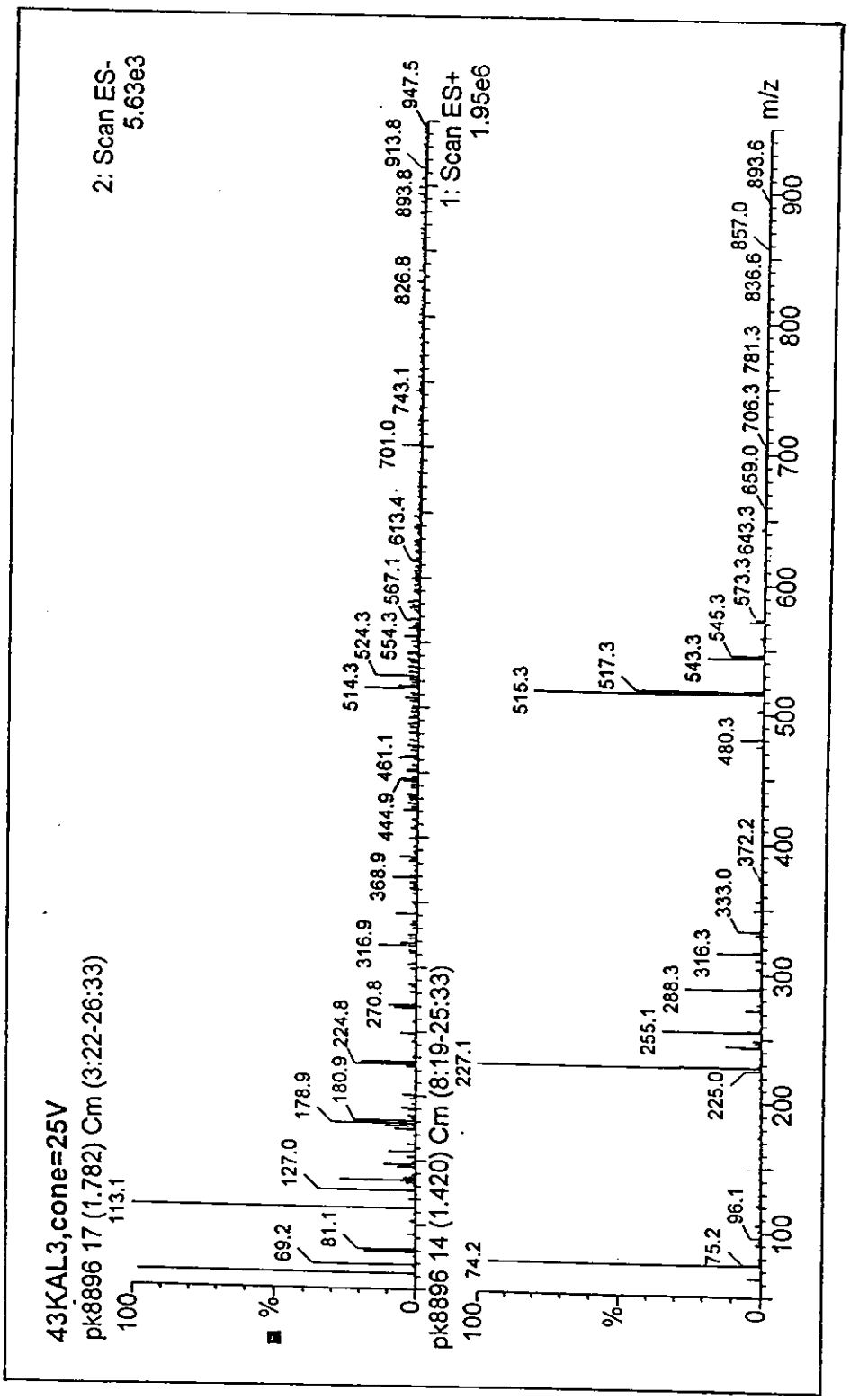

Figure 2 Electrospray mass spectrum of dmazpy ligand.

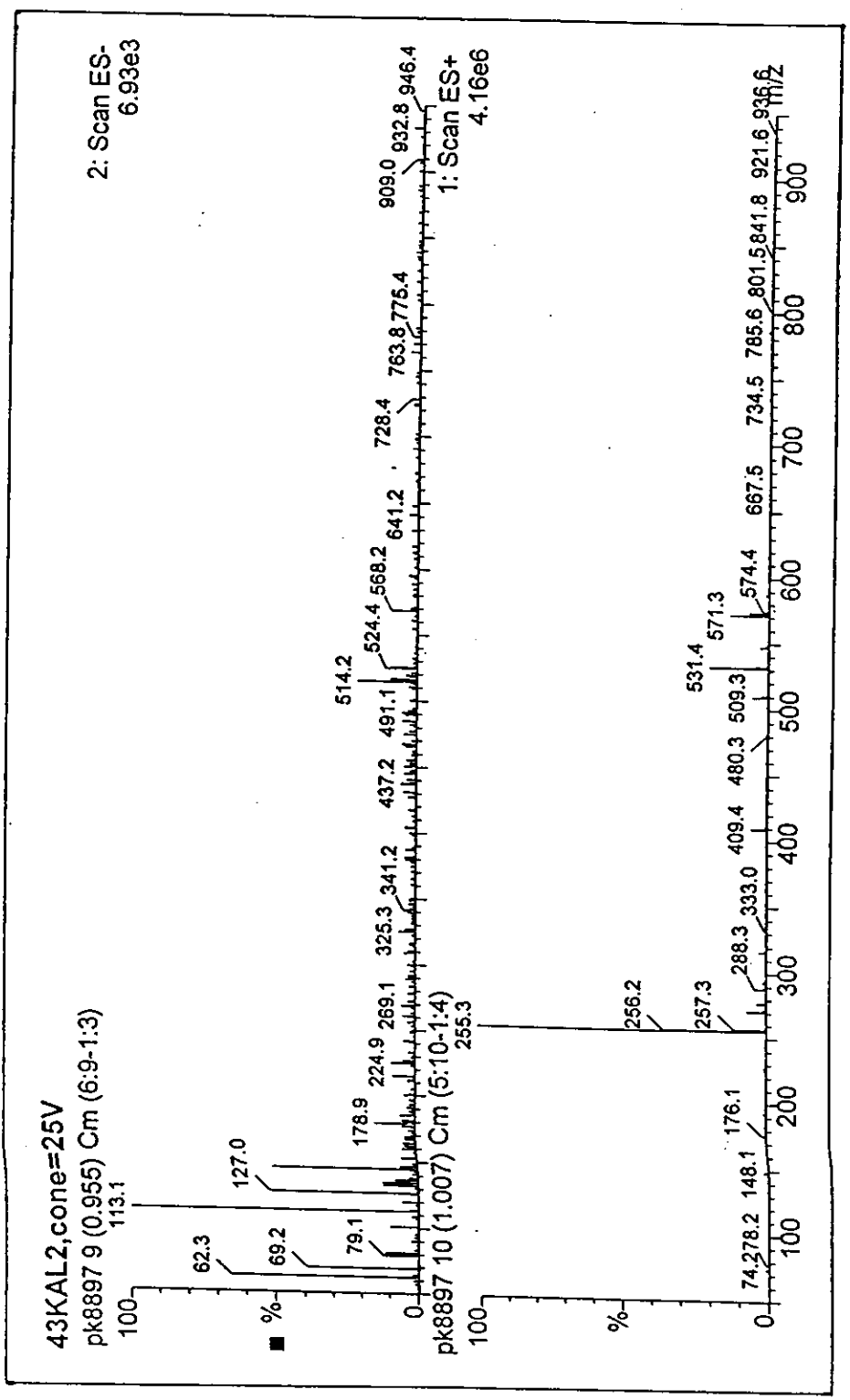

Figure 3 Electrospray mass spectrum of deazpy ligand.

3.1.2.3. UV-Visible absorption spectroscopy

UV-Visible absorption spectroscopy is the method to study the electronic transitions of the ligands. The UV-Visible absorption spectra of dmazpy and deazpy ligands in acetonitrile solution are shown in Figure 4 and 5, respectively. Electronic spectra of dmazpy and deazpy were recorded in eight solvents: hexane, acetone, acetonitrile, methanol, ethanol, *N,N*-dimethylformamide (DMF), and dimethyl sulfoxide (DMSO). The spectroscopic data is summarized in Table 5.

Table 5 The UV-Visible absorption spectroscopic data of dmazpy and deazpy ligands.

Solvent	λ_{max} nm, (ε x10^{-4} M^{-1} cm^{-1})		Cut-off Solvent (nm)
	Dmazpy	Deazpy	
Hexane	260(1.12) 398(3.29)	266(0.83) 410(2.56)	190
Acetone	422(2.66)	430(2.60)	320
Acetonitrile	270(1.05) 422(3.32)	272(1.23) 432(4.22)	190
Ethanol	274(1.44) 430(3.38)	276(1.22) 440(4.66)	200
Methanol	272(0.37) 434(2.95)	276(1.00) 444(3.63)	200
DMF	428(1.73)	438(2.29)	270
DMSO	272(1.35) 434(2.93)	270(1.42) 444(2.06)	250

The absorption spectra of dmazpy and deazpy ligand in this series of solvents showed intense bands at 260-285 nm ($\varepsilon \sim$ 3000-10,000 $M^{-1}cm^{-1}$) in UV region which referred to $\pi \rightarrow \pi^*$ (1) transition, and bands at 395-480 nm ($\varepsilon \sim$ 30,000 M^{-1} cm^{-1}) in visible region which belonged to $\pi \rightarrow \pi^*$ (2). On the other hand, azpy ligand showed absorption band in UV region which was assigned as $\pi \rightarrow \pi^*$ transition, and the broad band in visible region which referred to $n \rightarrow \pi^*$ transition. Dmazpy and deazpy ligands had $\pi \rightarrow \pi^*$ transition at the lowest energy, whereas those in azpy was $n \rightarrow \pi^*$ transition.

In addition, dmazpy and deazpy exhibited slightly solvent effect. The solvent polarity led to bathochromic shift of $\pi \rightarrow \pi^*$ (2) transition.

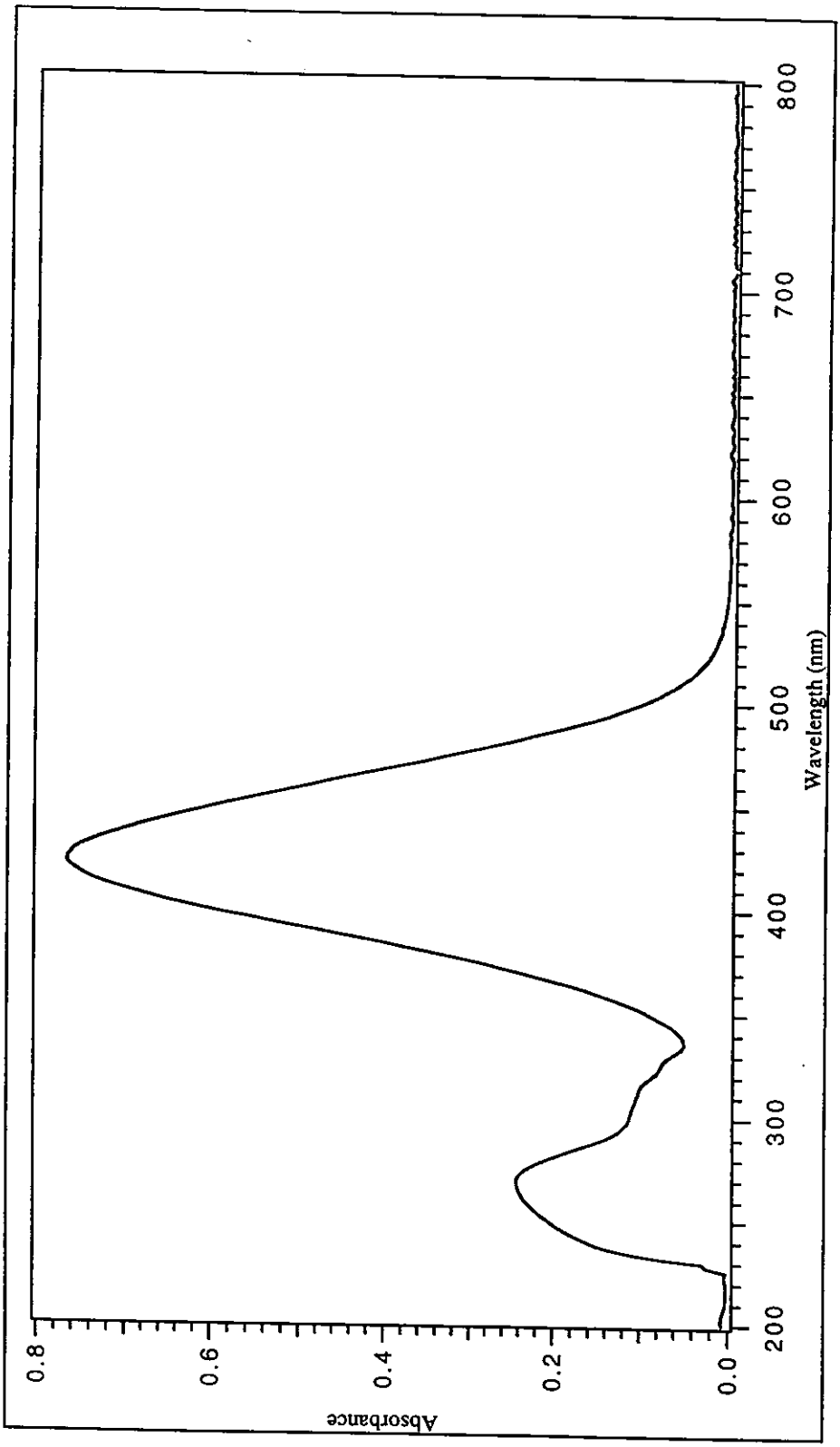

Figure 4 UV-Visible absorption spectrum of dmazpy ligand in acetonitrile.

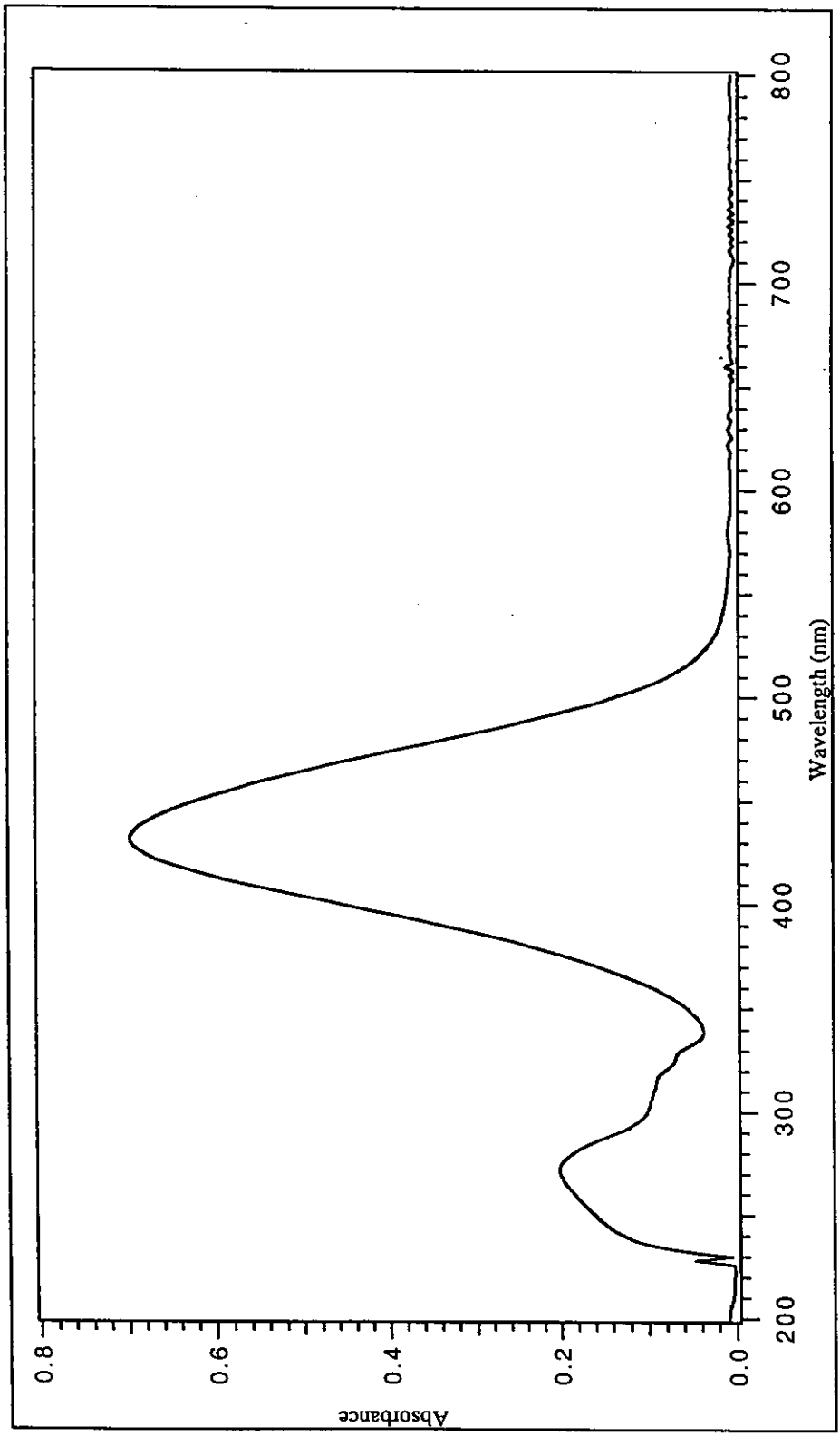

Figure 5 UV-Visible absorption spectrum of deazpy ligand in acetonitrile.

3.1.2.4. Infrared spectroscopy

Infrared spectra of dmazpy and deazpy ligands were recorded in the range 4000-370 cm^{-1} and shown in Figure 6 and 7, respectively. The interesting intense vibration frequencies of ligands were C=C, C=N, N=N (azo) stretching vibration and C-H bending of para disubstituted benzene. The summary of infrared spectroscopic data is listed in Table 6.

Table 6 Infrared spectroscopic data of dmazpy and deazpy ligands.

Vibration modes	Frequencies (cm^{-1})	
	dmazpy	deazpy
C=N	1610	1599
C=C	1447	1517
N=N	1402	1394
C-H bending of para disubstituted benzene	823	833
C-H bending of ethyl chain	-	789

Infrared spectra of dmazpy and deazpy ligands showed many vibrations of different intensities below 1,600 cm^{-1}. The most important peak was N=N stretching which used to consider the π-acid property in azo complexes. The N=N stretching of dmazpy and deazpy ligands showed the intense peak at 1402 and 1394 cm^{-1}, respectively. Meanwhile, the N=N stretching frequency of azpy ligand appeared at higher frequency, 1420 cm^{-1} (Krause and Krause, 1980).

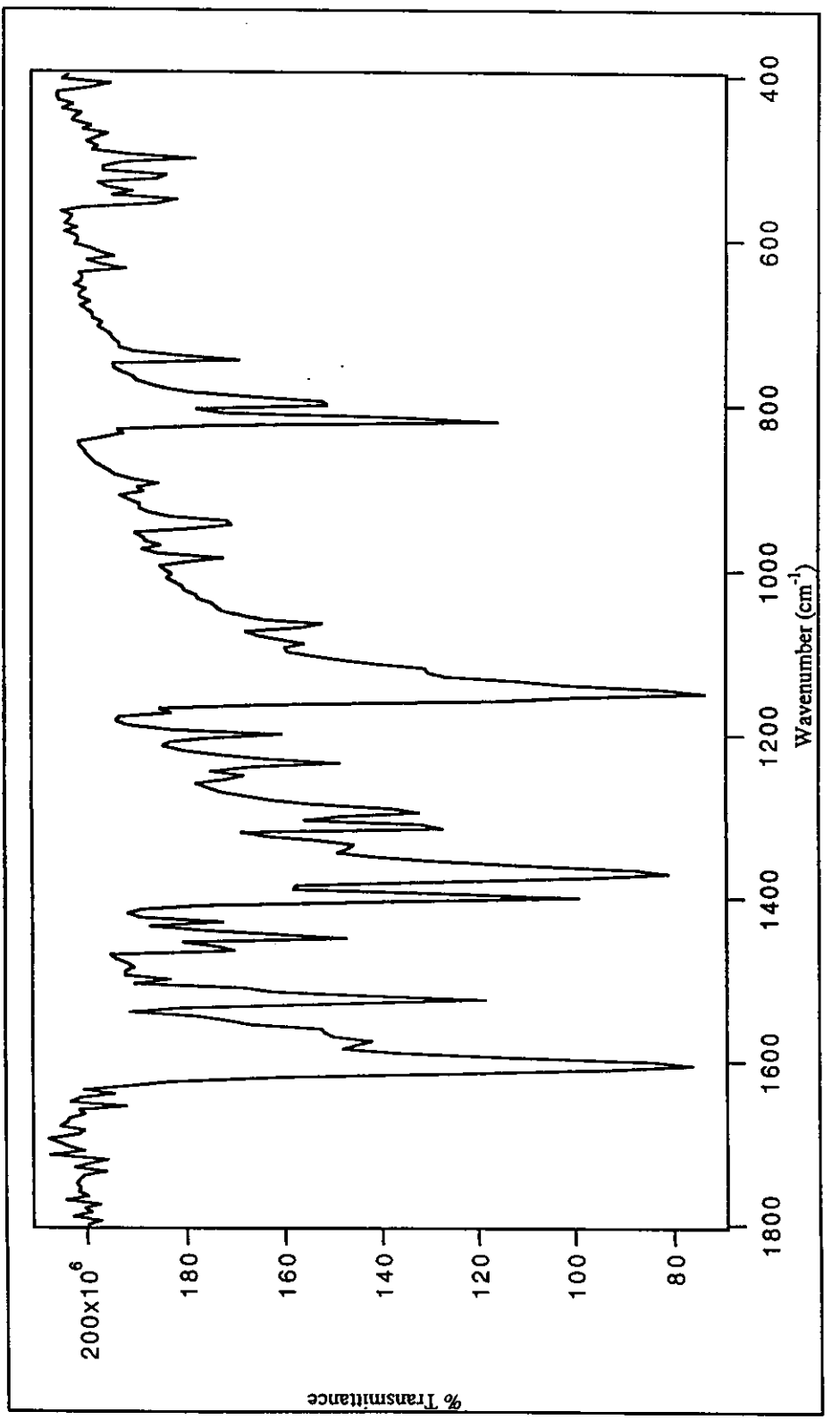

Figure 6 IR spectrum of 2-(4'-*N*,*N*-dimethylaminophenylazo)pyridine (dmazpy).

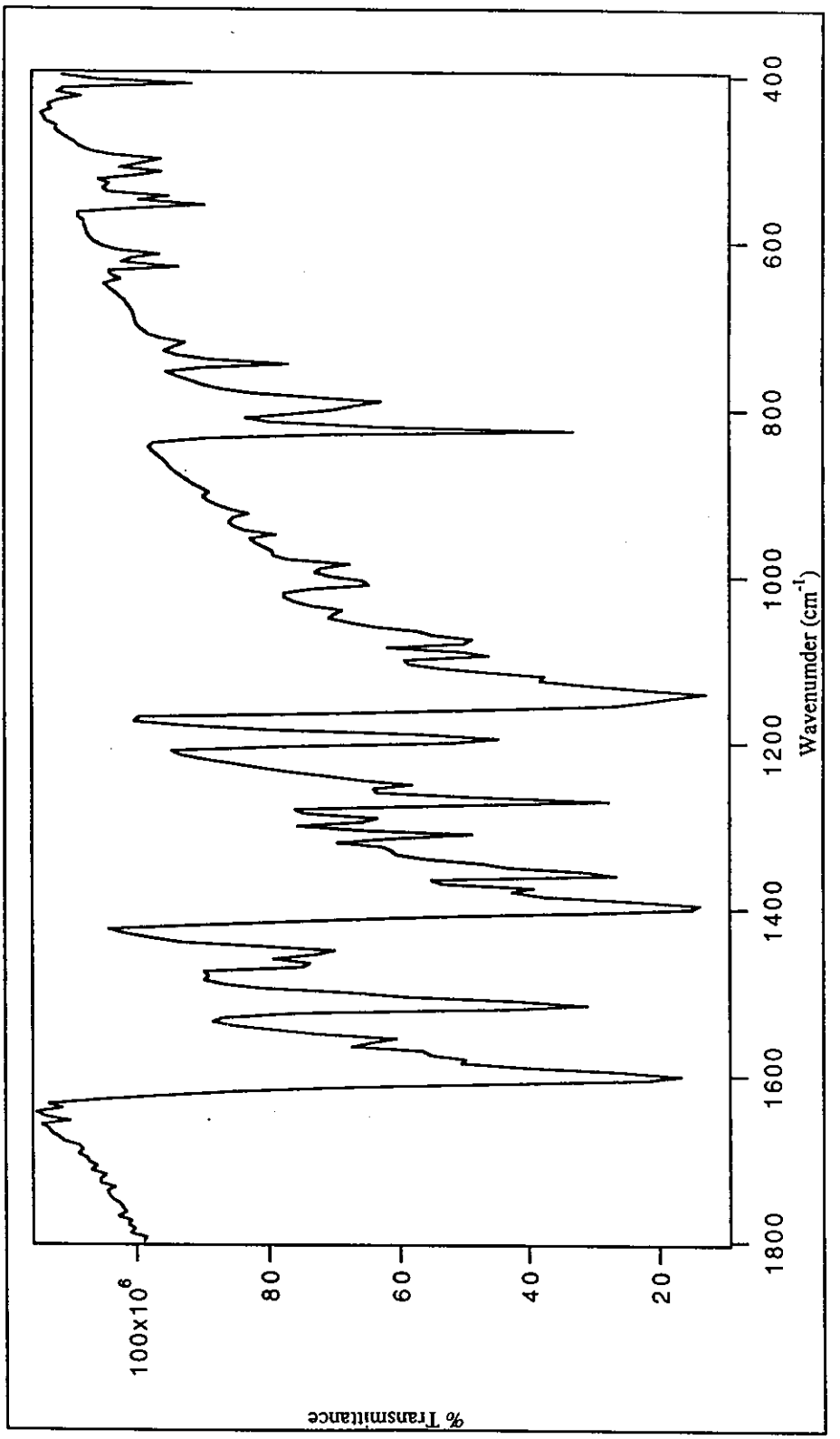

Figure 7 IR spectrum of 2-(4'-*N*,*N*-diethyl aminophenylazo)pyridine (deazpy).

3.1.2.5. Nuclear magnetic resonance spectroscopy

^{1}H NMR spectroscopy is an important technique to determine molecular structure. The ^{1}H NMR spectra of ligands are recorded in $CDCl_3$.The ^{1}H NMR spectrum of dmazpy and deazpy are shown in Figure 8 and 9, respectively. The chemical shift (δ, ppm) and J-coupling (Hz) of dmazpy and deazpy ligands are reported in Table 7 and 8.

Table 8 ^{1}H NMR spectroscopic data of dmazpy ligand.

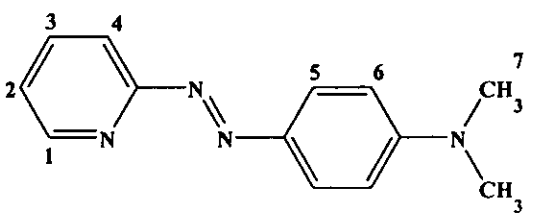

H-position	δ (ppm)	Amount of H	Peak	J-coupling (Hz)
1	8.68	1	ddd	5.0, 1.8, 0.5
5	8.01	2	d	9.5
3	7.83	1	ddd	8.5, 7.5, 2.0
4	7.76	1	d	8.5
2	7.29	1	ddd	7.5, 1.0, 5.0
6	6.76	2	d	9.0
7	3.10	6	s	-

d = doublet, ddd = doublet of doublet of doublet, s = singlet

Table 8 ^{1}H NMR spectroscopic data of deazpy ligands.

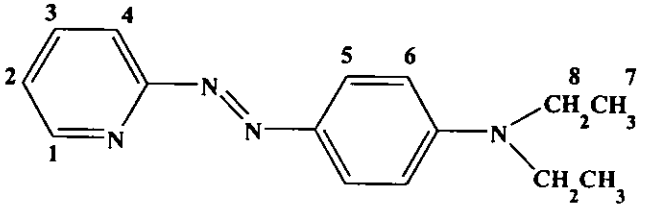

H-position	δ (ppm)	Amount of H	Peak	J-coupling (Hz)
1	8.68	1	d	5.0
5	7.99	2	d	9.0
3	7.82	1	ddd	5.0, 8.0, 2.0
4	7.75	1	d	8.0
2	7.27	1	ddd	6.5, 2.0, 4.5
6	6.72	2	d	9.0
8	3.46	4	q	7.5, 7.0, 7.0
7	1.24	6	t	7.0, 7.5

d = doublet, ddd= doublet of doublet of doublet, t = triplet, q = quartet

The ^{1}H NMR data of dmazpy is similar to deazpy. The types of protons in dmazpy ligand are divided into seven groups, while those in deazpy are divided into eight groups. The detail of each signal could be explained below.

The proton H1 is on pyridine located next to pyridine nitrogen atom, which occurs at most downfield. The signal is splitted by proton H2 (J = 5.0 Hz), H3 (J = 1.8 Hz) and H4 (J = 0.5 Hz). The signal appears as doublet of doublet of doublet.

The proton H2 is located next to proton H1. The resonance occurs as doublet of doublet of doublet. The splitting of doublet of doublet of doublet peaks is observed for

coupling with proton H1 (J = 4.5-5 Hz) and H3 (J = 6.5-7.5 Hz). Each of doublet peaks is splitted to doublet peaks (J = 1-2 Hz) from long range coupling with proton H4.

The proton H3 is opposite to pyridine nitrogen. This proton shows the signal at higher chemical shift than proton H2, because proton H3 locates at para position. The signal appears as doublet of doublet of doublet peaks. It is splitted by proton H2 (J = 7.5 Hz), H4 (J = 8.5 Hz) and H1 (J = 2 Hz).

The Proton H4 is located next to proton H3 and effected by nitrogen of azo function. The signal occurs at downfield more than proton H2 and H3. The signal shows as doublet of doublet peaks. It is splitted by proton H3 (J = 8-8.5 Hz).

The proton H5 are two equivalent protons on phenyl ring located closed to azo nitrogen. The proton H5 interacts with proton H6 and the signal shows as doublet peaks (J = 8-8.5 Hz).

The proton H6 are two equivalent protons located next to proton H5. The splitting pattern is doublet of doublet (J = 9 Hz).

The proton H7 are the methyl protons. The signal of dmazpy ligand appears as singlet peak of 6 protons. The signal of deazpy ligand occurs as triplet peaks, due to the methylene protons (J = 7, 7.5 Hz).

The proton H8 are the methylene protons of deazpy ligand. The signal of this proton is quartet peaks from the interaction with methyl proton (J = 7, 7.5, 7 Hz).

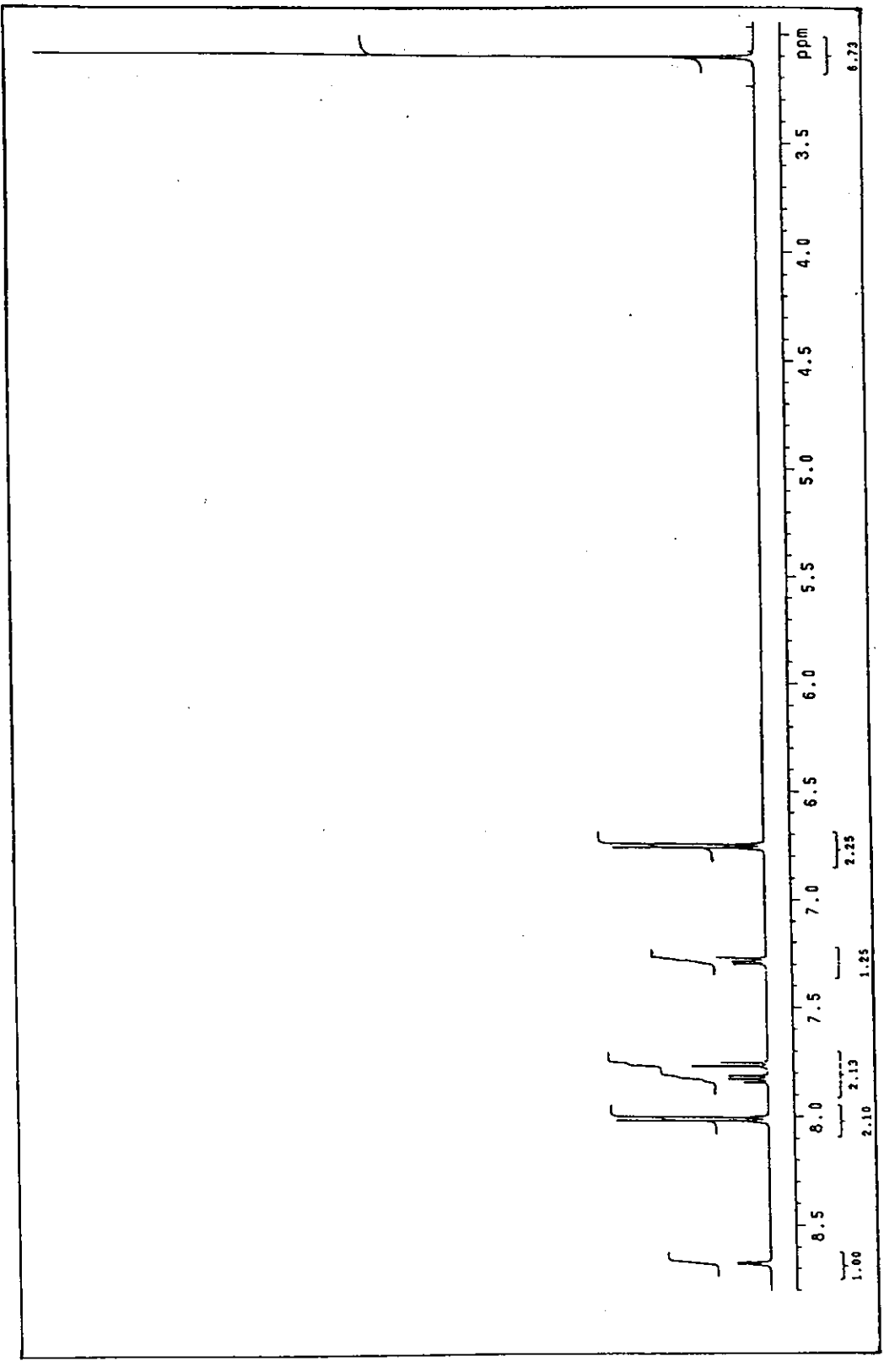

Figure 8 ^{1}H NMR spectrum of dmazpy ligand.

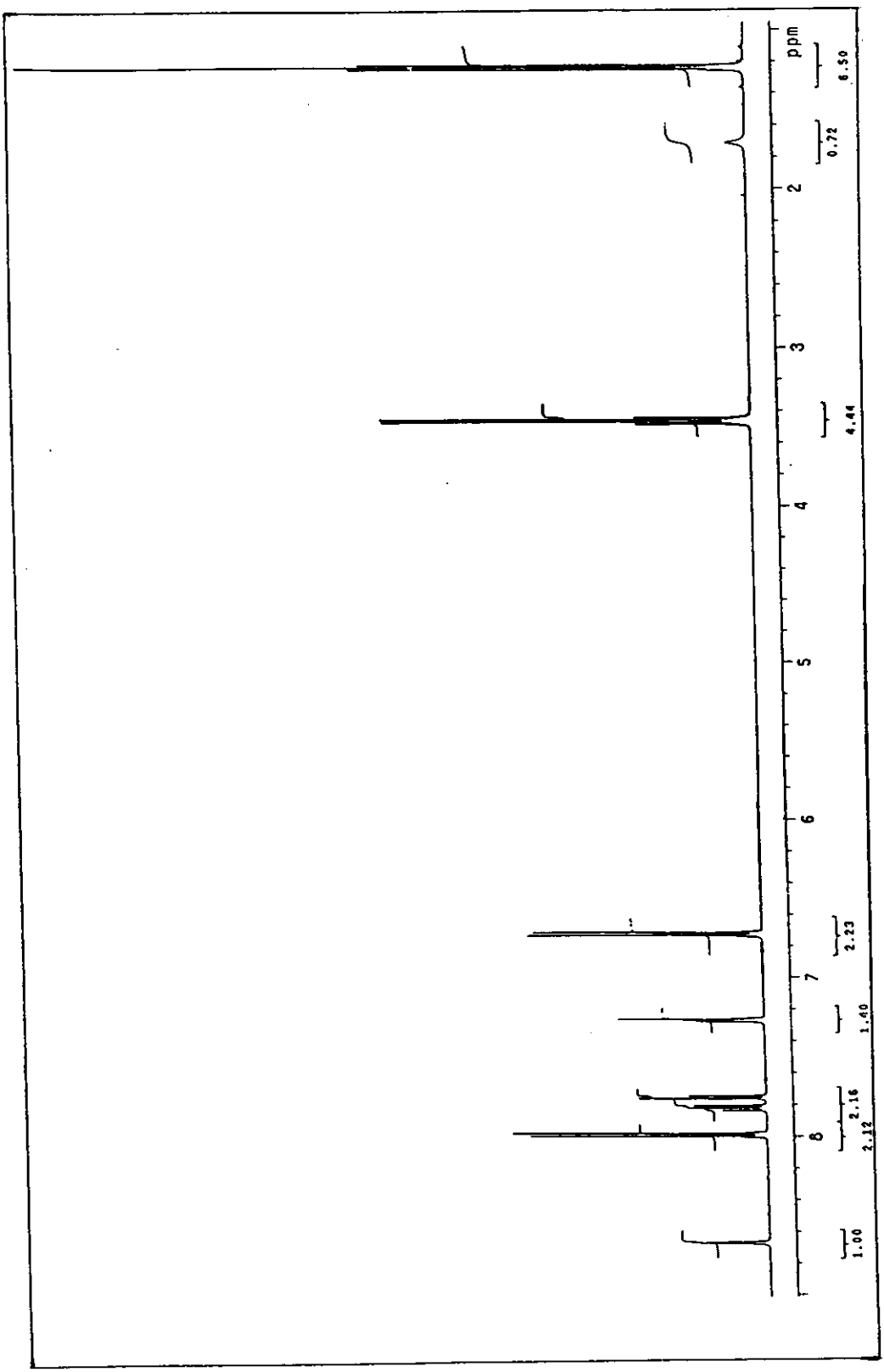

Figure 9 ^{1}H NMR spectrum of deazpy ligand.

3.1.2.6. Cyclic voltammetry

The cyclic voltammetry is an important technique to study the electrochemistry of the ligands. An electrochemistry behavior of the dmazpy was similar to that of deazpy. The four peaks were observed. The two peaks were in reduction potential range (negative potential) and the other peaks were in oxidation potential range (positive potential). Whereas, azpy ligand did not show any peaks in positive potential. Cyclic voltammetric data of azpy, dmazpy and deazpy ligands are summarized in Table 10. The potentials were compared with the potential of ferrocene couple ($E_{1/2}$ = 0 V, ΔE_p = 68 mV). The cyclic voltammogram of dmazpy and deazpy ligands were recorded in acetonitrile solution as shown in Figure 10 and 11, respectively.

In this experiment, the different scan rates were used to check the couple or the redox reaction. The couple giving equal anodic and cathodic currents was referred to reversible couple. On other hand, the unequal currents were referred to the unequally transfer of the electron in the reduction and oxidation. This led to irreversible couple.

Table 9 Cyclic voltammetric data of azpy, dmazpy and deazpy ligands in 0.1 M TBAH acetonitrile at scan rate 50 mV/s. (ferrocene as an internal standard, ΔE_p = 68 mV).

Compound	$E_{1/2}$, V (ΔE_p, mV)		
	peak	Oxidation	Reduction
Azpy		-	-1.58(171)
Dmazpy	I	+0.53(84)	-1.76[a]
	II	+0.74(84)	
Deazpy	I	+0.60(96)	-1.71[a]
	II	+0.81(84)	

a = irreversible cathodic peak

Reduction range

The cathodic peaks at -1.76 V (for dmazpy) and —1.71 V (for deazpy) in reduction potential were irreversible peaks eventhough high scan rate (500, 1000, 2000 mV/s) were obtained. In both dmazpy and deazpy ligands, the anodic peak showed at —1.262 V, but this anodic peak could not occur spontaneously. Comparison with azpy ligand, the reduction potential acted as a reversible couple at $E_{1/2}$ = -1.58 V (ΔE_p = 171 mV) which had two electrons transfer process related to the ΔE_p of ferrocene.

Oxidation range

The cyclic voltammogram of dmazpy showed two quasi-reversible couples at +0.53 V (ΔE_p = 84 mV) and +0.74 V (ΔE_p = 84 mV). The deazpy ligand gave similar results and two quasi-reversible couples occurred at +0.60 V (ΔE_p = 96

mV) and +0.80 V (ΔE_p = 84 mV). The couple I was studied in the range 400-700 mV. The cyclic voltammograms showed the irreversible peaks at low scan rate (50, 100 mV/s). However, this couple became clearly quasi-reversible peaks at higher scan rate (200-2000 mV/s). This couple was one electron transfer compared with ferrocene couple. This couple occurred spontaneously (Figure 50, Appendix A). The couple II was occurred from the couple I species in the range 750-1150 mV (Figure 51, Appendix A).

Azpy ligand had only one peak in reduction range. The difference might be due to substituent effects in dmazpy and deazpy molecules. The cyclic voltammograms of the starting material of both ligands, *N,N*-dimethyl-4-nitrosoaniline and *N,N*-diethyl-4-nitrosoaniline were studied to confirm this information. In the oxidation ranges, cyclic voltammogram of both substances showed quasi-reversible couples (Figure 52, Appendix A) at the closed potential to couple I of ligands.

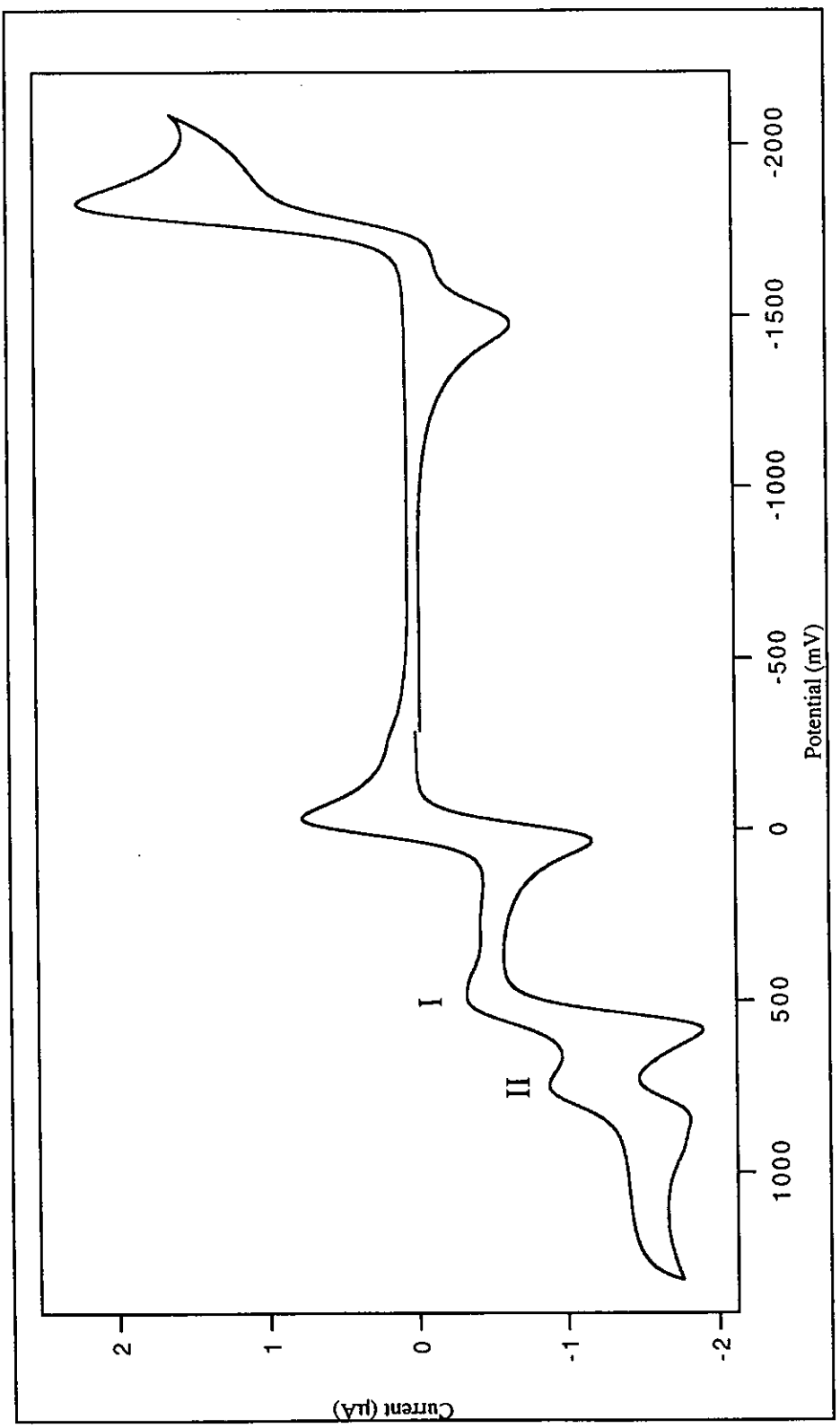

Figure 10 Cyclic Voltammogram of 2-(4'-*N*,*N*-dimetylaminophenylazo)pyridine (scan rate 50 mV/s).

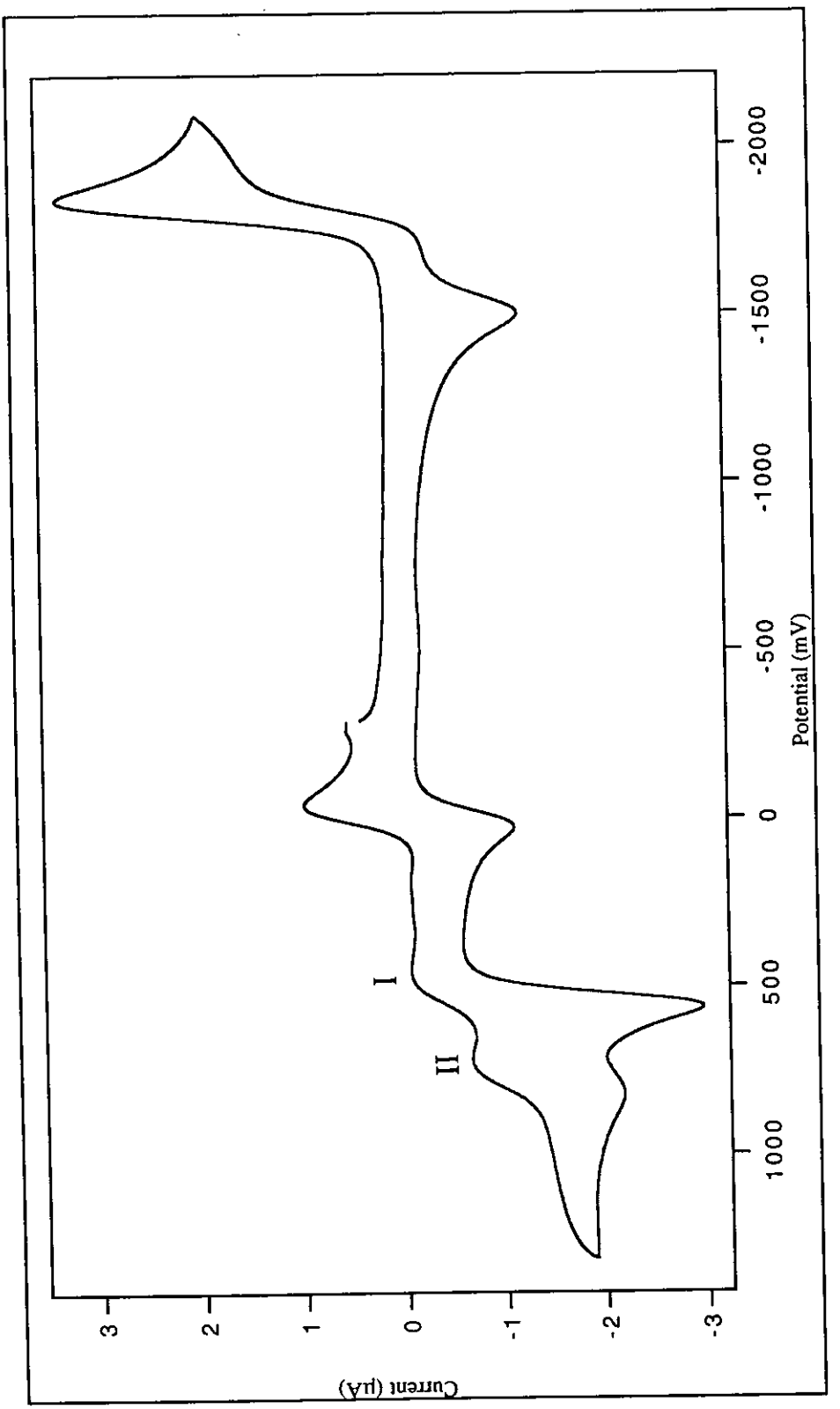

Figure 11 Cyclic Voltammogram of 2-(4'-*N*,*N*-diethylaminophenylazo)pyridine (scan rate 50 mV/s).

3.1.2.7. X-ray diffractometer

The X-ray crystallography is the most important technique to identify the geometries of the ligands. The single crystals of 2-(4'-*N*,*N*-dimethylaminophenylazo)pyridine (dmazpy) were grown by slowly diffusion of hexane into the ethylacetate solution. The crystallographic data are listed in Table 10-12. The crystal structure of dmazpy is shown in Figure 12.

The single crystals of 2-(4'-*N*,*N*-diethylaminophenylazo)pyridine (deazpy) were grown by slowly evaporation of ethanol. The crystallographic data are listed in Table 13-15. The crystal structure of deazpy is shown in Figure 13.

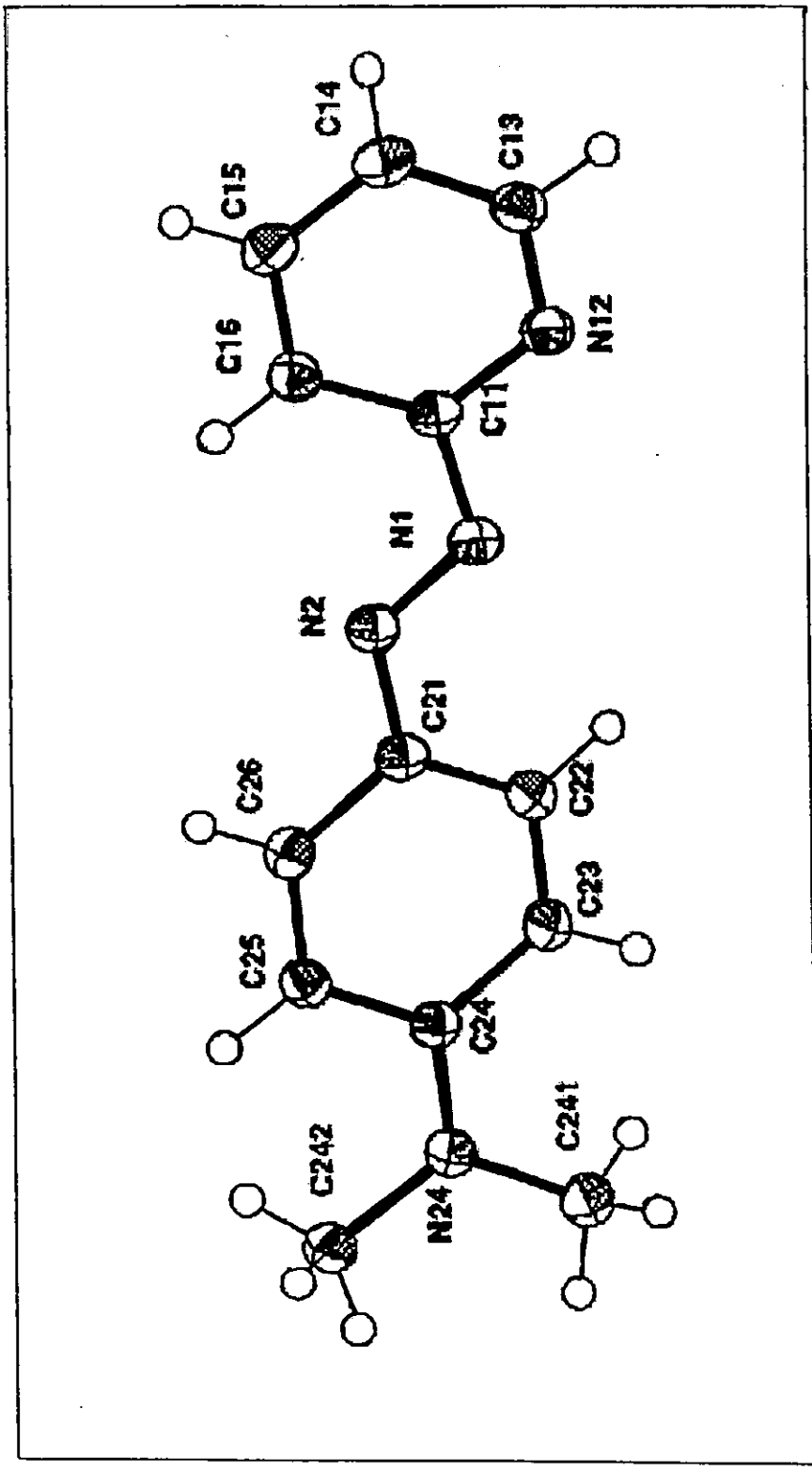

Figure 12 The structure of dmazpy ligand.

Table 10 The crystallographic data for dmazpy.

Empirical formula	$C_{13}H_{14}N_4$
Formula weight	226.28
Crystal system	monoclinic
Space group	$P_{121}/n1$
Unit cell dimensions	a = 6.1840(12) Å, $\alpha = 90°$
	b = 19.877(4) Å, $\beta = 95.43(3)°$
	c = 9.4710(19) Å, $\gamma = 90°$
Volume	1158.9(4) $Å^3$
Z	4
Temperature	153 K
Wavelength	0 .71073 nm
Density (calculated)	1.297 mg/m^3
Absorption coefficient	0.082 mm^{-1}
Index ranges	$-8 < h < 8, 0 < k < 26, 0 < l < 12$
Goodness-of-fit on F^2	1.192
R indices (all data)	$R = 0.043, R_w = 0.052$

Table 11 Non-hydrogen interatomic distances of dmazpy.

Atoms	Distance (Angstroms)
N(1)-C(11)	1.435(2)
N(1)-N(2)	1.270(1)
C(11)-N(12)	1.343(2)
C(11)-C(16)	1.397(2)
N(12)-C(13)	1.346(2)
C(13)-C(14)	1.385(2)
C(14)-C(15)	1.391(2)
C(15)-C(16)	1.385(2)
N(2)-C(21)	1.403(2)
C(21)-C(22)	1.404(2)
C(21)-C(26)	1.400(2)
C(22)-C(23)	1.379(2)
C(23)-C(24)	1.427(2)
C(24)-N(24)	1.364(2)
C(24)-C(25)	1.413(2)
N(24)-C(241)	1.455(2)
N(24)-C(242)	1.456(2)
C(25)-C(26)	1.381(2)

Table 12 Non-hydrogen interbond angles of dmazpy.

Atom	Angles (degrees)
C(11)-N(1)-N(2)	111.9(1)
N(1)-C(11)-N(12)	112.8(1)
N(1)-C(11)-C(16)	123.8(1)
N(12)-C(11)-C(16)	123.4(1))
C(11)-N(12)-C(13)	116.8(1)
N(12)-C(13)-C(14)	124.2(1)
C(13)-C(14)-C(15)	118.0(1)
C(14)-C(15)-C(16)	119.3(1)
C(11)-C(16)-C(15)	118.4(1)
N(1)-N(2)-C(21)	116.0(1)
N(2)-C(21)-C(22)	125.9(1)
N(2)-C(21)-C(26)	115.5(1)
C(22)-C(21)-C(26)	118.6(1)
C(21)-C(22)-C(23)	120.7(1))
C(22)-C(23)-C(24)	121.0(1)
C(23)-C(24)-N(24)	121.3(1)
C(23)-C(24)-C(25)	117.6(1)
N(24)-C(24)-C(25)	121.1(1)
C(24)-N(24)-C(241)	120.8(1)
C(24)-N(24)-C(242)	120.5(1)
C(241)-N(24)-C(242)	118.7(1)
C(24)-C(25)-C(26)	120.6(1)
C(21)-C(26)-C(25)	121.5(1)

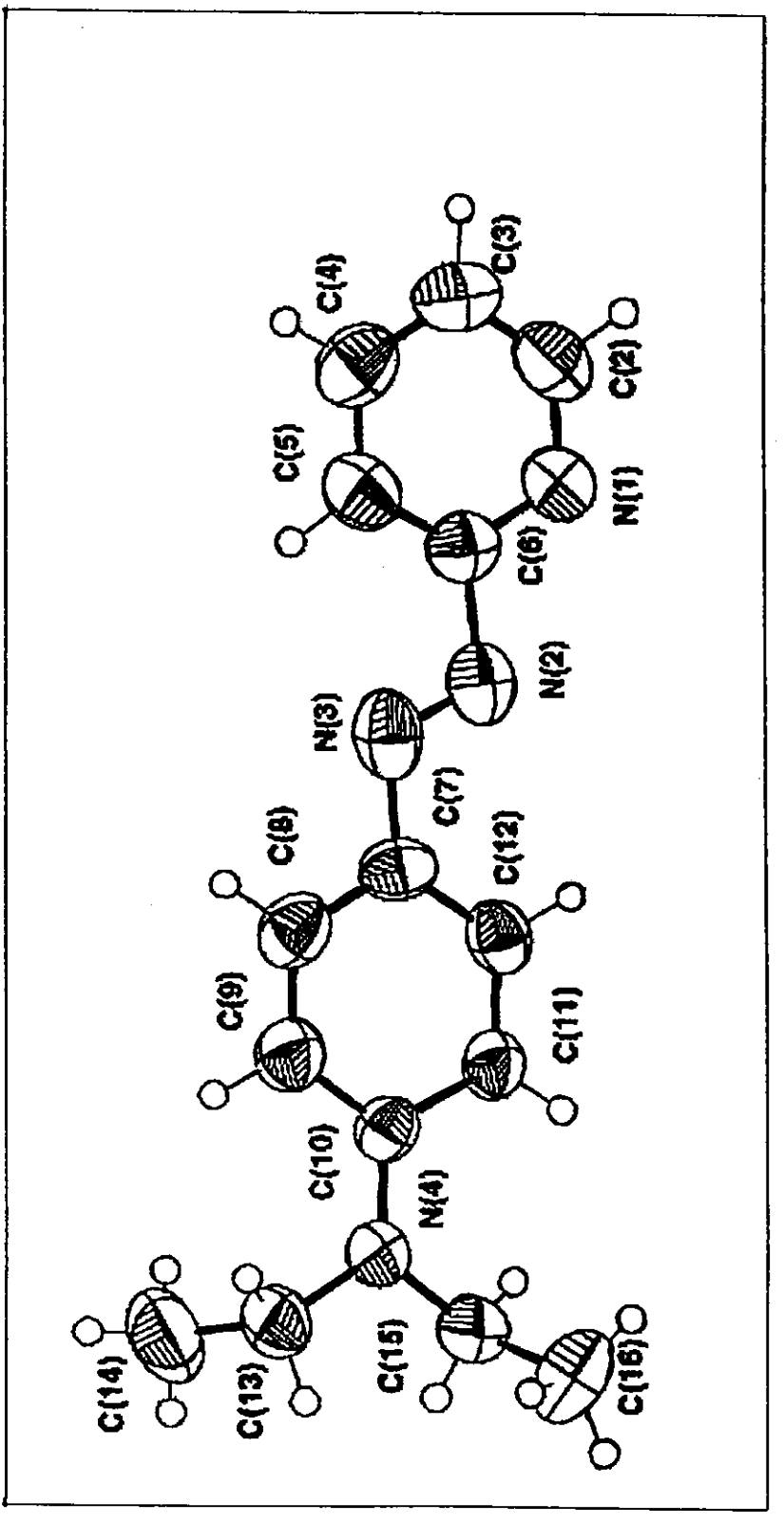

Figure 13 The structure of deazpy ligand.

Table 13 The crystallographic data for deazpy.

Empirical Formula	$C_{15}H_{18}N_4$
Formula weight	254.33
Crystal system	orthorhombic
Space group	P_{212121}
Unit cell dimensions	a = 7.4811 Å, $\alpha = 90°$
	b = 9.1005 Å, $\beta = 90°$
	c = 21.0371 Å, $\gamma = 90°$
Volume	1432.24(4) $Å^3$
Z	4
Temperature	296.2 K
Wavelength	0.71073 nm
Density (calculated)	1.179 mg/m^3
Absorption coefficient	0.073 nm^{-1}
Index ranges	$-9 < h < 0$, $-11 < k < 0$, $-26 < l < 0$
Goodness-of-fit on F^2	2.778
R indices (all data)	R = 0.0446, $R_w = 0.0360$

Table 14 Non-hydrogen interatomic distances of deazpy.

Atoms	Distance (Angstroms)
N(1)-C(2)	1.344(4)
N(1)-C(6)	1.324(4)
N(2)-N(3)	1.193(3)
N(2)-C(6)	1.497(3)
N(3)-C(7)	1.462(4)
N(4)-C(10)	1.363(3)
N(4)-C(13)	1.471(3)
N(4)-C(15)	1.461(3)
C(2)-C(3)	1.353(5)
C(3)-C(4)	1.372(6)
C(4)-C(5)	1.366(5)
C(5)-C(6)	1.365(4)
C(7)-C(8)	1.376(4)
C(7)-C(12)	1.395(4)
C(8)-C(9)	1.353(4)
C(9)-C(10)	1.407(4)
C(10)-C(11)	1.415(4)
C(11)-C(12)	1.375(4)
C(13)-C(14)	1.507(4)
C(15)-C(16)	1.501(4)

Table 15 Non-hydrogen interatomic angles of deazpy.

Atoms	Angles (degrees)
C(2)-N(1)-C(6)	115.2(3)
N(3)-N(2)-C(6)	108.7(2)
N(2)-N(3)-C(7)	112.6(2)
C(10)-N(4)-C(13)	122.2(2)
C(10)-N(4)-C(15)	122.2(2)
C(13)-N(4)-C(15)	115.5(2)
N(1)-C(2)-C(3)	125.8(3)
C(2)-C(3)-C(4)	116.9(3)
C(3)-C(4)-C(5)	119.3(3)
C(4)-C(5)-C(6)	119.1(3)
N(1)-C(6)-N(2)	111.1(2)
N(1)-C(6)-C(5)	123.6(3)
N(2)-C(6)-C(5)	125.3(2)
N(3)-C(7)-C(8)	113.6(2)
N(3)-C(7)-C(12)	126.9(2)
C(8)-C(7)-C(12)	119.5(2)
C(7)-C(8)-C(9)	121.0(3)
C(8)-C(9)-C(10)	121.8(3)
N(4)-C(10)-C(9)	121.0(2)
N(4)-C(10)-C(11)	122.3(2)
C(9)-C(10)-C(11)	116.8(2)

Table 15 (continued).

Atoms	Angles (degrees)
C(10)-C(11)-C(12)	121.0(3)
C(7)-C(12)-C(11)	120.0(2)
N(4)-C(13)-C(14)	113.0(2)
N(4)-C(15)-C(16)	113.8(2)

3.2. Preparation and Characterization of Complexes

3.2.1 Preparation of complexes

Reaction between $Ru(tpy)Cl_3$ and dmazpy in refluxing ethanol/water in a presence of NEt_3 and LiCl afforded a product mixture. The mixture was partially isolated by column chromatography on siliga gel with 2:1 acetone/water as the eluent. The $[Ru(tpy)(dmazpy)NO_2]PF_6$ was synthesized by a reaction involving Ag (I) abstraction of chlorine from [Ru(tpy)(dmazpy)Cl]Cl in acetone/water. Introduction of the NO_2^- ligand in tenfold excess led to the desired complex. $[Ru(tpy)(dmazpy)CH_3CN](PF_6)_2$ was obtained by reaction of [Ru(tpy)(dmazpy) Cl]Cl with $AgNO_3$ in acetonitrile solution and purified by column chromatography on siliga gel with acetonitrile as the eluent. $[Ru(tpy)(deazpy)X]^{n+}$, where $X = Cl^-$, NO_2^- and CH_3CN were synthesized similarly to $[Ru(tpy)(dmazpy)X]^{n+}$, where $X = Cl^-$, NO_2^- and CH_3CN. $[Ru(tpy)(dmazpy)Cl]PF_6$ and $[Ru(tpy)(deazpy)Cl]PF_6$ complexes were very soluble in alcohol, DMSO and DMF. Whereas, $[Ru(tpy)(dmazpy)NO_2]PF_6$ and $[Ru(tpy)(deazpy)NO_2]PF_6$ complexes were very soluble in alcohol, acetonitrile, DMSO and DMF.

$[Ru(tpy)(dmazpy)CH_3CN](PF_6)_2$ and $[Ru(tpy)(deazpy)CH_3CN](PF_6)_2$ complexes were obtained in low yield. $[Ru(tpy)(dmazpy)CH_3CN](PF_6)_2$ and $[Ru(tpy)(deazpy)CH_3CN](PF_6)_2$ complexes were not stable in air and easily decomposed. Then, those complexes were not characterized by all methods. $[Ru(tpy)(dmazpy)CH_3CN](PF_6)_2$ and $[Ru(tpy)(deazpy)CH_3CN](PF_6)_2$ complexes were very soluble in methanol, acetonitrile, acetone, DMSO and DMF. Some of the physical properties of complexes were summarized in Table 16.

Table 16 The physical properties of complexes.

Complex	Physical properties		
	Appearance	Color	Melting point (^{O} C)
$[Ru(tpy)(dmazpy)Cl]PF_6$	Needle	black	236-238
$[Ru(tpy)(dmazpy)NO_2]PF_6$	Rod like	green	250-254
$[Ru(tpy)(deazpy)Cl]PF_6$	Needle	black	284-286
$[Ru(tpy)(deazpy)NO_2]PF_6$	Rod like	green	288-290

3.2.2 Characterization of complexes

The chemistry of dmazpy and deazpy complexes were determined by using these techniques:

- Elemental analysis
- The electrospray and the FAB mass spectrometry
- UV-Visible absorption spectroscopy
- Infrared spectroscopy
- Proton Nuclear Magnetic Resonance spectroscopy
- Cyclic Voltammetry
- X-ray Diffractometer

3.2.2.1. Elemental analysis

Elemental analysis is a principle method to determine composition of elements in the complexes. Therefore, the elements in the complexes are confirmed by this method.

Table 17 Elemental analysis data of $[Ru(tpy)(dmazpy)X]PF_6$ and $[Ru(tpy)(deazpy)X]PF_6$ complexes , where $X = Cl^-, NO_2^-$.

Complex	%C		%N		%H	
	Calcd	Found	Calcd	Found	Calcd	Found
$[Ru(tpy)(dmazpy)Cl]PF_6$	45.36	44.11	3.40	3.36	13.24	12.81
$[Ru(tpy)(dmazpy)NO_2]PF_6$	44.72	44.22	3.35	3.04	14.91	14.00
$[Ru(tpy)(deazpy)Cl]PF_6$	46.83	44.57	3.80	4.02	12.75	12.47
$[Ru(tpy)(deazpy)NO_2]PF_6$	46.20	44.46	3.75	3.74	14.74	14.38

3.2.2.2 The electrospray and the FAB mass spectroscopy

The electrospray and the FAB mass spectra of $[Ru(tpy)(dmazpy)X]^{n+}$ and $[Ru(tpy)(deazpy)X]^{n+}$ complexes , where $X = Cl^-, NO_2^-$ and CH_3CN were displayed in Figure 14-22. The important electrospray and the FAB mass spectroscopic data of complexes with the corresponding relative abundance were listed in Table 18-21.

Table 18 Electrospray mass spectroscopic data of [Ru(tpy)(dmazpy)Cl]Cl and [Ru(tpy)(dmazpy)X]PF_6 complexes , where X = Cl^-, NO_2^-.

m/z	Unit	Equivalent species	Rel. Abun.
[Ru(tpy)(dmazpy)Cl]Cl			
596.0	$[Ru(tpy)(dmazpy)Cl]^+$	$[M]^+$	100
595.0	$[Ru(tpy)(dmazpy)Cl-H]^+$	$[M-H]^+$	60
594.0	$[Ru(tpy)(dmazpy)Cl-2H]^+$	$[M-2H]^+$	40
[Ru(tpy)(dmazpy)Cl]PF_6			
597.8	$[Ru(tpy)(dmazpy)Cl+H]^+$	$[M+H]^+$	95
595.7	$[Ru(tpy)(dmazpy)Cl-H]^+$	$[M-H]^+$	100
594.7	$[Ru(tpy)(dmazpy)Cl-2H]^+$	$[M-2H]^+$	50
258.3	$[Ru(py-H)(py)]^+$	$[Ru(py-H)(py)]^+$	40
[Ru(tpy)(dmazpy)NO_2]PF_6			
609.1	$[Ru(tpy)(dmazpy)NO_2+2H]^+$	$[M+2H]^+$	60
607.1	$[Ru(tpy)(dmazpy)NO_2]^+$	$[M]^+$	100
606.0	$[Ru(tpy)(dmazpy)NO_2-H]^+$	$[M-H]^+$	55
605.1	$[Ru(tpy)(dmazpy)NO_2-2H]^+$	$[M-2H]^+$	45

M = $[Ru(tpy)(dmazpy)X]^{n+}$

Table 19 FAB mass spectroscopic data of $[Ru(tpy)(dmazpy)CH_3CN](PF_6)_2$ complex.

m/z	Unit	Equivalent species	Rel. Abun.
$[Ru(tpy)(dmazpy)CH_3CN](PF_6)_2$			
915	$[Ru(tpy)(dmazpy)CH_3CN](PF_6)_2 + Na^+$	$[M+2PF_6]+Na^+$	70
747	$[Ru(tpy)(dmazpy)CH_3CN]^+(PF_6)$	$[M+PF_6]^+$	84
727	$[Ru(tpy)(dmazpy)H_2O+3H]^+(PF_6)$	$[M-CH_3CN +H_2O+3H+PF_6]^+$	58
602	$[Ru(tpy)(dmazpy)CH_3CN]^{2+}$	$[M]^{2+}$	100

$M = [Ru(tpy)(dmazpy)X]^{n+}$

Table 20 Electrospray mass spectroscopic data of [Ru(tpy)(deazpy)Cl]Cl and $[Ru(tpy)(deazpy)Cl]PF_6$ complexes.

m/z	Unit	Equivalent species	Rel. Abun.
[Ru(tpy)(deazpy)Cl]Cl			
624.1	$[Ru(tpy)(deazpy)Cl]^+$	$[M]^+$	100
280.0	$[Ru(deazpy\text{-}N(C_2H_5)_2+3H]^+$	$[M\text{-}N(C_2H_5)_2+3H]^+$	30
103.7	$[Ru+2H]^+$	$[Ru+2H]^+$	85
$[Ru(tpy)(deazpy)Cl]PF_6$			
626.0	$[Ru(tpy)(deazpy)Cl+2H]^+$	$[M+2H]^+$	70
624.1	$[Ru(tpy)(deazpy)Cl]^+$	$[M]^+$	100
623.1	$[Ru(tpy)(deazpy)Cl\text{-}H]^+$	$[M\text{-}H]^+$	60
622.1	$[Ru(tpy)(deazpy)Cl\text{-}2H]^+$	$[M\text{-}2H]^+$	40

$M = [Ru(tpy)(deazpy)X]^{n+}$

Table 21 FAB mass spectroscopic data of $[Ru(tpy)(deazpy)NO_2]PF_6$ and $[Ru(tpy)(deazpy)CH_3CN](PF_6)_2$ complexes.

m/z	Unit	Equivalent species	Rel. Abun.
$[Ru(tpy)(deazpy)NO_2]PF_6$			
722	$[Ru(tpy)(deazpy)NO_2+H$ $-2(CH_2CH_3)]PF_6$	$[M+H$ $-2(CH_2CH_3)]PF_6$	55
713	$[Ru(tpy)(deazpy)-NO_2$ $-2CH_2CH_3]PF_6$	$[M-NO_2$ $-CH_2CH_3]PF_6$	60
635	$[Ru(tpy)(deazpy)NO_2]^+$	$[M]^+$	40
607	$[Ru(tpy)(deazpy)NO_2+H$ $-CH_2CH_3]^+$	$[M+H-CH_2CH_3]^+$	100
$[Ru(tpy)(deazpy)CH_3CN](PF_6)_2$			
943	$[Ru(tpy)(deazpy)CH_3CN](PF_6)_2$ $+Na^+$	$[M+2PF_6]+Na^+$	46
775	$[Ru(tpy)(deazpy)CH_3CN]^+(PF_6)$	$[M+PF_6]^+$	60
608	$[Ru(tpy)(deazpy)H_2O]^{2+}$	$[M-CH_3CN+H_2O]^{2+}$	100

$M = [Ru(tpy)(deazpy)X]^{n+}$

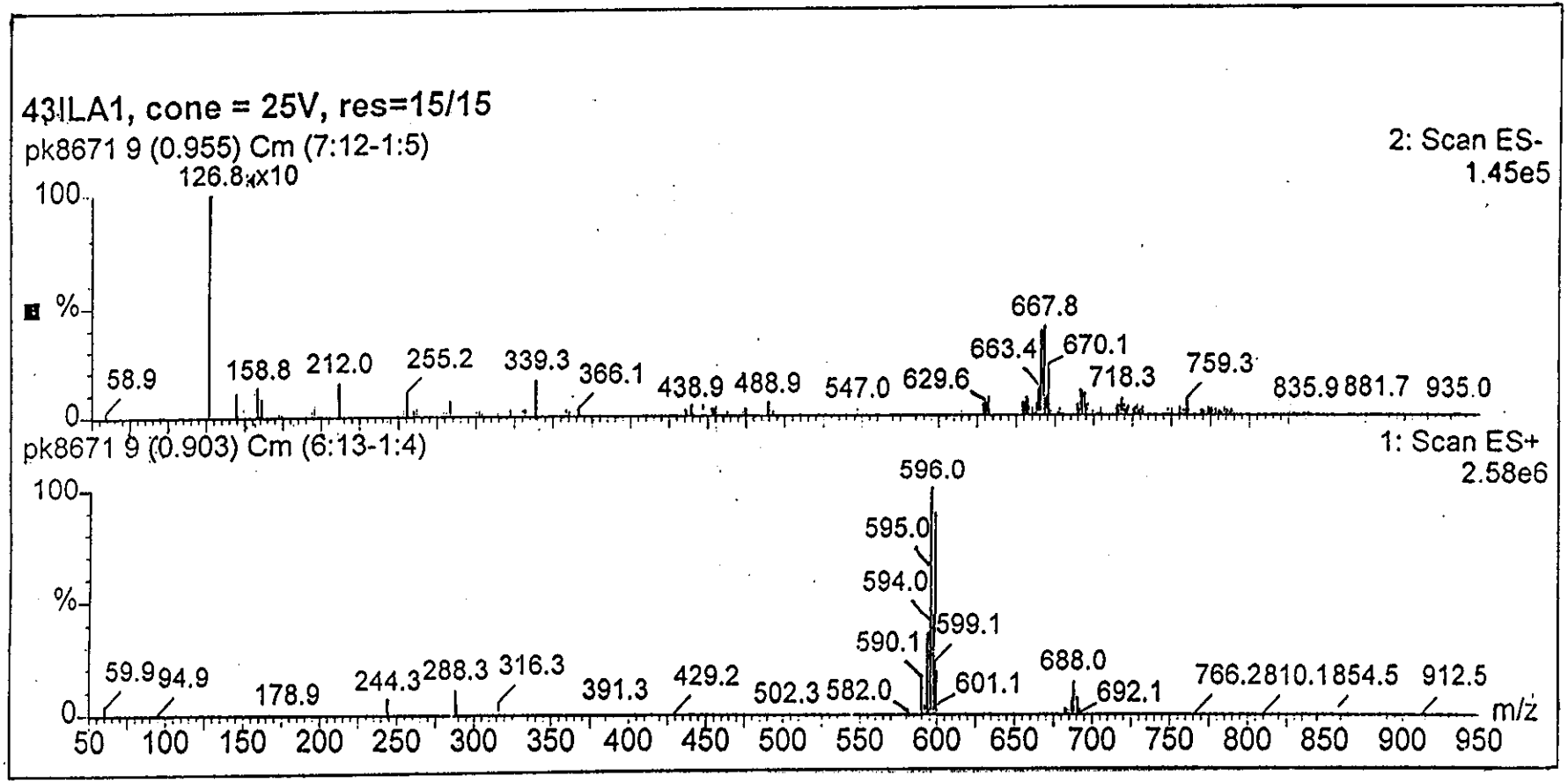

Figure 14 Electrospray mass spectrum of [Ru(tpy)(dmazpy)Cl]Cl complex.

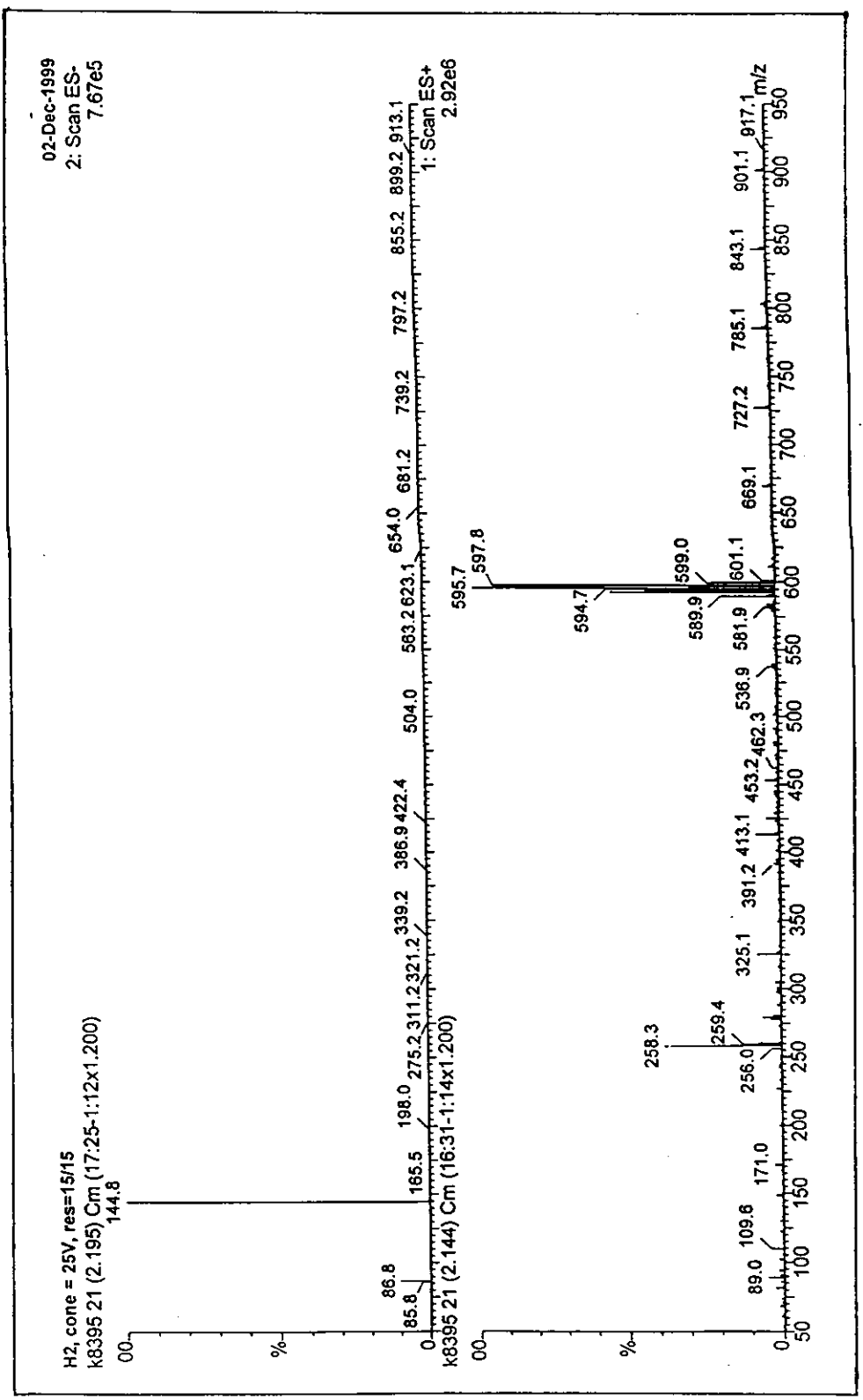

Figure 15 Electrospray mass spectrum of $[Ru(tpy)(dmazpy)Cl]PF_6$ complex.

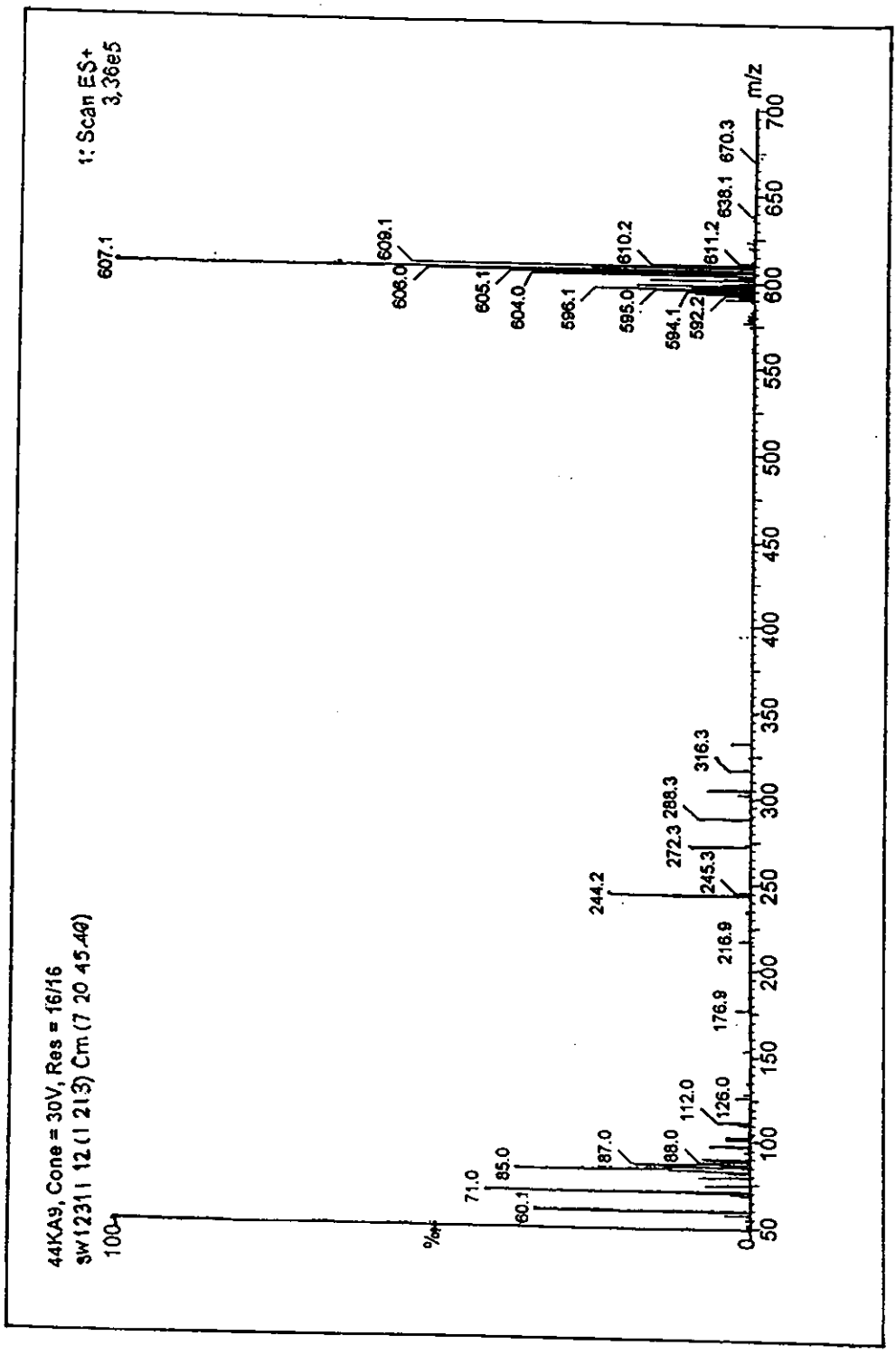

Figure 16 Electrospray mass spectrum of $[Ru(tpy)(dmazpy)NO_2]PF_6$ complex.

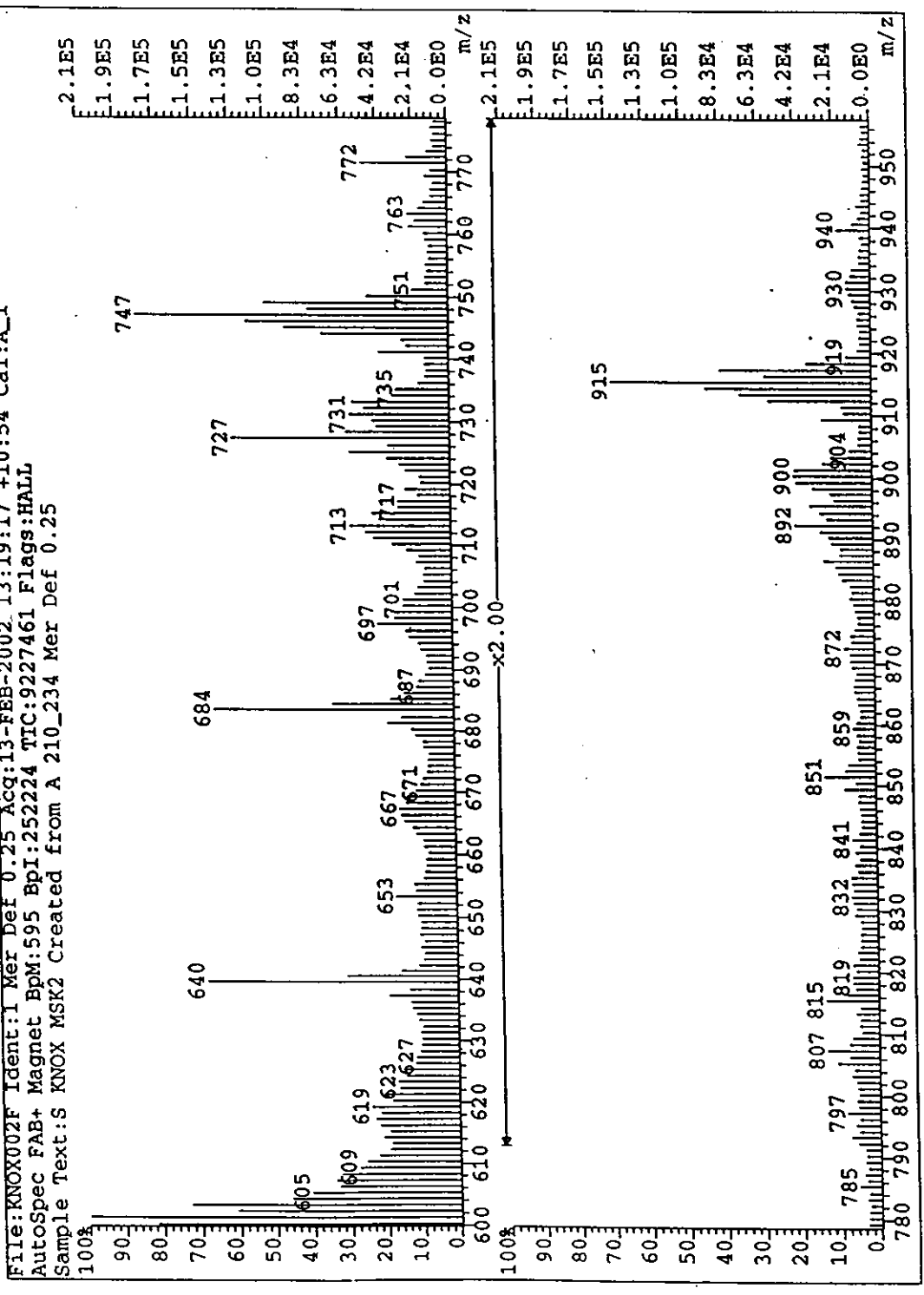

Figure 17 FAB mass spectrum of $[Ru(tpy)(dmazpy)CH_3CN](PF_6)_2$ complex.

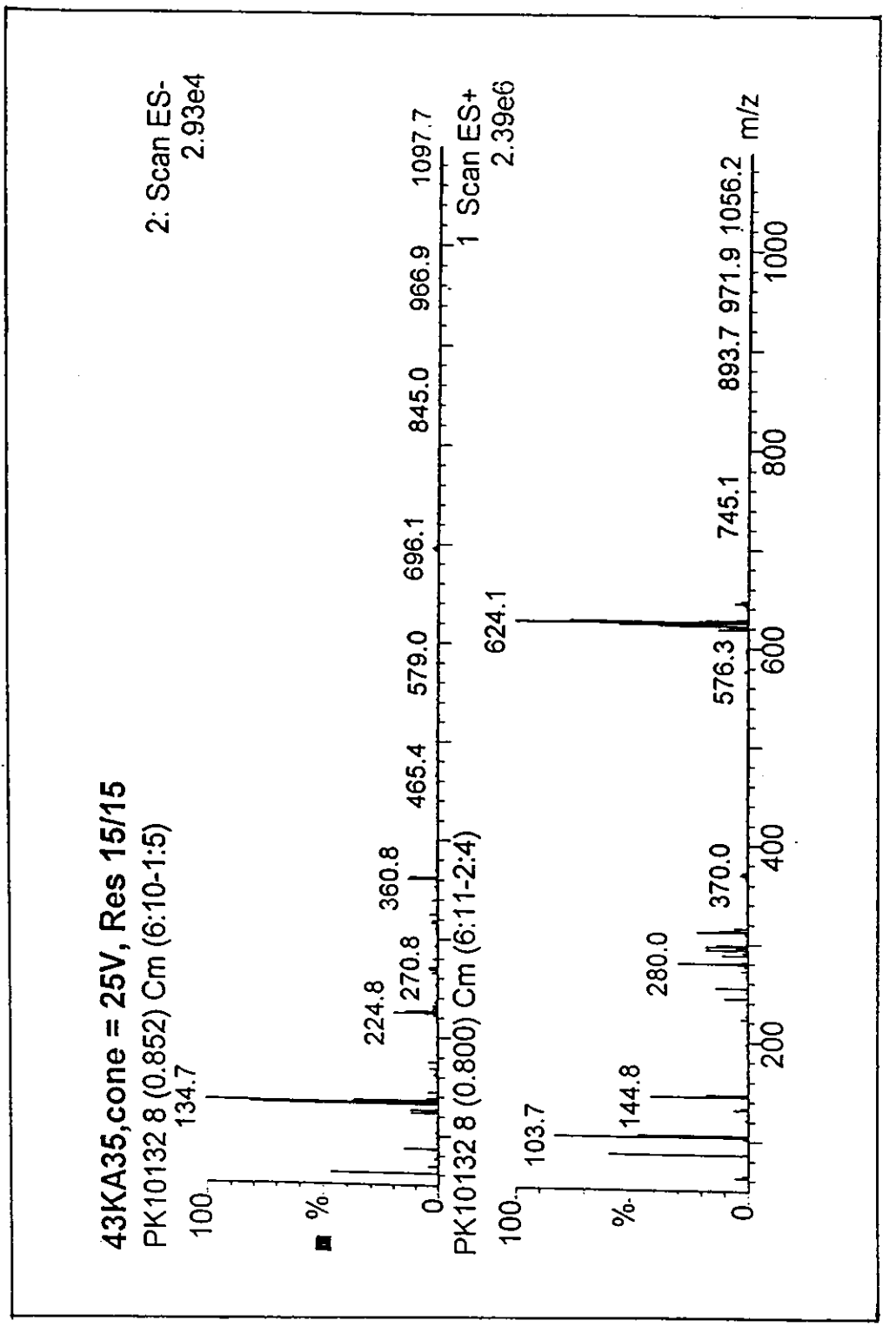

Figure 18 Electrospray mass spectrum of [Ru(tpy)(deazpy)Cl]Cl complex.

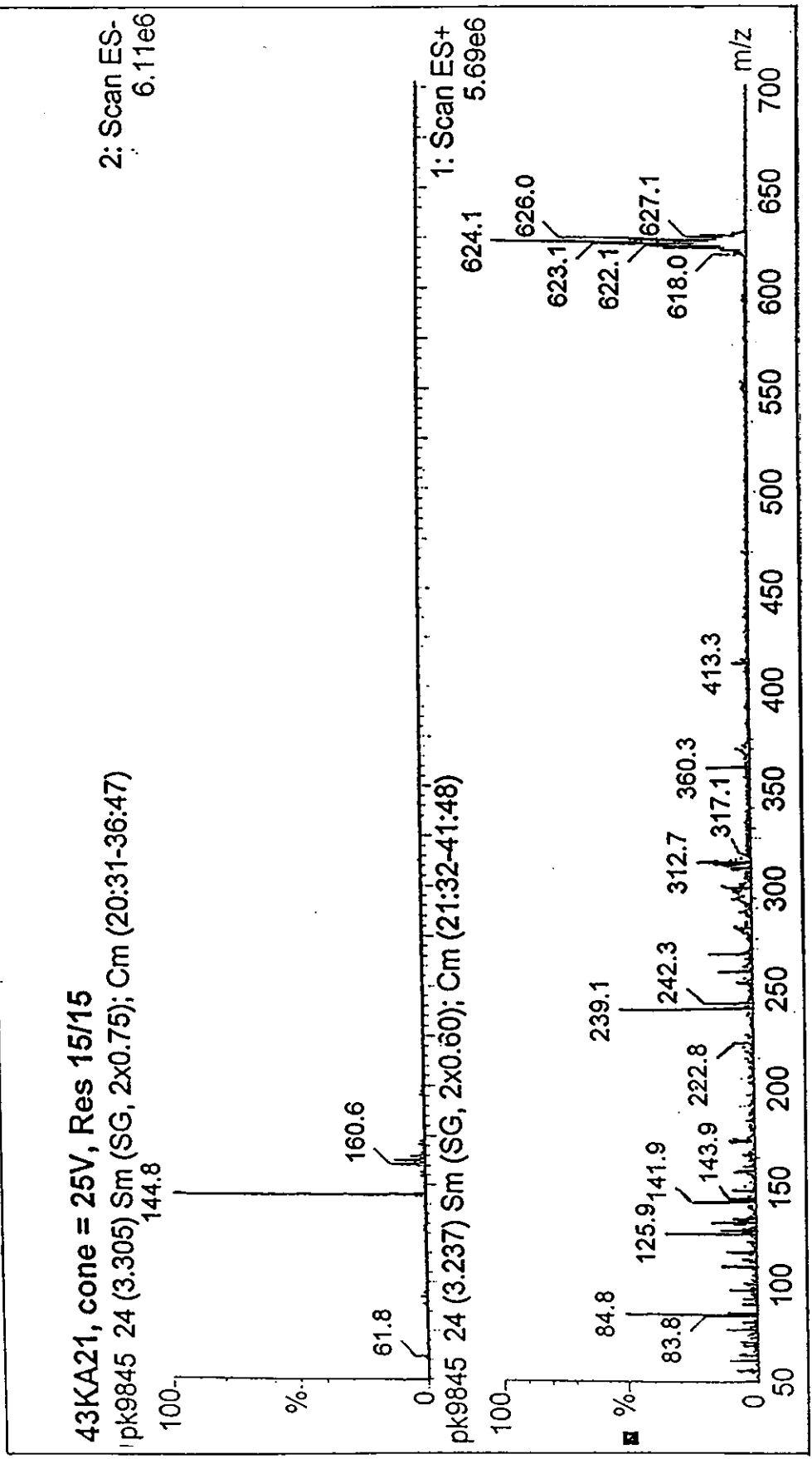

Figure 19 Electrospray mass spectrum of $[Ru(tpy)(deazpy)Cl]PF_6$ complex.

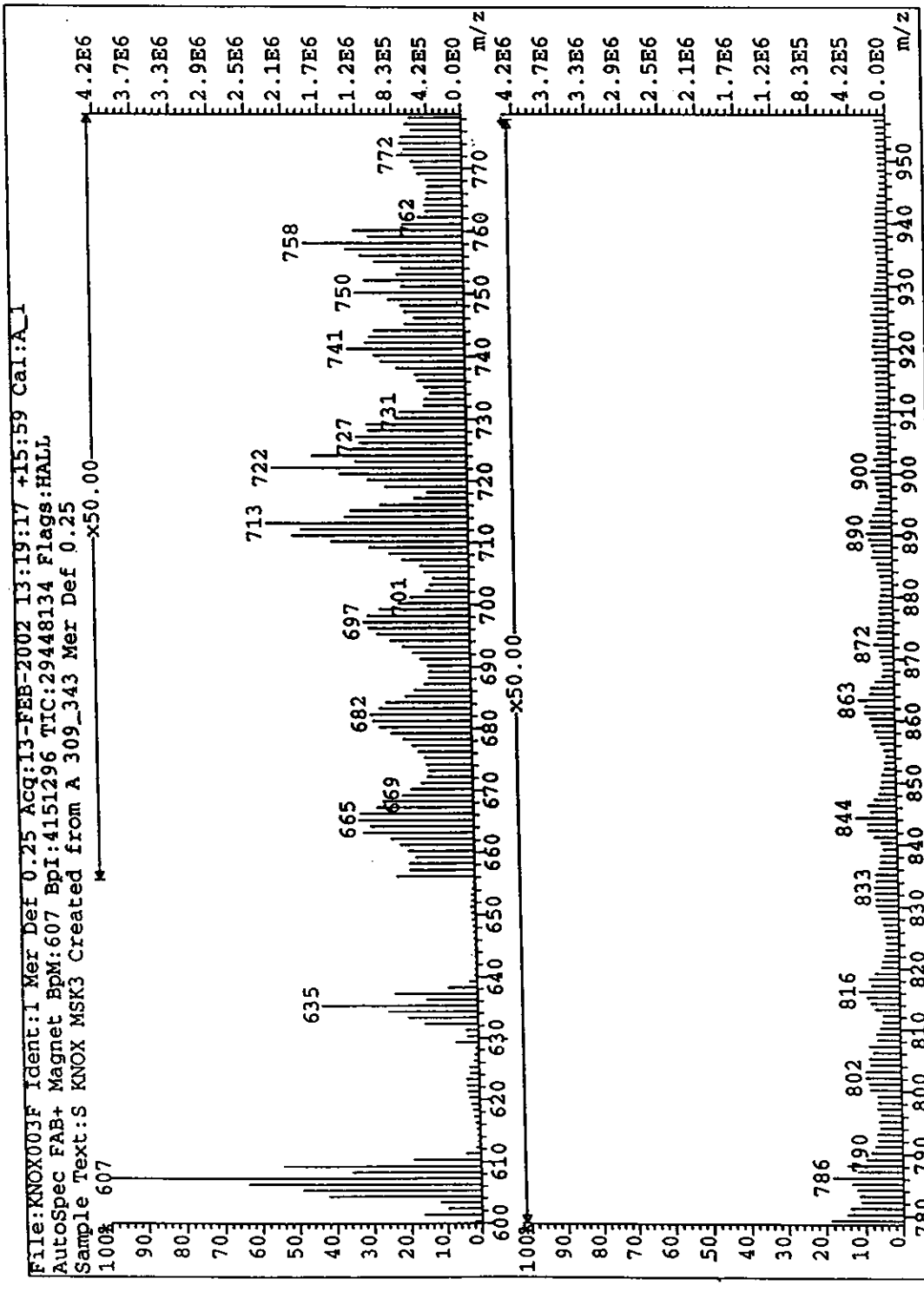

Figure 20 FAB mass spectrum of $[Ru(tpy)(deazpy)NO_2]PF_6$ complex.

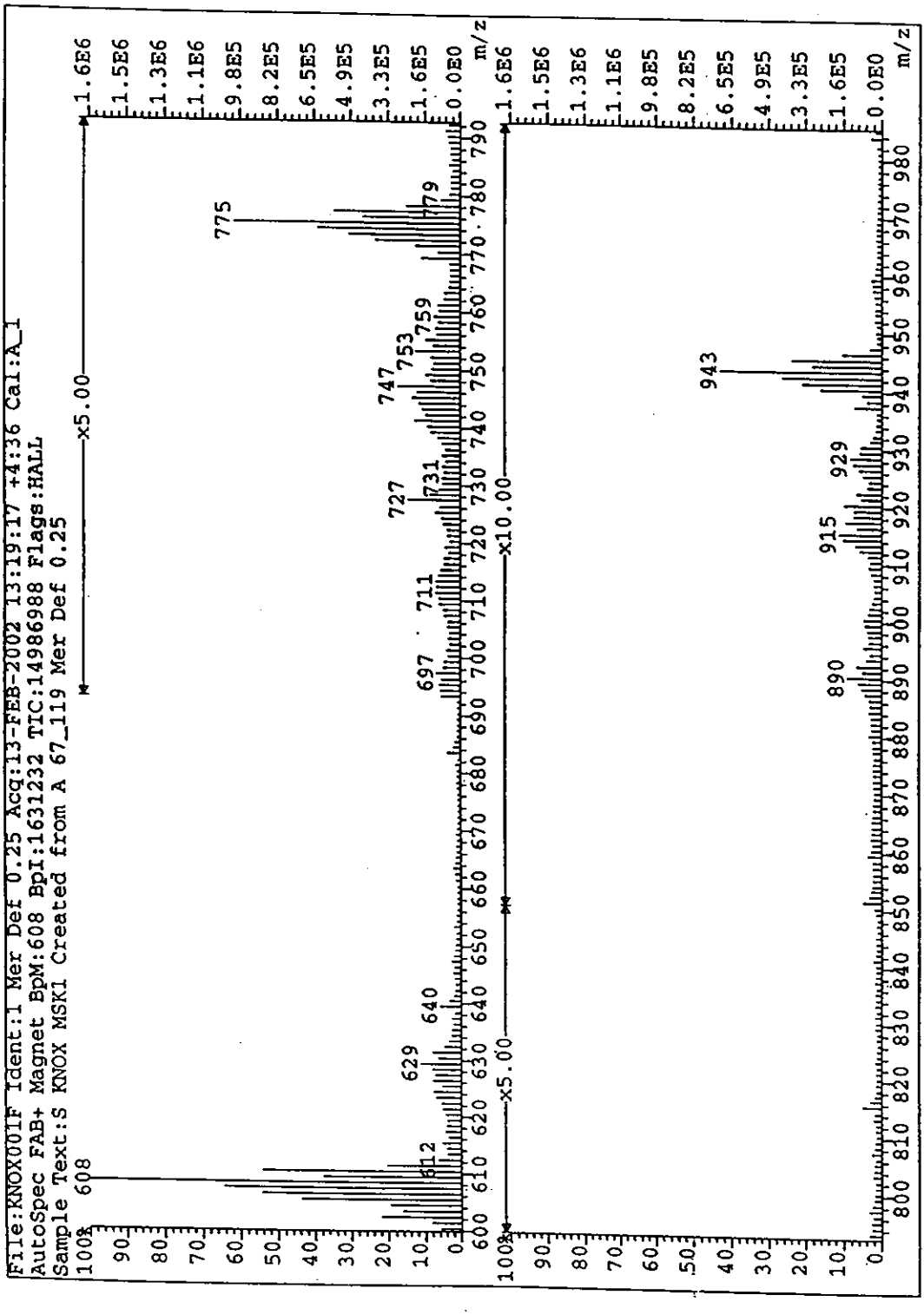

Figure 21 FAB mass spectrum of $[Ru(tpy)(deazpy)CH_3CN](PF_6)_2$ complex.

3.2.2.3. UV-Visible absorption spectroscopy

The UV-Visible absorption spectra of $[Ru(tpy)(dmazpy)X](PF_6)_n$ and $[Ru(tpy)(deazpy)X](PF_6)_n$ complexes , where X = Cl^-, NO_2^- and CH_3CN in acetonitrile solution are shown in Figure 22-27. Electronic spectra of [Ru(tpy)(dmazpy)X]$(PF_6)_n$ and $[Ru(tpy)(deazpy)X](PF_6)_n$ complexes , where X = Cl^-, NO_2^- and CH_3CN were recorded in six solvents; acetone, acetonitrile, ethanol, methanol, *N,N*-dimetylformamide (DMF), and dimethyl sulfoxide (DMSO) are listed in Table 22-23.

The absorption spectra of complexes were recorded in both ultraviolet (200-400 nm) and visible (400-800 nm) regions. The intense bands in UV region belonged to the electronic transition of dmazpy and tpy ligands. In the visible region, each complex exhibited intense two broad bands, which referred to metal-to-ligand charge transfer (MLCT).

Table 22 UV-Visible absorption spectroscopic data of $[Ru(tpy)(dmazpy)X](PF_6)_n$ complexes , where X = Cl^-, NO_2^- and CH_3CN in various solvents.

Solvent	λ_{max} nm, (ε x10^{-4} M^{-1} cm^{-1})		
	RudmCl	RudmNO_2	RudmCH_3CN
Acetone	500(1.53), 574(1.54)	506(1.57), 572(1.26)	496(1.38), 572(1.34)
Acetonitrile	274(2.90), 312(2.73)	272(2.37), 302(2.30)	272(1.90), 298(1.96)
	498(2.37), 570(1.42)	504(1.67), 572(1.22)	494(1.33), 568(1.26)
Ethanol	274(2.44), 312(2.36)	272(2.36), 302(2.39)	274(1.54), 300(1.62)
	498(2.11), 574(1.33)	506(1.77), 576(1.38)	498(1.10), 578(1.12)
Methanol	274(2.99), 312(2.81)	272(2.61), 300(2.50)	272(1.17), 300(1.13)
	500(2.46), 572(1.51)	502(1.79), 574(1.38)	498(1.31), 576(1.23)
DMF	276(2.37), 316(2.29)	274(2.98), 302(2.70)	286(3.02), 322(1.99)
	504(1.94), 576(1.18)	510(1.72), 578(1.22)	500(2.01), 576(1.82)
DMSO	276(4.38), 316(4.06)	276(6.25), 306(6.16)	288(2.24), 334(1.52)
	506(2.75), 580(1.34)	510(4.16), 582(3.21)	502(1.44), 578(1.39)

RudmCl = $[Ru(tpy)(dmazpy)Cl]PF_6$

RudmNO_2 = $[Ru(tpy)(dmazpy)NO_2]PF_6$

RudmCH_3CN = $[Ru(tpy)(dmazpy)CH_3CN](PF_6)_2$

Table 23 UV-Visible absorption spectroscopic data of $[Ru(tpy)(deazpy)X](PF_6)_n$ complexes , where X = Cl^-, NO_2^- and CH_3CN in various solvents.

Solvent	λ_{max} nm, (ε x10^{-4} M^{-1} cm^{-1})		
	RudeCl	RudeNO_2	RudeCH_3CN
Acetone	504(2.94), 582(1.89)	508(2.22), 584(1.98)	496(1.84), 574(1.60)
Acetonitrile	274(3.08), 312(3.04)	272(2.69), 302(2.80)	272(2.57), 298(2.67)
	502(2.72), 582(1.78)	506(2.17), 582(1.79)	496(1.88), 572(1.60)
Ethanol	274(2.97), 312(2.88)	272(3.28), 302(3.45)	272(2.50), 300(2.61)
	502(2.62), 584(1.75)	508(2.68), 586(2.37)	498(1.84), 578(1.66)
Methanol	274(3.14), 312(3.13)	272(3.68), 300(3.49)	274(2.53), 300(2.34)
	502(2.78), 582(1.77)	506(2.53), 582(2.23)	500(1.79), 578(1.33)
DMF	276(3.74), 314(3.48)	274(1.45), 304(1.45)	274(2.89), 286(2.92)
	506(3.07), 584(1.77)	512(1.05), 586(0.88)	500(1.82), 578(1.59)
DMSO	276(3.64), 316(3.57)	276(3.73), 306(3.75)	290(3.28), 334(2.31)
	508(3.12), 584(2.12)	512(2.89), 584(2.45)	502(2.34), 582(2.15)

RudeCl = $[Ru(tpy)(deazpy)Cl]PF_6$

RudeNO_2 = $[Ru(tpy)(deazpy)NO_2]PF_6$

RudeCH_3CN = $[Ru(tpy)(deazpy)\ CH_3CN](PF_6)_2$

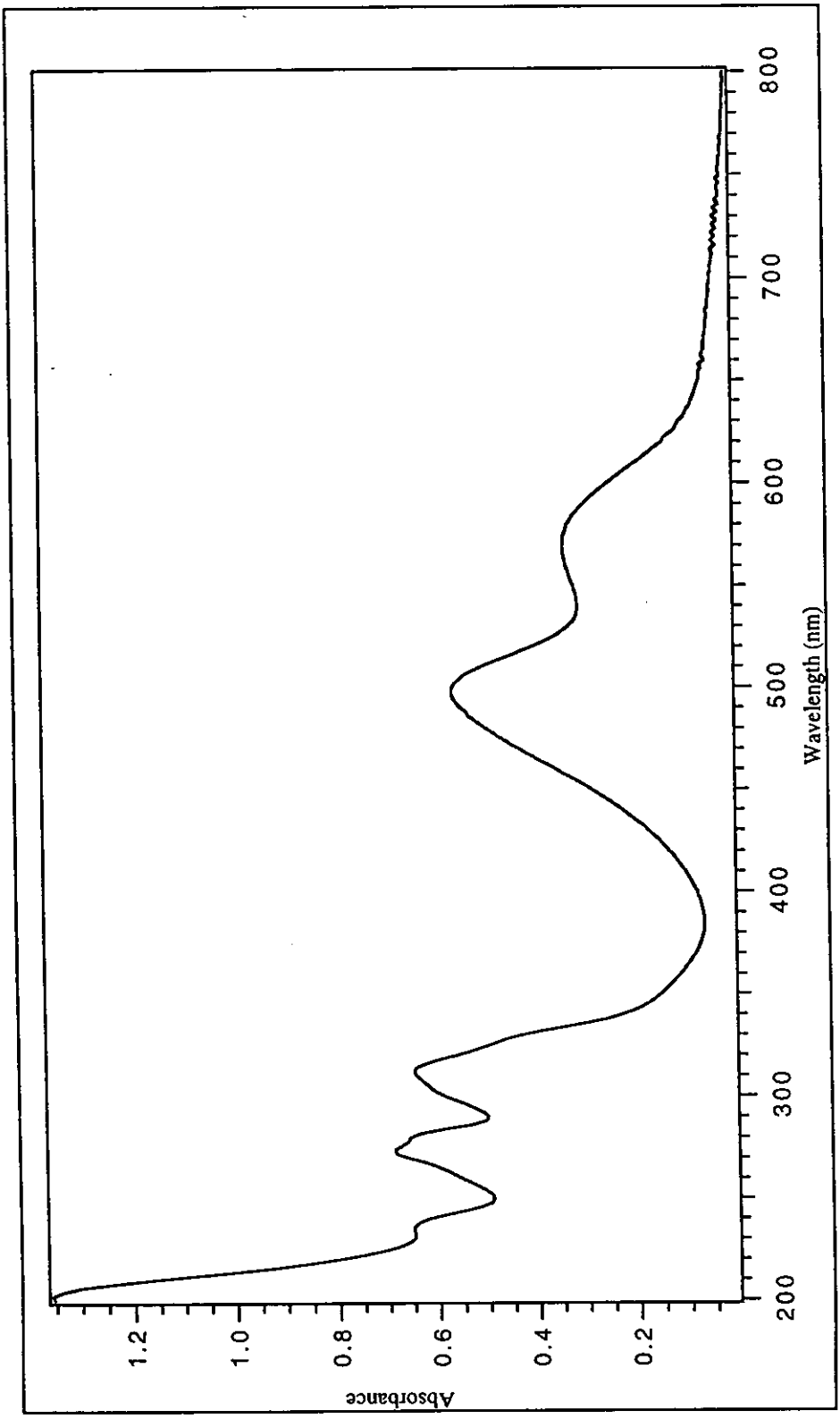

Figure 22 UV-Visible absorption spectrum of $[Ru(tpy)(dmazpy)Cl]PF_6$ in acetonitrile.

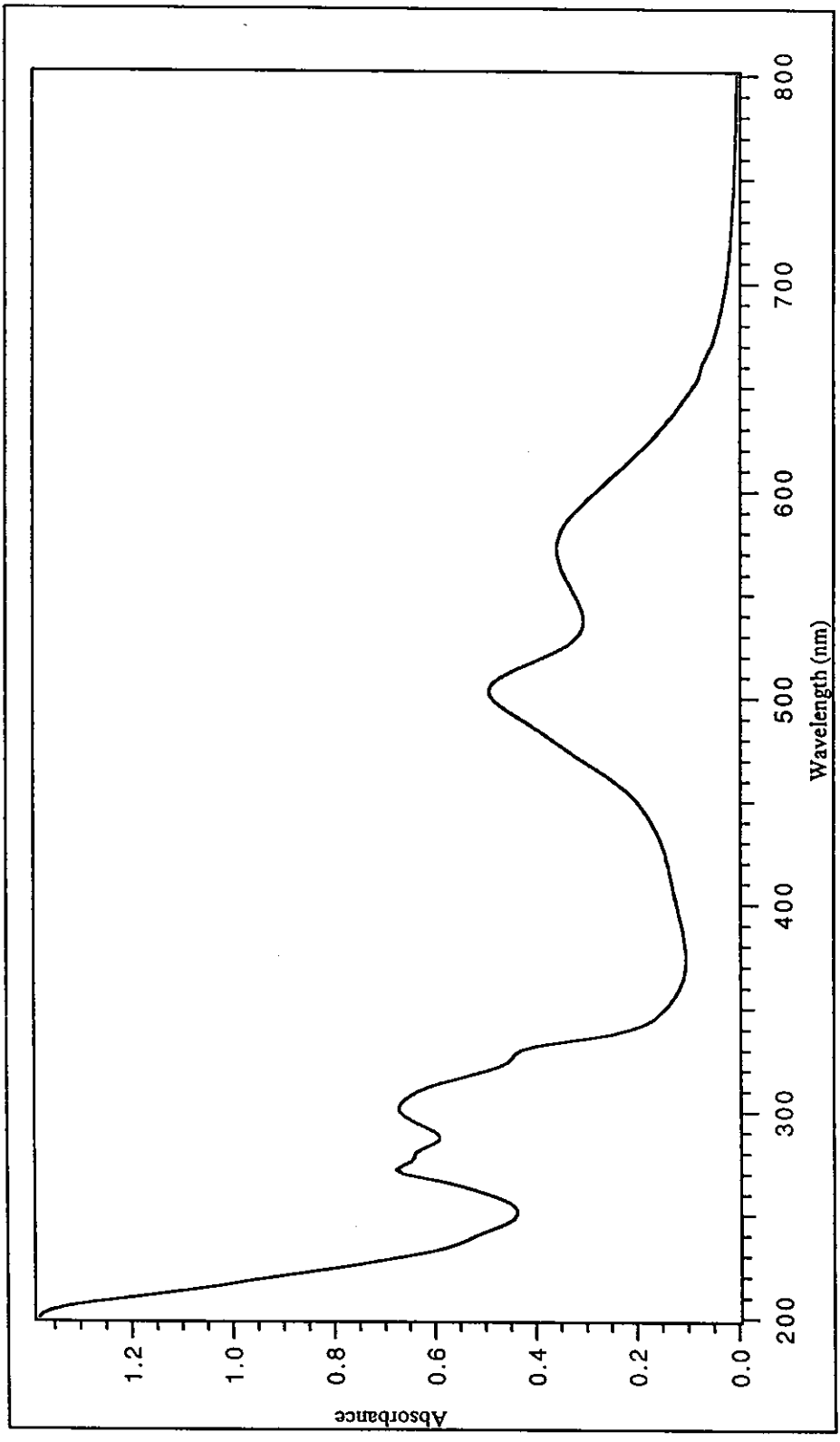

Figure 23 UV-Visible absorption spectrum of $[Ru(tpy)(dmazpy)NO_2]PF_6$ in acetonitrile.

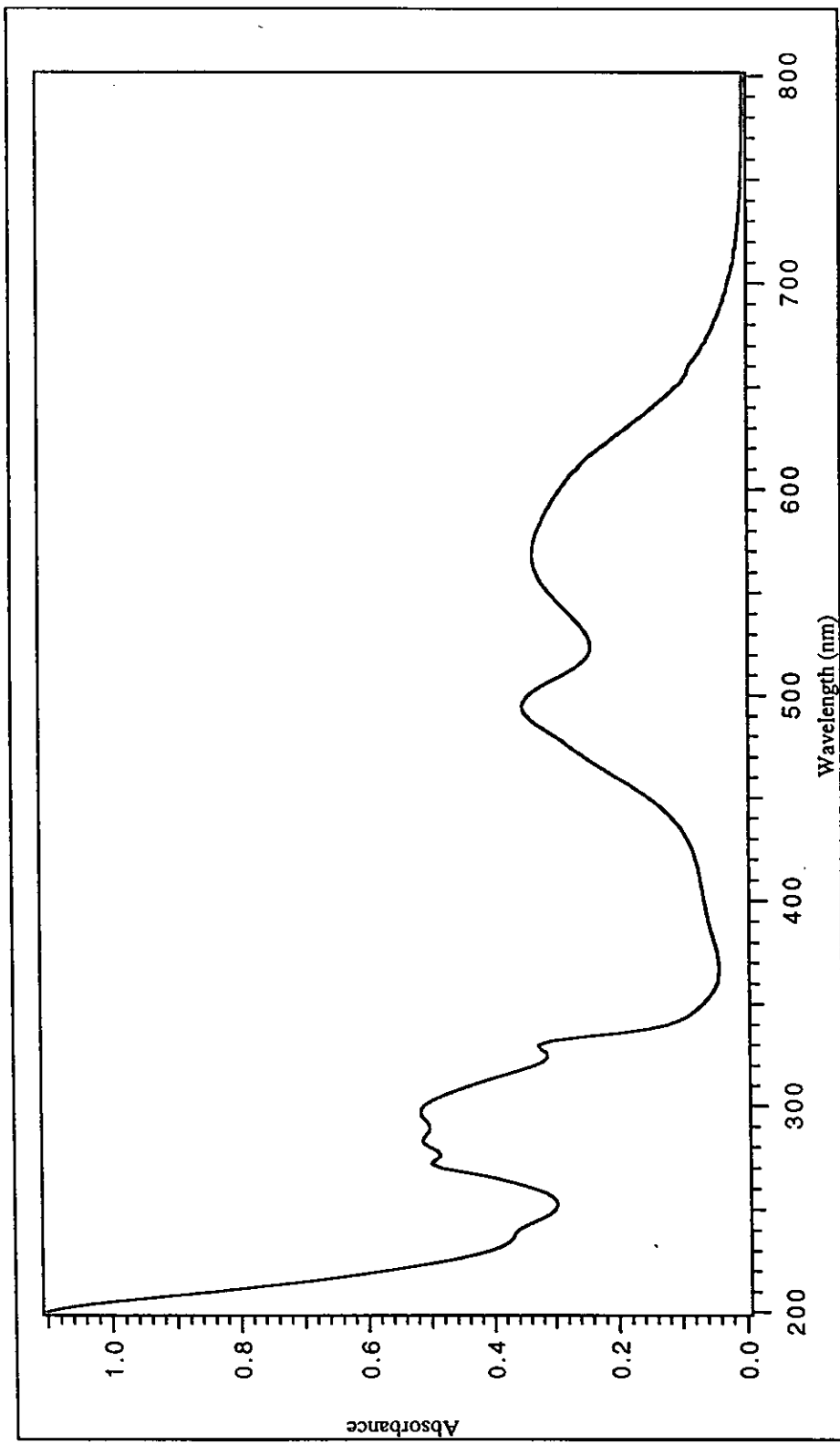

Figure 24 UV-Visible absorption spectrum of $[Ru(tpy)(dmazpy)CH_3CN](PF_6)_2$ in acetonitrile.

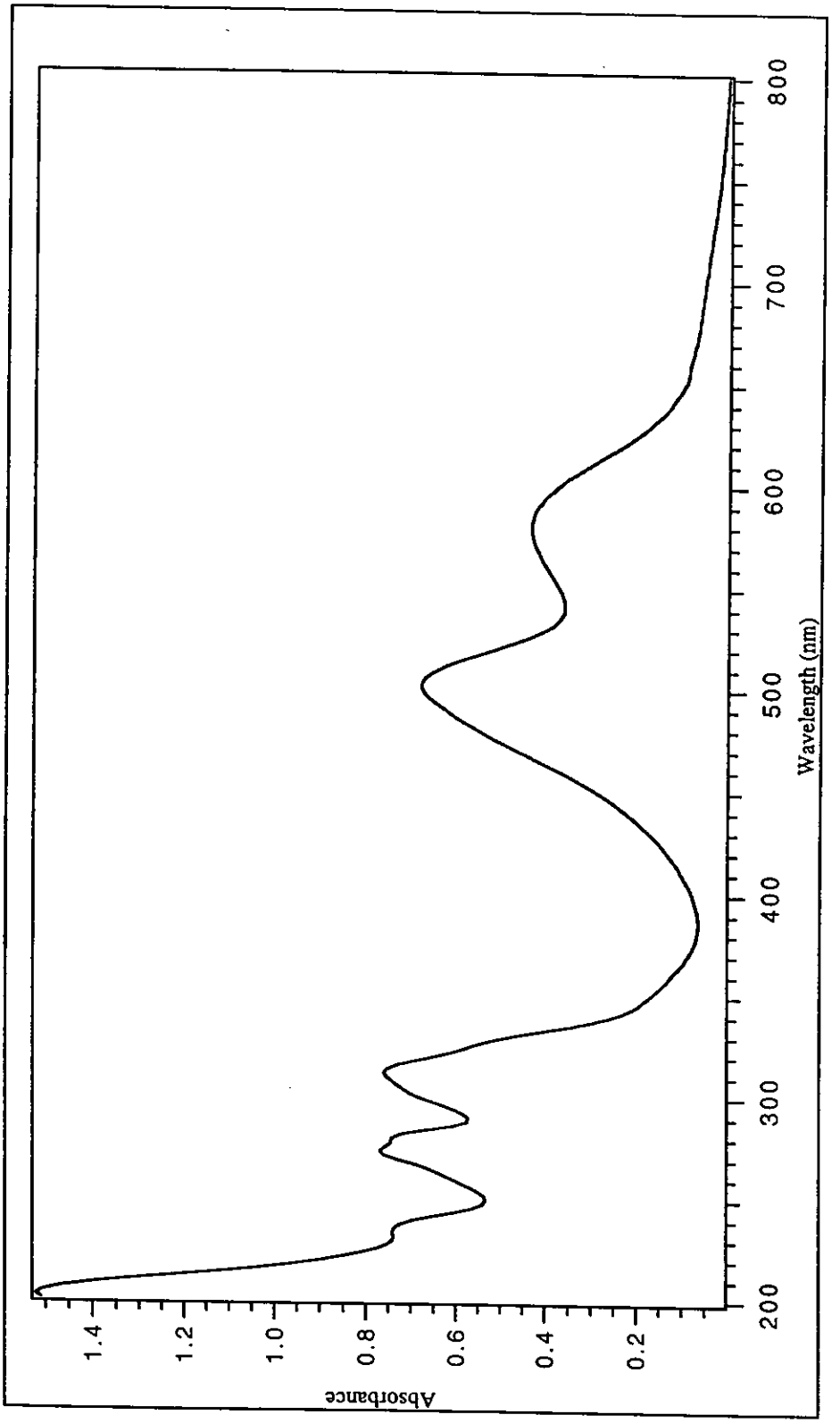

Figure 25 UV-Visible absorption spectrum of [Ru(tpy)(deazpy)Cl]PF_6 in acetonitrile.

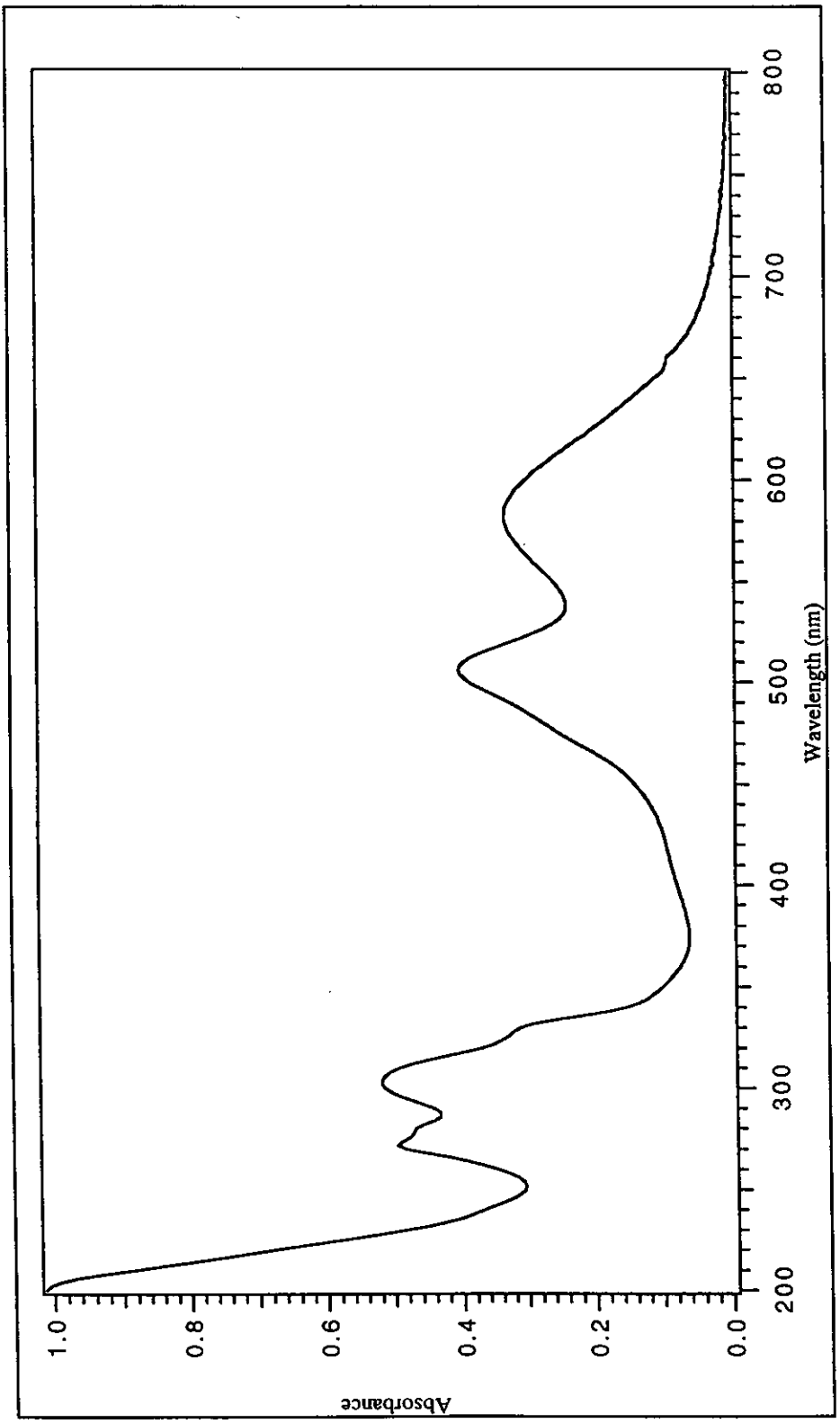

Figure 26 UV-Visible absorption spectrum of $[Ru(tpy)(deazpy)NO_2]PF_6$ in acetonitrile.

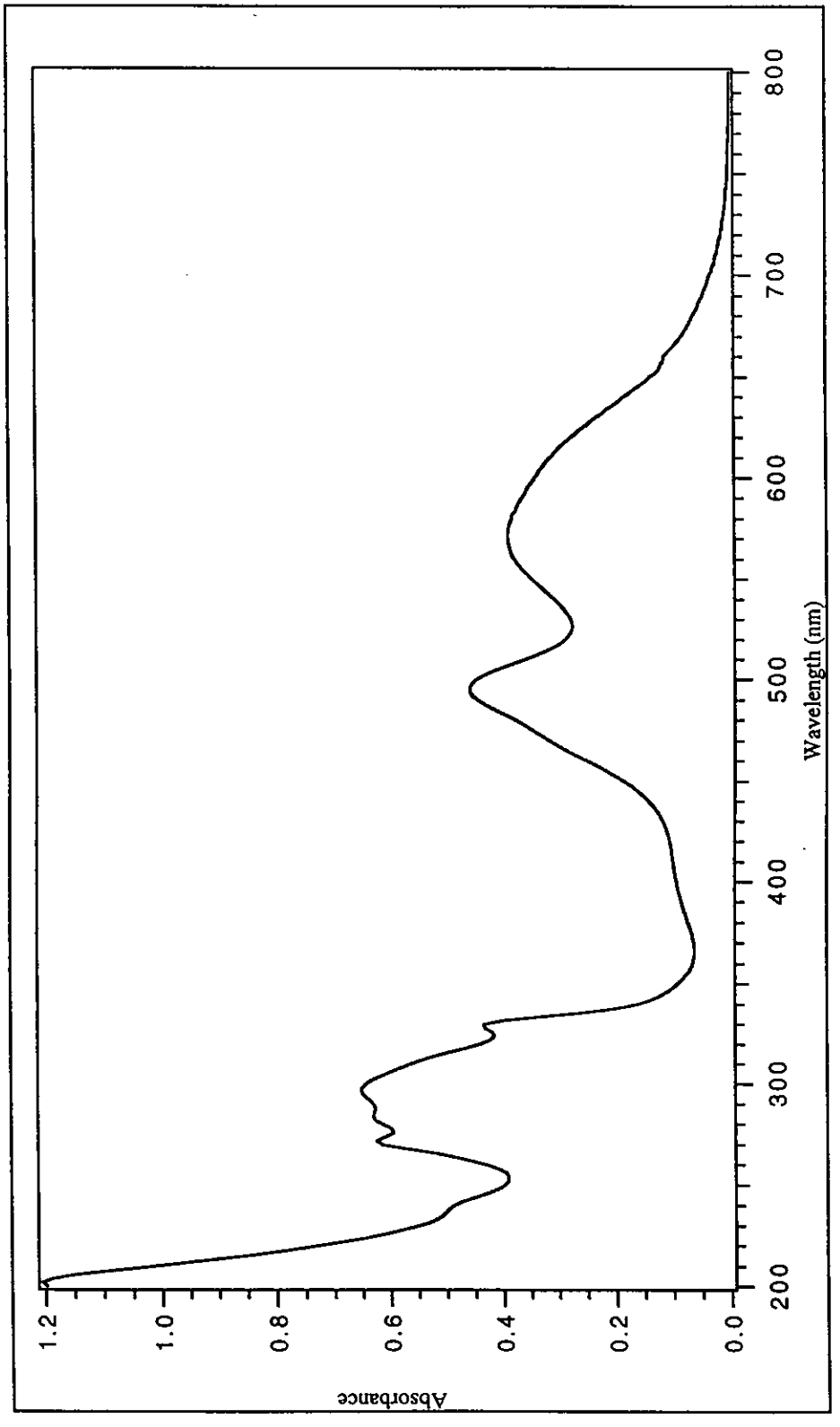

Figure 27 UV-Visible absorption spectrum of $[Ru(tpy)(deazpy)CH_3CN](PF_6)_2$ in acetonitrile.

3.2.2.4. Infrared spectroscopy

Vibrational spectra in the region 4000-370 cm^{-1}, could be used to give information about ligands coordinated to the ruthenium center. Infrared spectroscopic data of $[Ru(tpy)(dmazpy)X](PF_6)_n$ and $[Ru(tpy)(deazpy)X](PF_6)_n$, where $X = Cl^-$, NO_2^- and CH_3CN, were important in the range 1600-500 cm^{-1}. The infrared spectra of complexes are shown in Figure 28-33. The summaries of the infrared spectroscopic data were listed in Table 24 and 25.

Table 24 Infrared spectroscopic data of $[Ru(tpy)(dmazpy)X](PF_6)_n$, where $X = Cl^-$, NO_2^- and CH_3CN.

Vibration modes	Frequencies (cm^{-1})		
	RudmCl	$RudmNO_2$	$RudmCH_3CN$
C=N	1597	1596	1596
C=C	1450	1449	1450
N=N	1294	1355	1294
C-H bending of para disubstituted benzene	773	773	773
NO_2 asymmetric stretching	-	1380	-
NO_2 symmetric stretching	-	1245	-

RudmCl = $[Ru(tpy)(dmazpy)Cl]PF_6$

$RudmNO_2$ = $[Ru(tpy)(dmazpy)NO_2]PF_6$

$RudmCH_3CN$ = $[Ru(tpy)(dmazpy)\ CH_3CN](PF_6)_2$

Table 25 Infrared spectroscopic data of $[Ru(tpy)(deazpy)X](PF_6)_n$, where X = Cl^-, NO_2^- and CH_3CN.

Vibration modes	Frequencies (cm^{-1})		
	RudeCl	$RudeNO_2$	$RudeCH_3CN$
C=N	1598	1595	1592
C=C	1450	1451	1451
N=N	1293	1359	1300
C-H bending of para disubstituted benzene	773	788	772
NO_2 asymmetric stretching	-	1384	-
NO_2 symmetric stretching	-	1272	-

RudeCl = $[Ru(tpy)(deazpy)Cl]PF_6$

$RudeNO_2$ = $[Ru(tpy)(deazpy)NO_2]PF_6$

$RudeCH_3CN$ = $[Ru(tpy)(deazpy)\ CH_3CN](PF_6)_2$

In general, characteristic peaks of all complexes were sharp peak of C=N stretching modes which were observed at frequencies in the range 1600-1550 cm^{-1}. The N=N (azo) stretching modes in complexes occurred in the spectral region 1360-1280 cm^{-1}. The N=N stretching frequency of each complexes were not similar. The N=N stretching modes in complexes were shifted to lower frequency from free ligands.

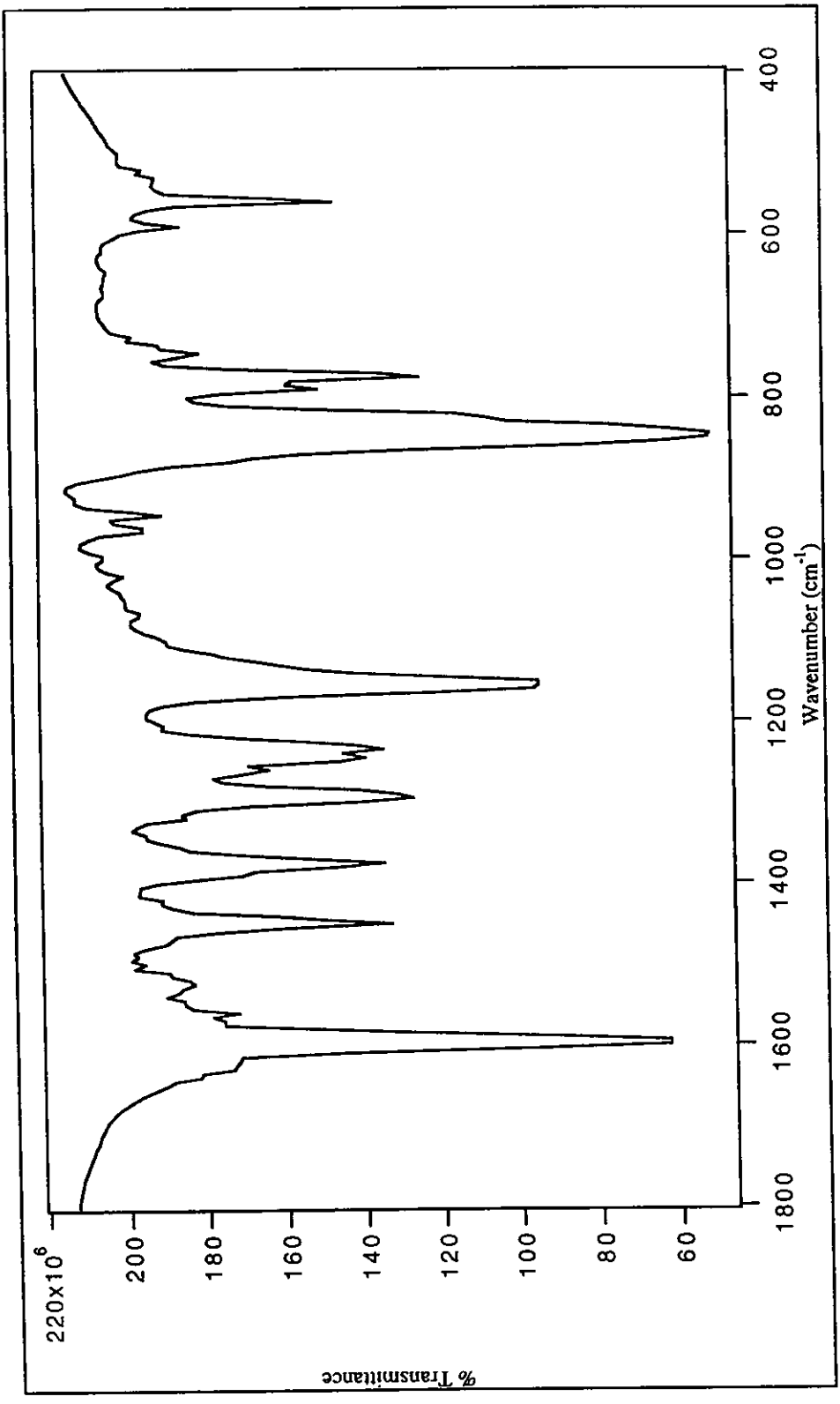

Figure 28 IR spectrum of $[Ru(tpy)(dmazpy)Cl]PF_6$ complex.

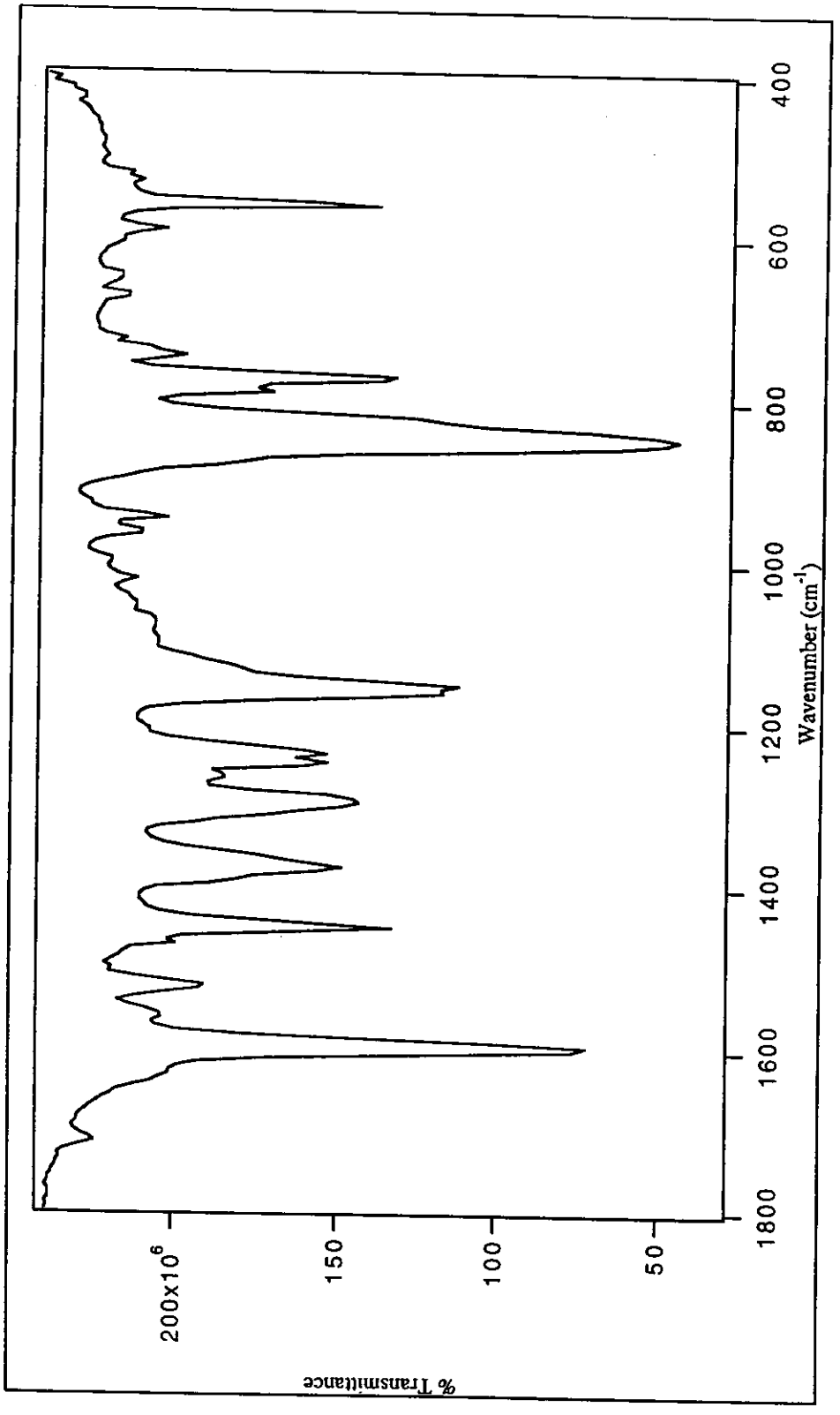

Figure 29 IR spectrum of $[Ru(tpy)(dmazpy)NO_2]PF_6$ complex.

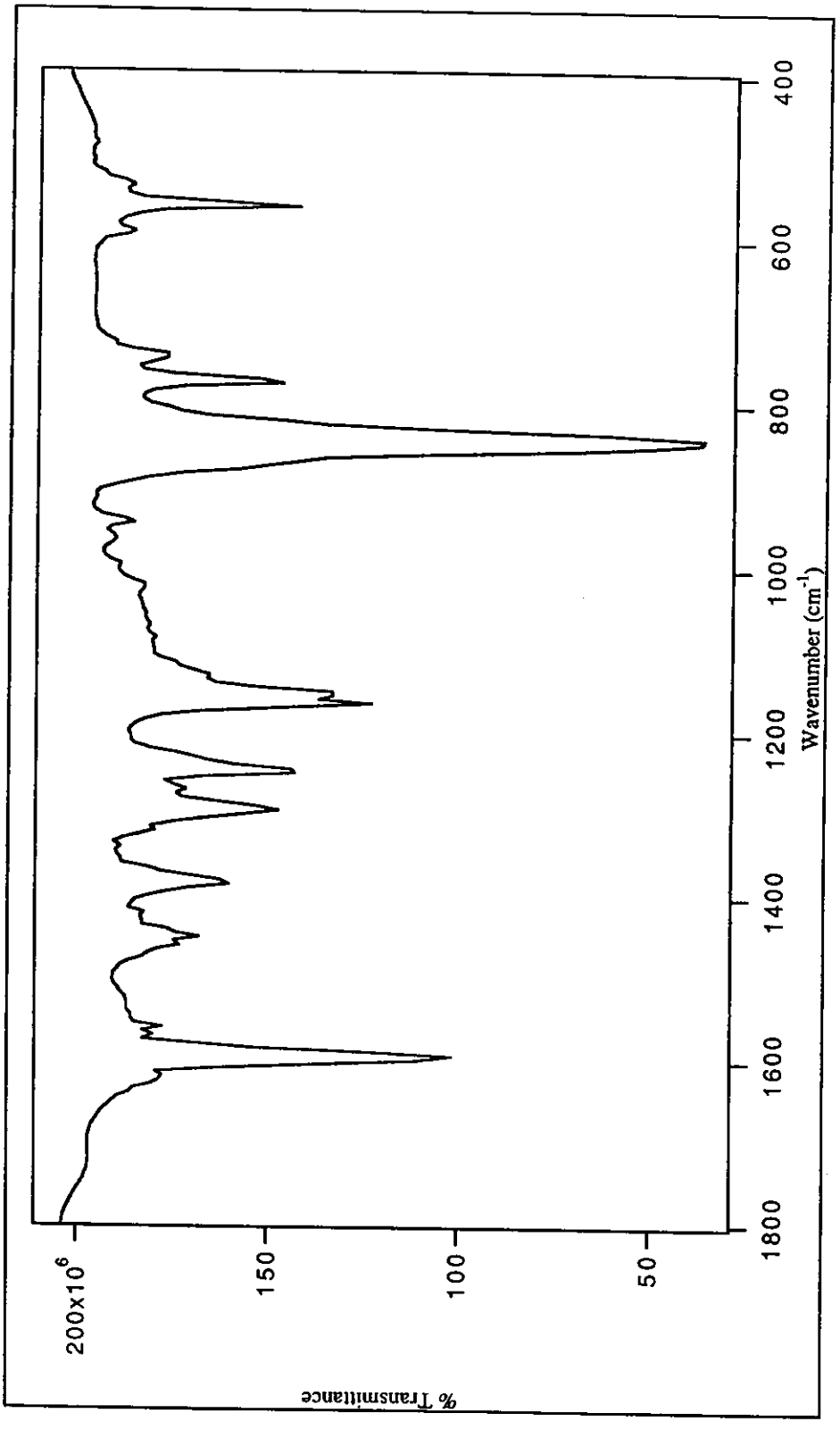

Figure 30 IR spectrum of $[Ru(tpy)(dmazpy)CH_3CN](PF_6)_2$ complex.

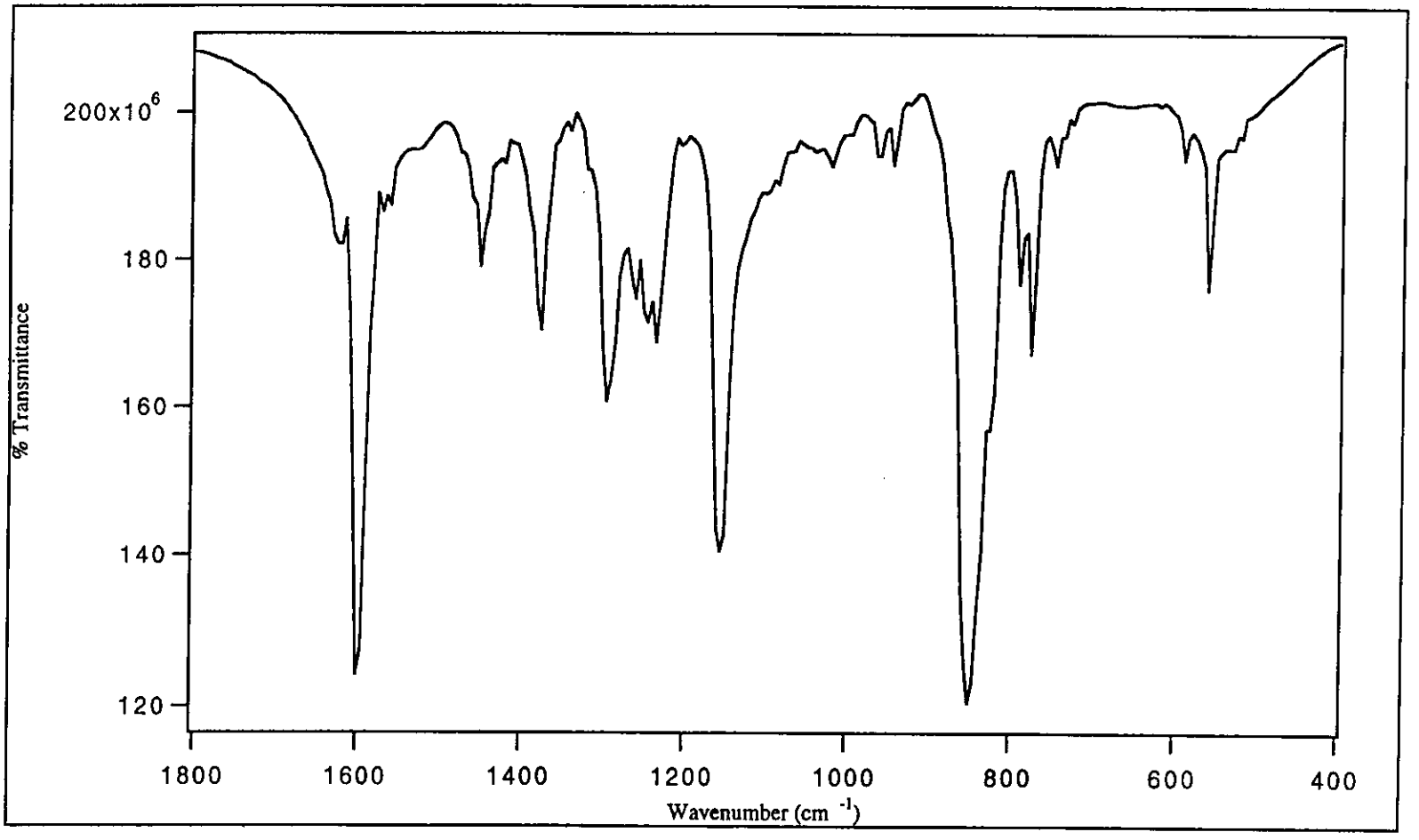

Figure 31 IR spectrum of $[Ru(tpy)(deazpy)CH_3CN](PF_6)_2$ complex.

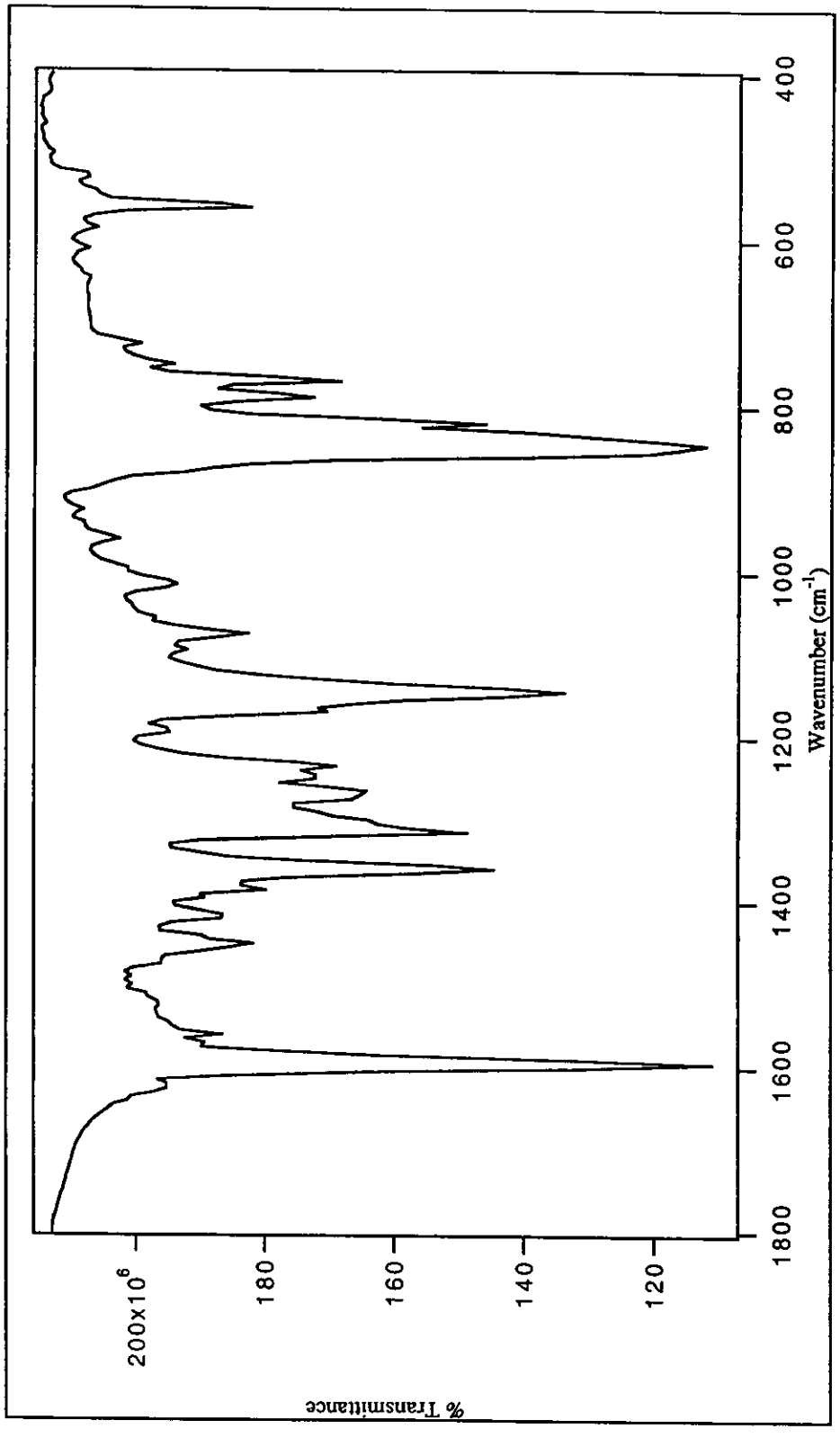

Figure 32 IR spectrum of $[Ru(tpy)(deazpy)NO_2]PF_6$ complex.

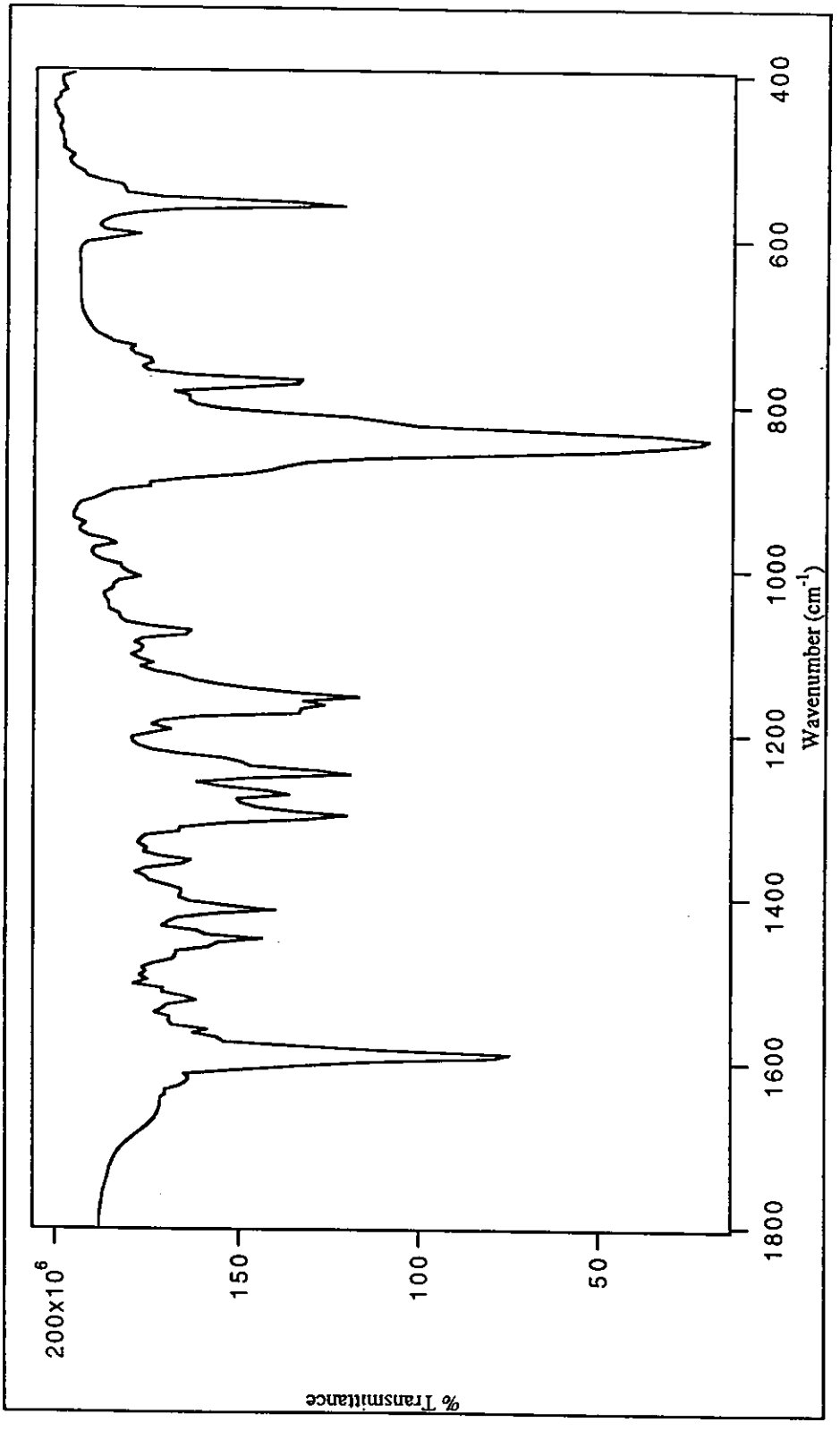

Figure 33 IR spectrum of $[Ru(tpy)(deapy)CH_3CN]PF_6$ complex.

3.2.2.5. Nuclear Magnetic resonance spectroscopy

^{1}H NMR spectroscopy is an important technique to determine molecular structure because the different protons in the molecular structure will show the different chemical shifts. Furthermore, ^{1}H NMR spectra exhibit the total number of protons in each complex, and their chemical shifts are related to their position in complexes. The ^{1}H NMR spectra of $[Ru(tpy)(dmazpy)X](PF_6)_n$ and $[Ru(tpy)(deazpy)X](PF_6)_n$, where X = Cl^-, and NO_2^-, H_2O, CH_3CN were recorded in d_6-DMSO. The ^{1}H NMR spectra of complexes are displayed in Figure 34-41. The ^{1}H NMR spectroscopic data of these complexes are given in Table 26 and 27.

Table 26 ^{1}H NMR spectroscopic data of $[Ru(tpy)(dmazpy)X](PF_6)_n$, where X = Cl^-, NO_2^-, H_2O and CH_3CN.

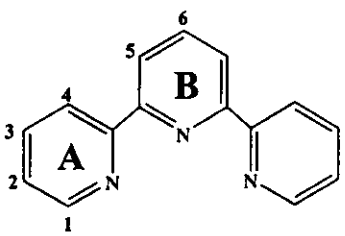

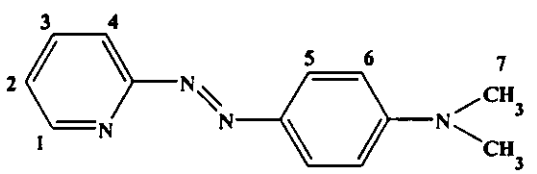

Proton	Number of protons	Chemical Shift, ppm			
		RudmCl	$RudmNO_2$	$RudmH_2O$	$RudmCH_3CN$
1	1	9.80(d)	9.48(d)	9.80(d)	9.64(d)
1A	2	8.71(m)	8.74(d)	8.70(m)	8.88(d)
4	1		8.70(m)		8.82(d)
5B	2	8.62(d)	8.61(d)	8.61(d)	8.76(d)
2	1	8.36(t)	8.40(t)	8.36(ddd)	8.50(m)
6B	1	8.28(t)	8.36(t)	8.29(t)	

Proton	Number of protons	Chemical Shift, ppm			
		RudmCl	$RudmNO_2$	$RudmH_2O$	$RudmCH_3CN$
2A	2	8.09(t)	8.12(t)	8.10(ddd)	8.22(ddd)
3	1	8.04(t)	8.0(t)	8.04(t)	8.06(t)
3A	2	7.47(t)	7.50(t)	7.47(t)	7.57(t)
4A	2	7.27(d)	7.35(d)	7.27(dd)	7.49(d)
5	2	6.62(d)	6.67(d)	6.62(d)	6.59(d)
6	2	6.28(d)	6.31(d)	6.28(d)	6.32(d)
7	6	2.87(s)	2.92(s)	2.87(s)	2.92(s)
CH_3CN	-	-	-	-	2.37(s)

RudmCl = $[Ru(tpy)(dmazpy)Cl]PF_6$

$RudmNO_2$ = $[Ru(tpy)(dmazpy)NO_2]PF_6$

$RudmH_2O$ = $[Ru(tpy)(dmazpy)H_2O](PF_6)_2$

$RudmCH_3CN$ = $[Ru(tpy)(dmazpy)CH_3CN](PF_6)_2$

^1H NMR spectra of $[Ru(tpy)(dmazpy)X](PF_6)_n$, where X = Cl^-, NO_2^-, H_2O and CH_3CN, showed many sharp resonances. In total thirteen resonances were expected for twenty-five hydrogens present in these complexes. There were seven signals for fourteen hydrogens of dmazpy ligand and only six signals for eleven hydrogens of tpy ligand, because a plane of symmetry splits the tpy ligand into two equal halves. ^1H NMR spectrum of $[Ru(tpy)(dmazpy)CH_3CN](PF_6)_2$ displayed fourteen resonances which referred to twenty-eight hydrogens. The hydrogens of acetonitrile showed a singlet peak.

Table 27 ^{1}H NMR spectroscopic data of $[Ru(tpy)(deazpy)X](PF_6)_n$, where X = Cl^-, NO_2^- and CH_3CN.

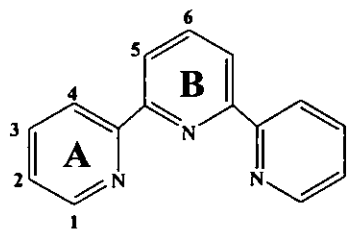

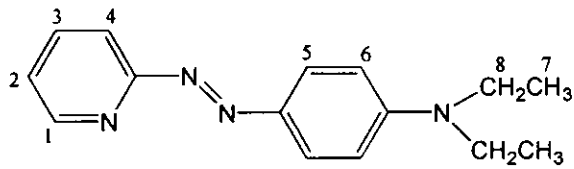

Proton	Number of protons	Chemical Shift, ppm			
		RudeCl	$RudeNO_2$	$RudmH_2O$	$RudeCH_3CN$
1	1	9.80(d)	9.46(d)	9.80(d)	9.63d)
1A	2	8.72(d)	8.73(d)	8.69(m)	8.88(d)
4	1	8.67(d)	8.68(d)		8.84(d)
5B	2	8.62(d)	8.62(d)	8.60(d)	8.77(d)
2	1	8.35(t)	8.48(m)	8.36(t)	8.51(t)
6B	1	8.28(t)		8.29(t)	8.27(ddd)
2A	2	8.07(ddd)	8.13(ddd)	8.10(ddd)	8.22(ddd)
3	1	8.15(t)	7.98(t)	8.02(t)	8.05(t)
3A	2	7.46(t)	7.51(t)	7.47(t)	7.57(t)
4A	2	7.27(d)	7.45(d)	7.28(d)	7.49(d)
5	2	6.62(d)	6.69(d)	6.63(d)	6.58(d)
6	2	6.26(d)	6.29(d)	6.27(d)	6.31(d)
8	4	3.27(q)	3.30(q)	3.27(q)	3.31(q)
7	6	1.00(t)	1.01(t)	1.00(t)	1.00(t)
CH_3CN	-	-	-	-	2.36(s)

RudeCl = $[Ru(tpy)(deazpy)Cl]PF_6$

$RudeNO_2$ = $[Ru(tpy)(deazpy)NO_2]PF_6$

$RudeH_2O$ = $[Ru(tpy)(deazpy)H_2O](PF_6)_2$

$RudeCH_3CN$ = $[Ru(tpy)(deazpy)CH_3CN](PF_6)_2$

^1H NMR spectra of $[Ru(tpy)(deazpy)X](PF_6)_n$, where X = Cl^-, NO_2^-, H_2O and CH_3CN, were slightly different from those of $[Ru(tpy)(dmazpy)X](PF_6)_n$. But the signals of the ethyl group were shown clearly.

Results from Table 26 and 27 showed that the proton H1 of pyridine ring in all complexes occurred at downfield chemical shift as doublet.

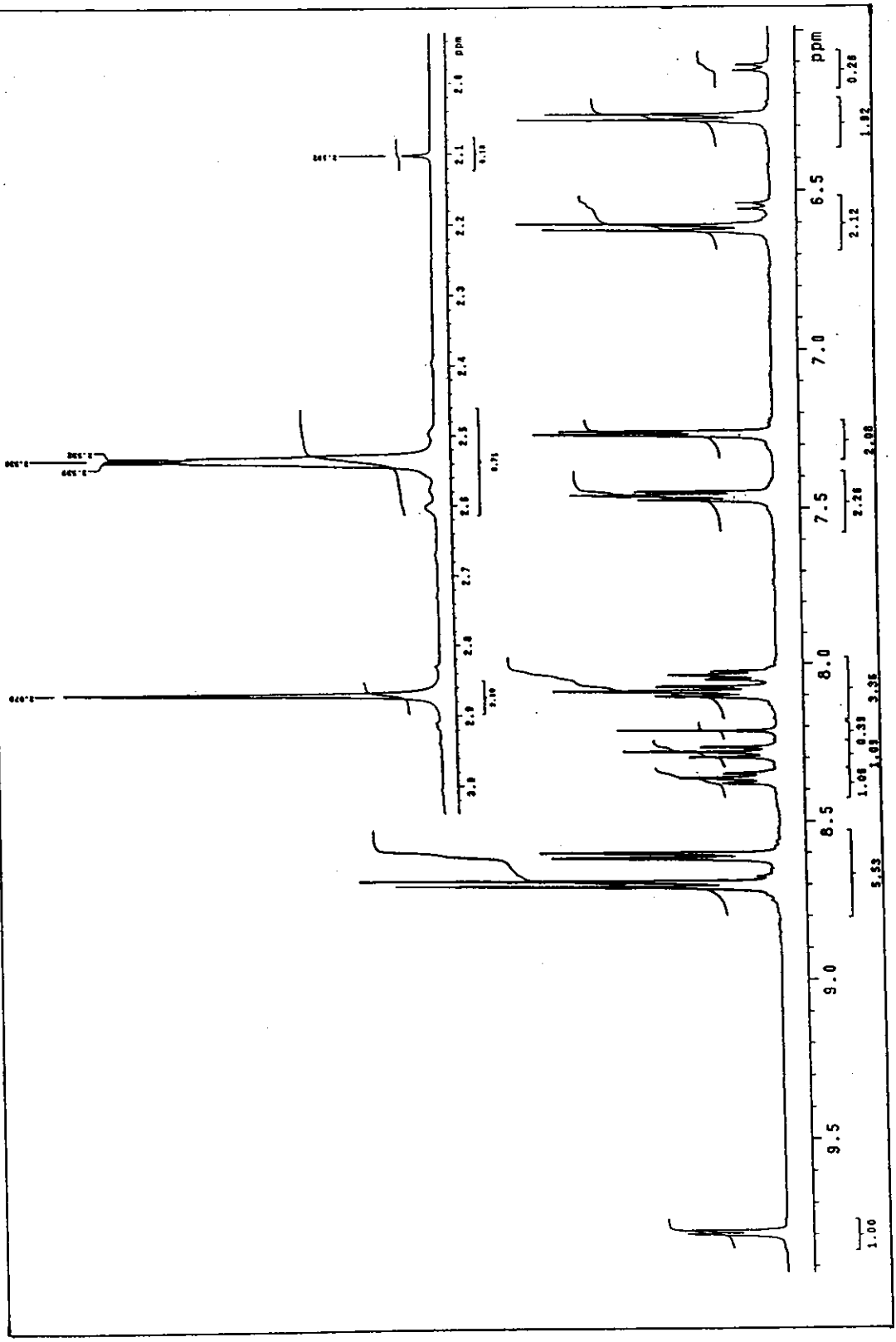

Figure 34 ^{1}H NMR spectrum of [Ru(tpy)(dmazpy)Cl]PF_6 complex.

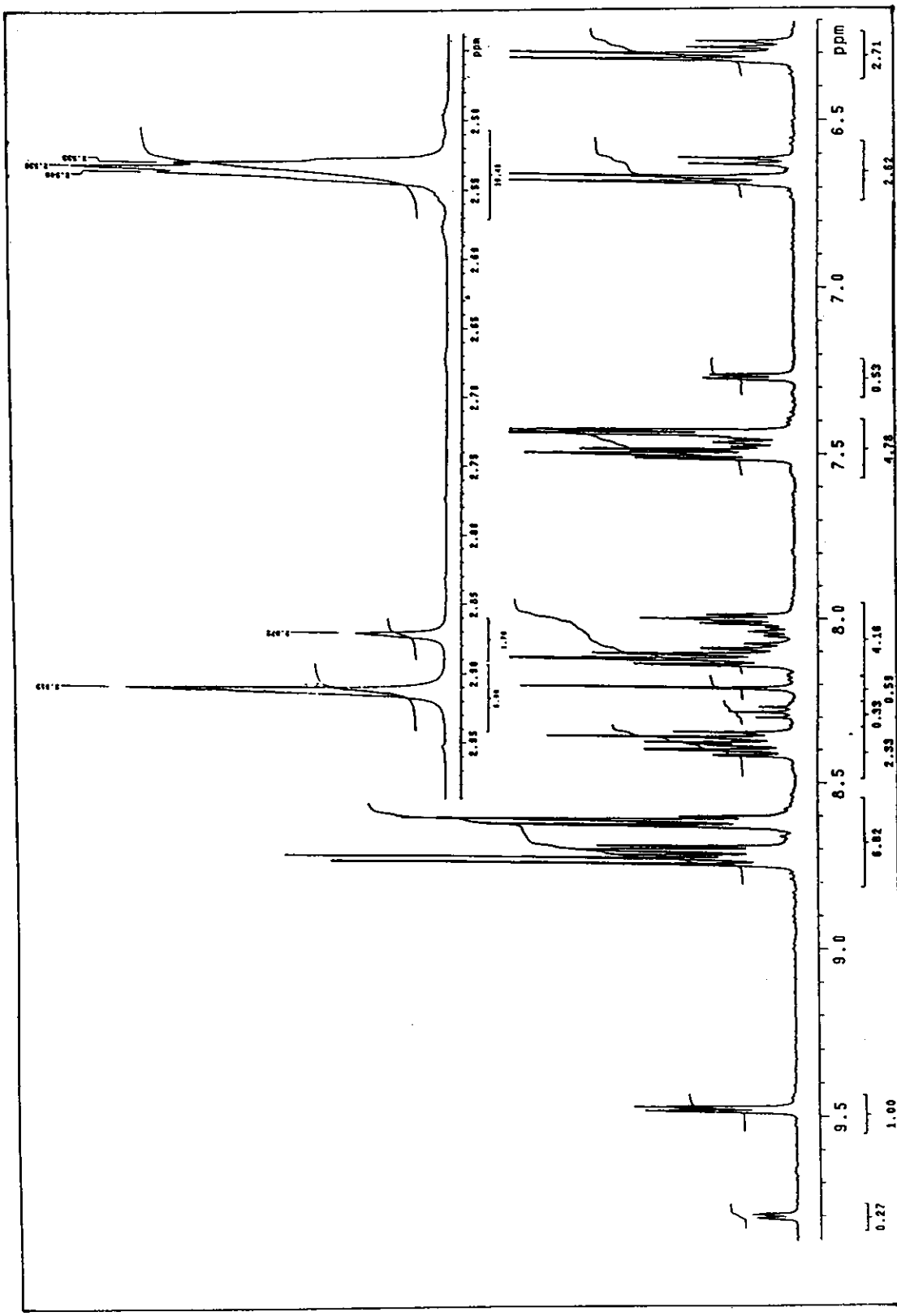

Figure 35 ^{1}H NMR spectrum of [Ru(tpy)(dmazpy)NO_2]PF_6 complex.

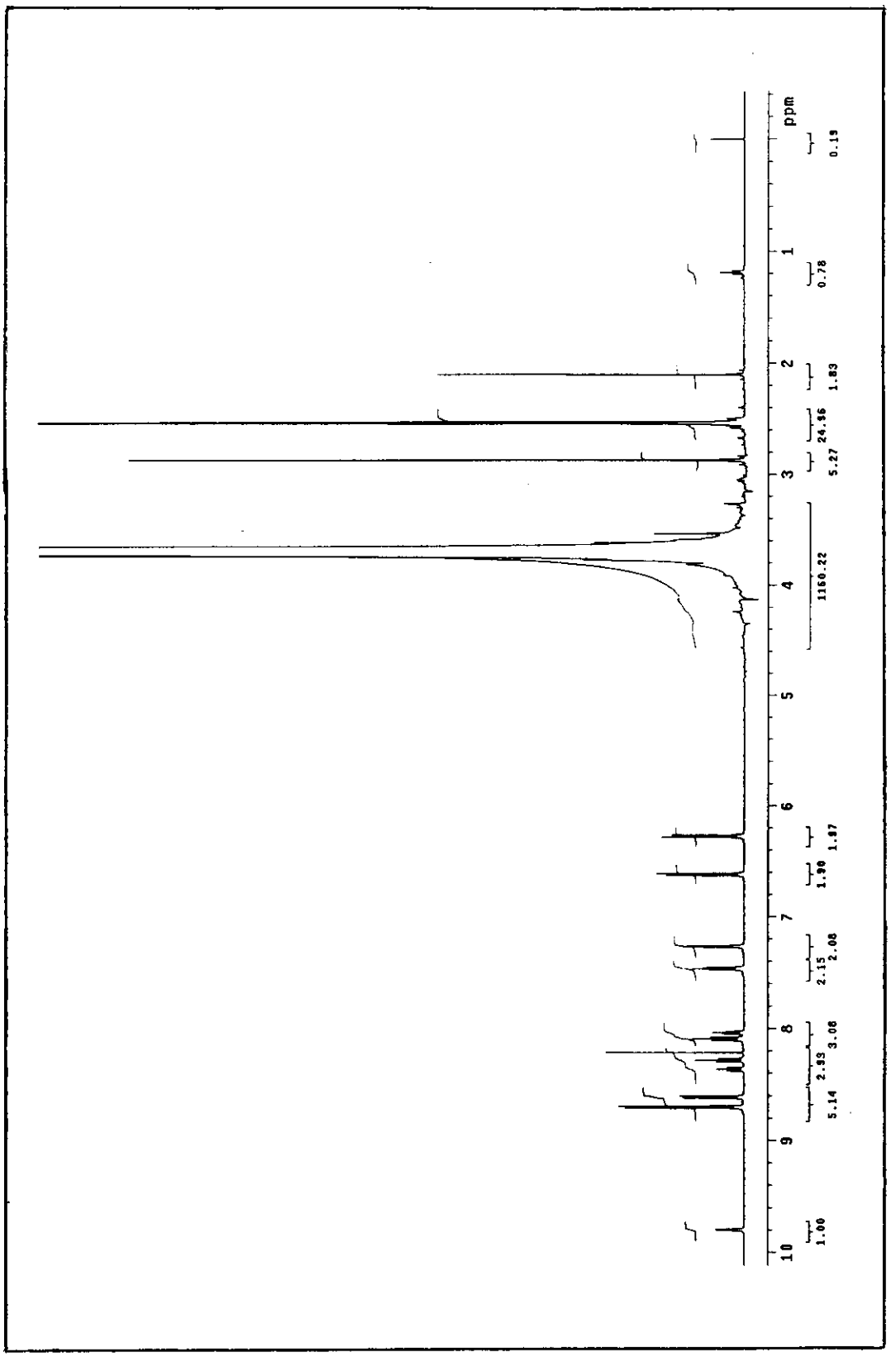

Figure 36 ^{1}H NMR spectrum of $[Ru(tpy)(dmazpy)H_2O](PF_6)_2$ complex.

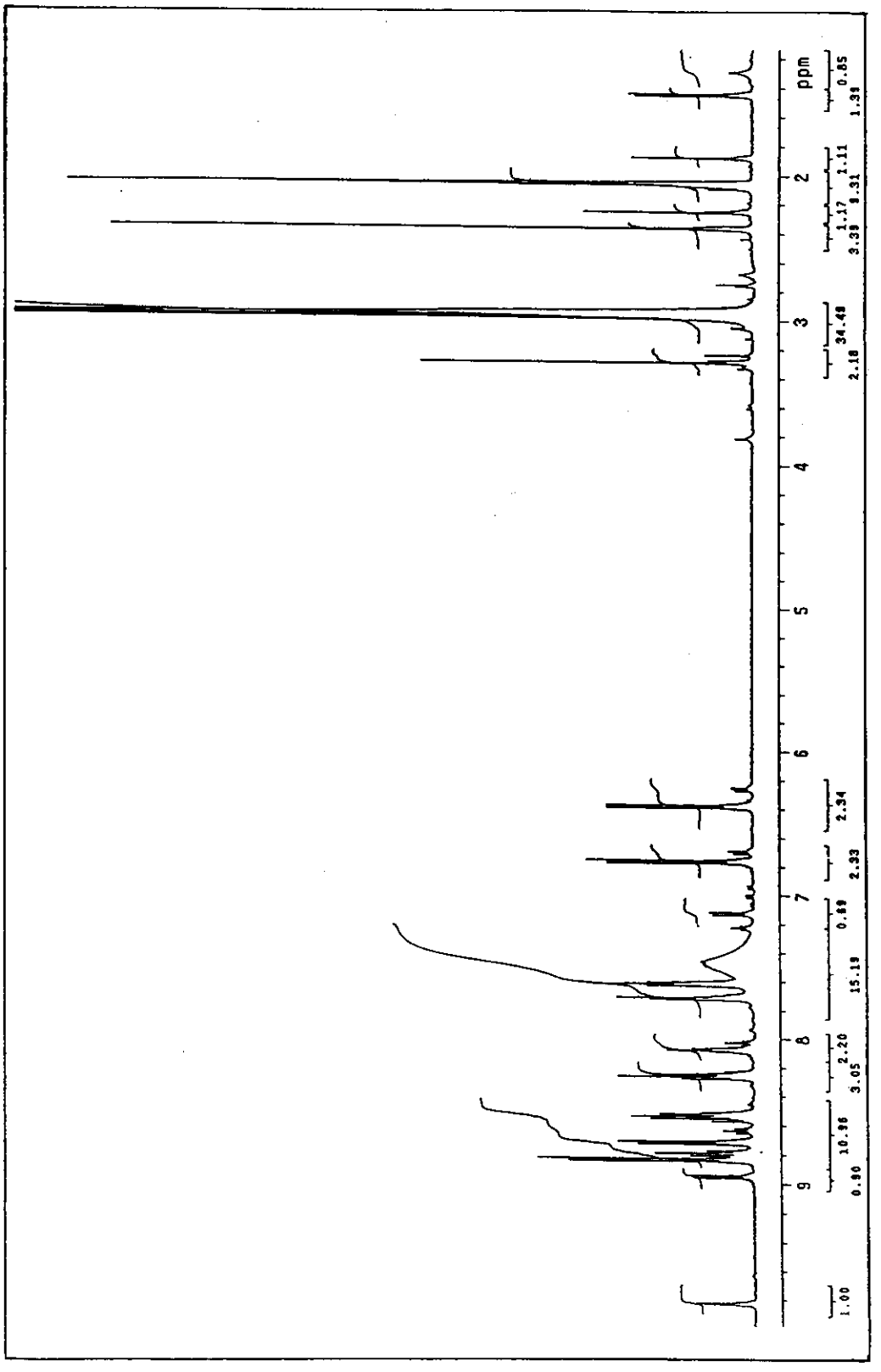

Figure 37 ^{1}H NMR spectrum of [Ru(tpy)(dmazpy)CH_3CN]$(PF_6)_2$ complex.

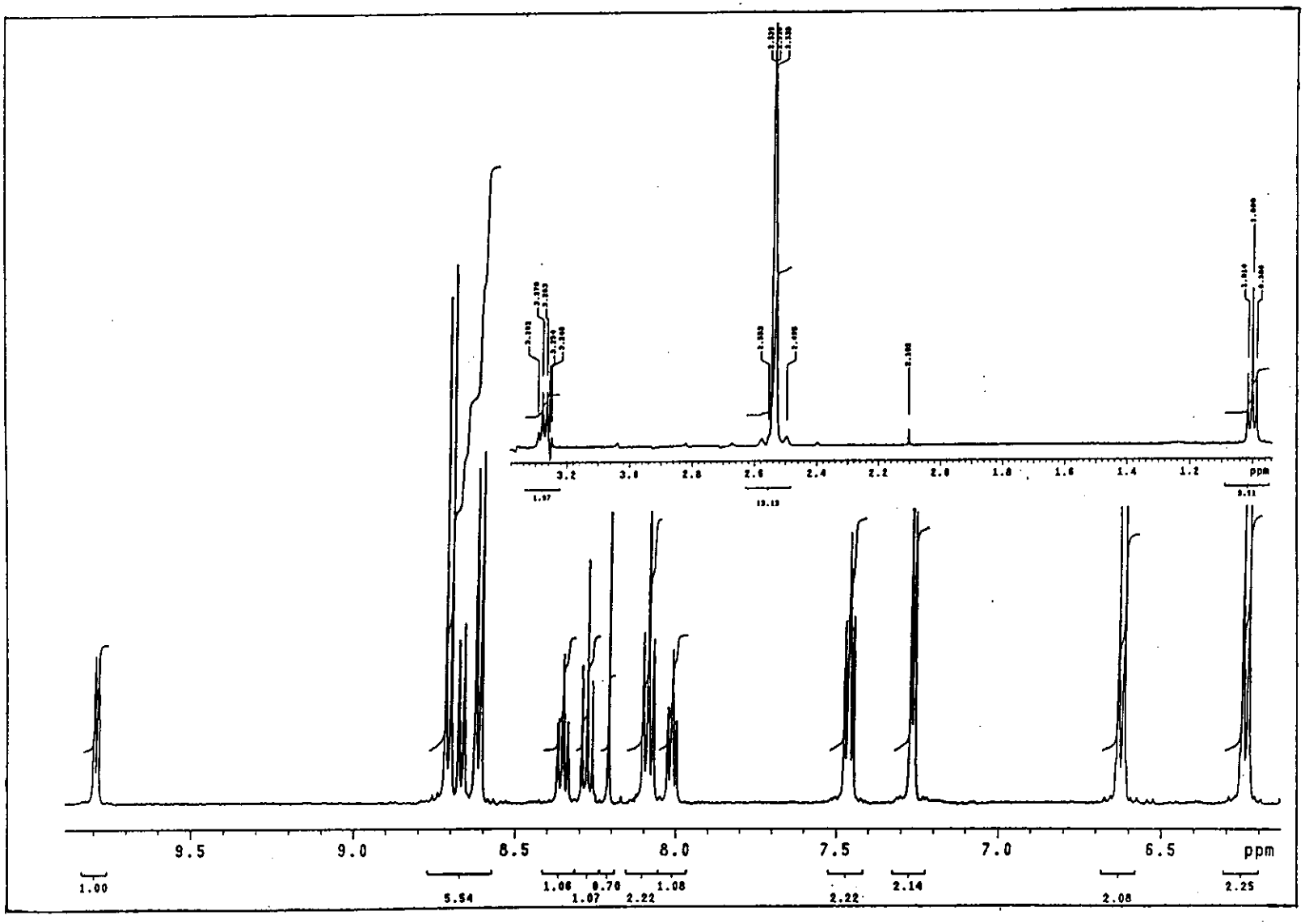

Figure 38 ^{1}H NMR spectrum of $[Ru(tpy)(deazpy)Cl]PF_6$ complex.

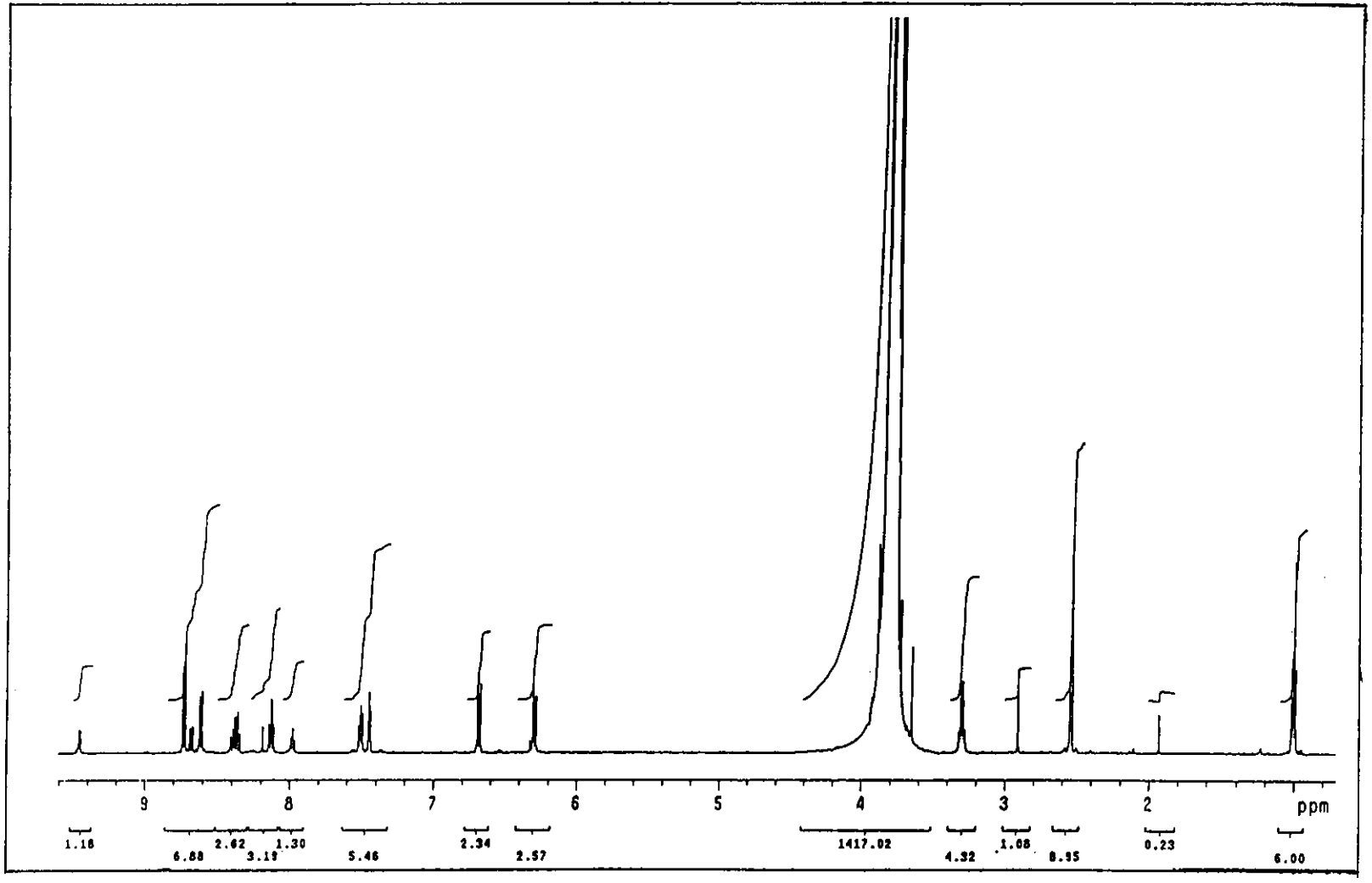

Figure 39 ^{1}H NMR spectrum of $[Ru(tpy)(deazpy)NO_2]PF_6$ complex.

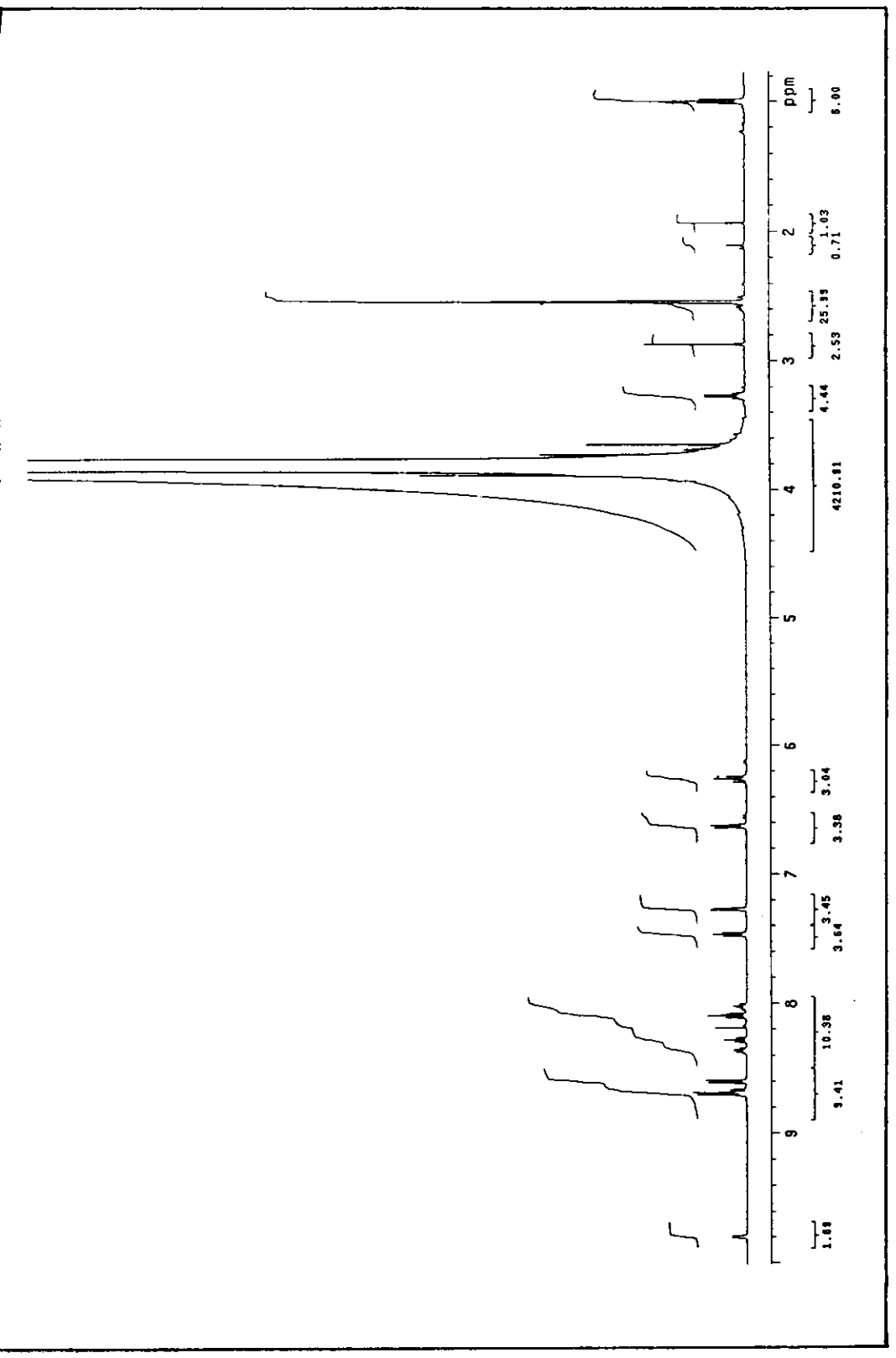

Figure 40 ^{1}H NMR spectrum of [Ru(tpy)(deazpy)H_2O][PF_6]$_2$ complex.

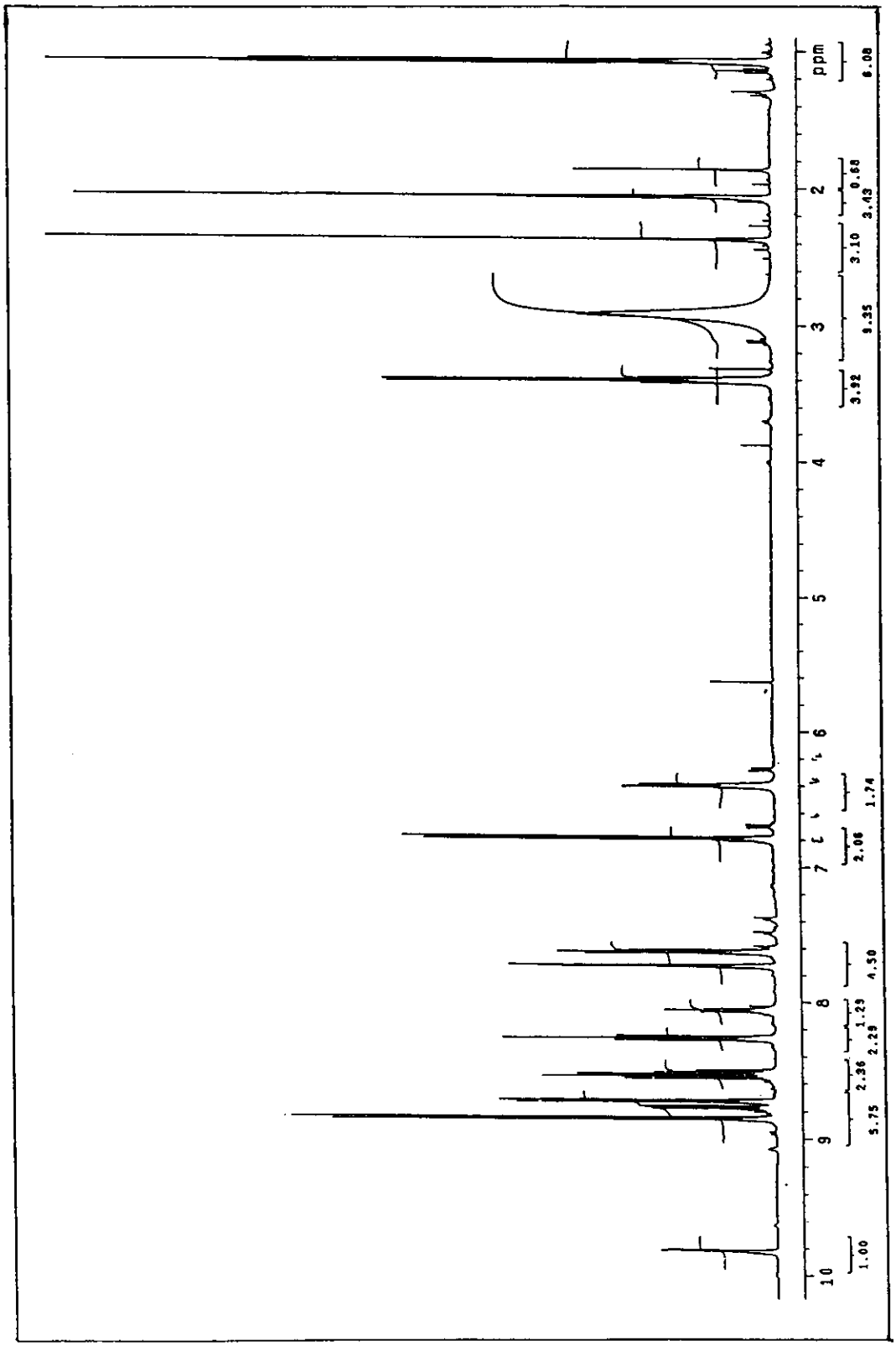

Figure 41 ^{1}H NMR spectrum of $[Ru(tpy)(deazpy)CH_3CN](PF_6)_2$ complex.

3.2.2.6. Cyclic voltammetry

Cyclic voltammetry is a method of studying the oxidation-reduction processes in detail. Cyclic voltammogram of [Ru(tpy)(dmazpy)X]PF_6 and [Ru (tpy) (deazpy)X]PF_6, where X = Cl^-, NO_2^- are shown in Figure 42-47. The summary of the cyclic voltammetric data is demonstrated in Table 28.

Table 28 Cyclic voltammetric data of [Ru(tpy)(dmazpy)X]PF_6 and [Ru(tpy) (deazpy)X]PF_6, where X = Cl^-, NO_2^- in 0.1 M TBAH acetonitrile solution at scan rate 50 mV/s (ferrocene as internal standard, ΔE_p = 68 mV)

Complex	$E_{1/2}$, V (ΔE_p, mV)			
	Oxidation range		Reduction range	
[Ru(tpy)(dmazpy)Cl]PF_6	III	+0.59(76)	I	-1.21(63)
	[Ru(II/III)]	+0.96(107)	II	-1.79(105)
[Ru(tpy)(dmazpy)NO_2]PF_6	III	+0.65(60)	I	-1.15(68)
	[Ru(II/III)]	+1.15[a]	II	-1.88(76)
[Ru(tpy)(deazpy)Cl]PF_6	III	+0.58(67)	I	-1.22(79)
	[Ru(II/III)]	+0.98(80)	II	-1.79(103)
[Ru(tpy)(deazpy)NO_2]PF_6	III	+0.64(68)	I	-1.17(64)
	[Ru(II/III)]	+1.18[a]	II	-1.89(62)

a = irreversible anodic peak

Cyclic voltammograms of $[Ru(tpy)(dmazpy)X]PF_6$ and $[Ru(tpy)(deazpy)X]PF_6$, where X = Cl^-, NO_2^-, gave similar patterns but the peak potentials were shifted. There were two couples in positive potential. One couple was ligand character and another couple was the redox of Ru (II/III). In addition, the two couples occurred in reduction range.

Oxidation range

The complexes were studied in the range 0-1400 mV. The couple III belonged to the ligand character, which occurred spontaneously. This couple was quasi-reversible couple with one electron transfer in comparison with ferrocence couple. The Ru (II/III) couple was quasi-reversible in $[Ru(tpy)(dmazpy)Cl]PF_6$ and $[Ru(tpy)(deazpy)Cl]PF_6$ complexes which could individually transfer one electron. Whereas, only oxidation peaks were observed in $[Ru(tpy)(dmazpy)NO_2]PF_6$ and $[Ru(tpy)(deazpy)NO_2]PF_6$ complexes.

Reduction range

The complexes were studied in the range -2000-0 mV. Two couples appeared in this range. In $[Ru(tpy)(dmazpy)Cl]PF_6$ and $[Ru(tpy)(deazpy)Cl]PF_6$ complexes the couple I was quasi-reversible couple when higher scan rates were applied, but was complete reversible couple in $[Ru(tpy)(dmazpy)NO_2]PF_6$ and $[Ru(tpy)(deazpy)NO_2]PF_6$ complexes at low scan rates (50, 100 mV/s). In all complexes, the couple II was occurred in the range -1500 to -2000 mV. The couple II was quasi-reversible couple when higher scan rates were obtained.

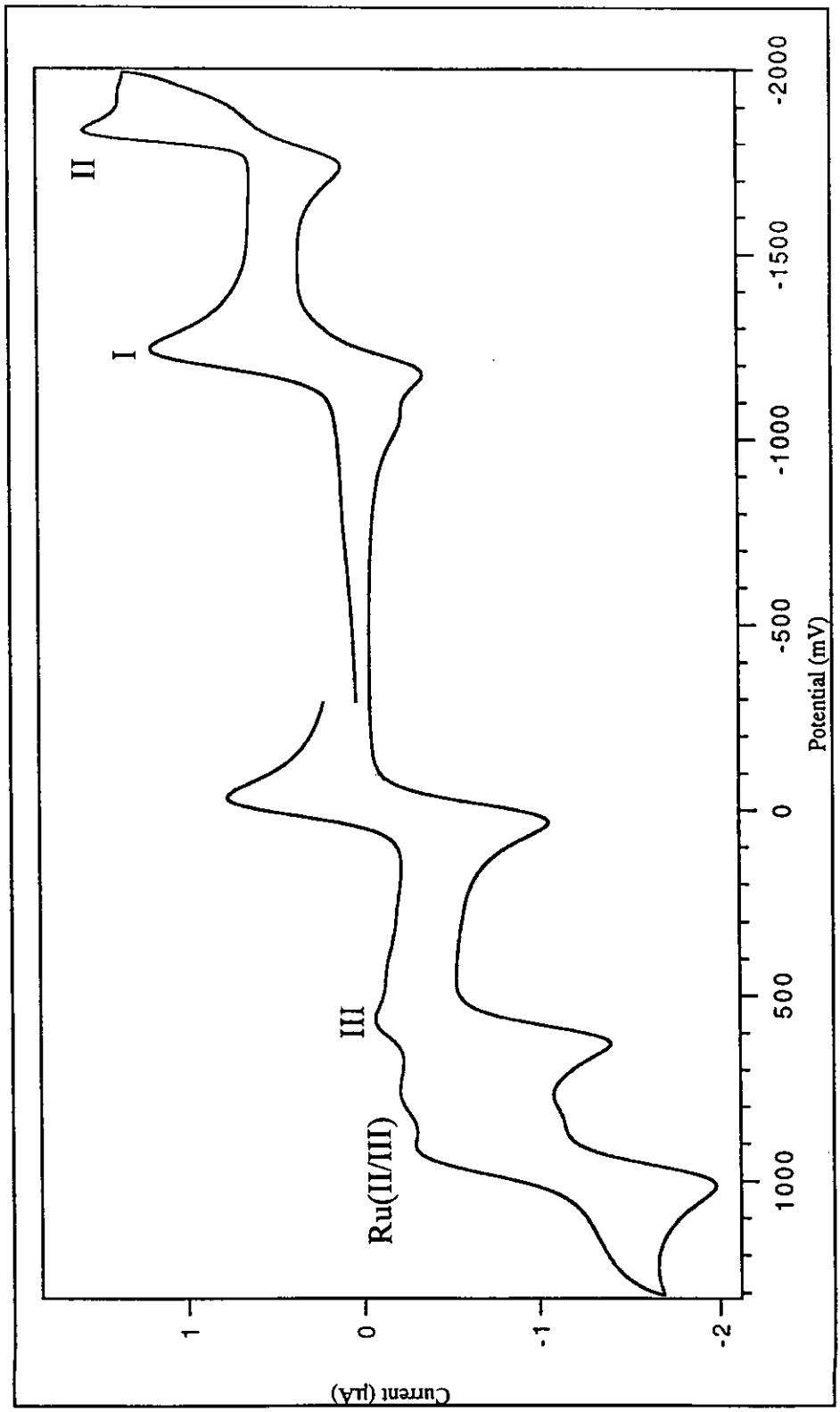

Figure 42 Cyclic voltammogram of $[Ru(tpy)(dmazpy)Cl]PF_6$ in acetonitrile (scan rate 50 mV/s).

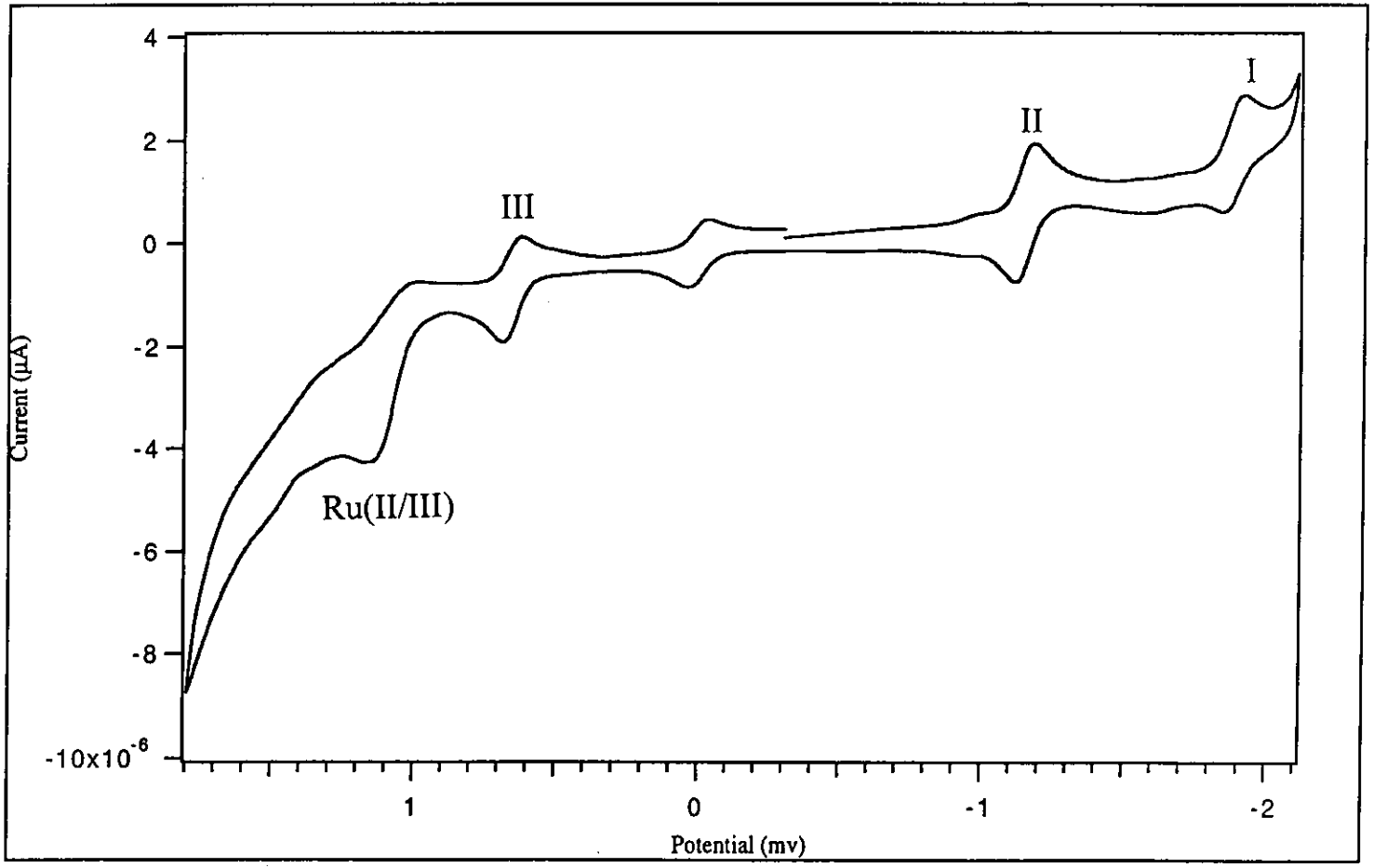

Figure 43 Cyclic votammogram of $[Ru(tpy)(dmazpy)NO_2]PF_2$ in acetonitrile (scan rate 50 mV/s).

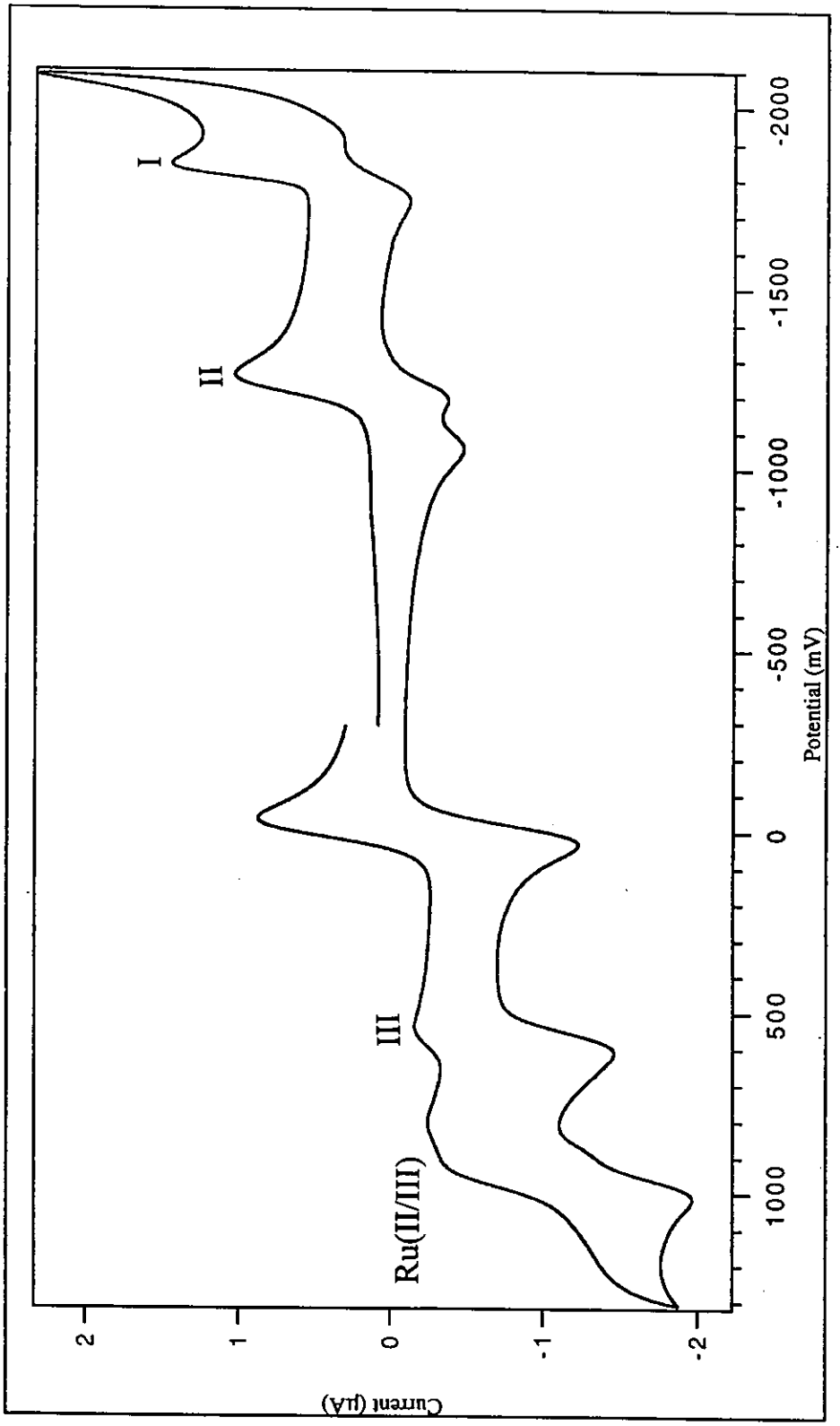

Figure 44 Cyclic voltammogram of [Ru(tpy)(deazpy)Cl]PF_6 in acetonitrile (scan rate 50 mV/s).

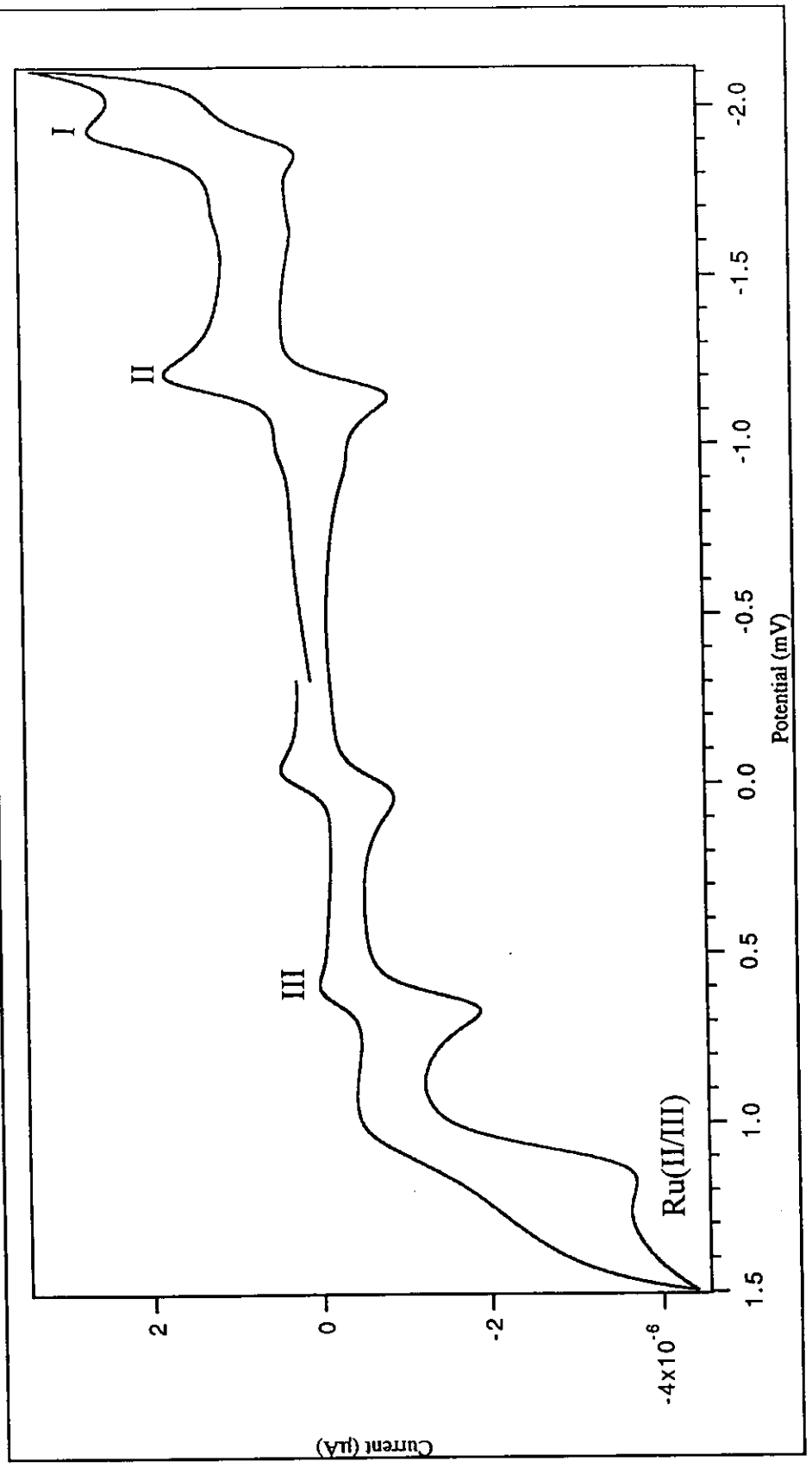

Figure 45 Cyclic voltammogram of $[Ru(tpy)(deazpy)NO_2]PF_6$ in acetonitrile (scan rate 50 mV/s).

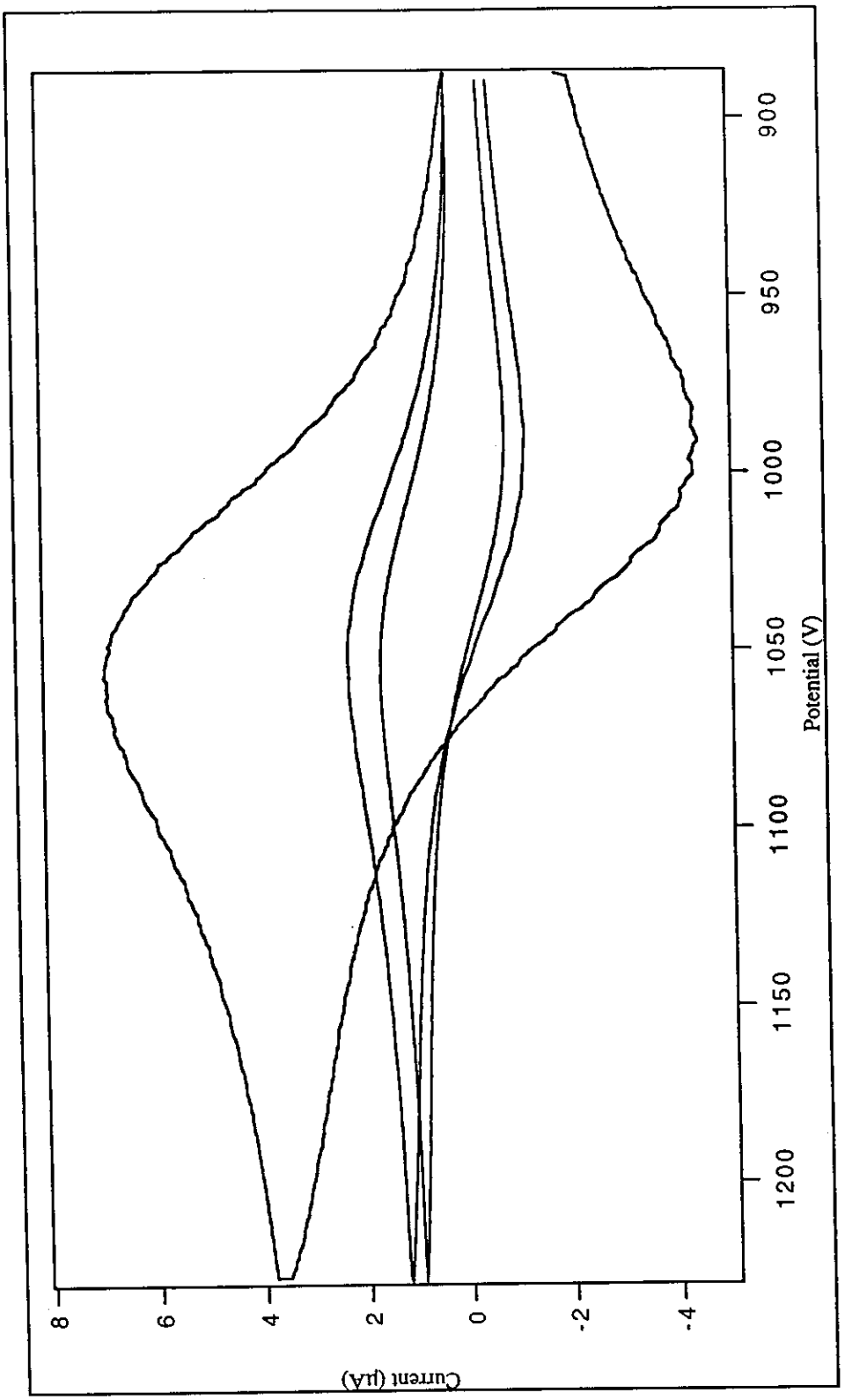

Figure 46 Cyclic voltammogram of quasi-reversible couples of $[Ru(tpy)(dmazpy)Cl]PF_6$ Complexes scanned with various scan rates (50, 100, 1000 mV/s).

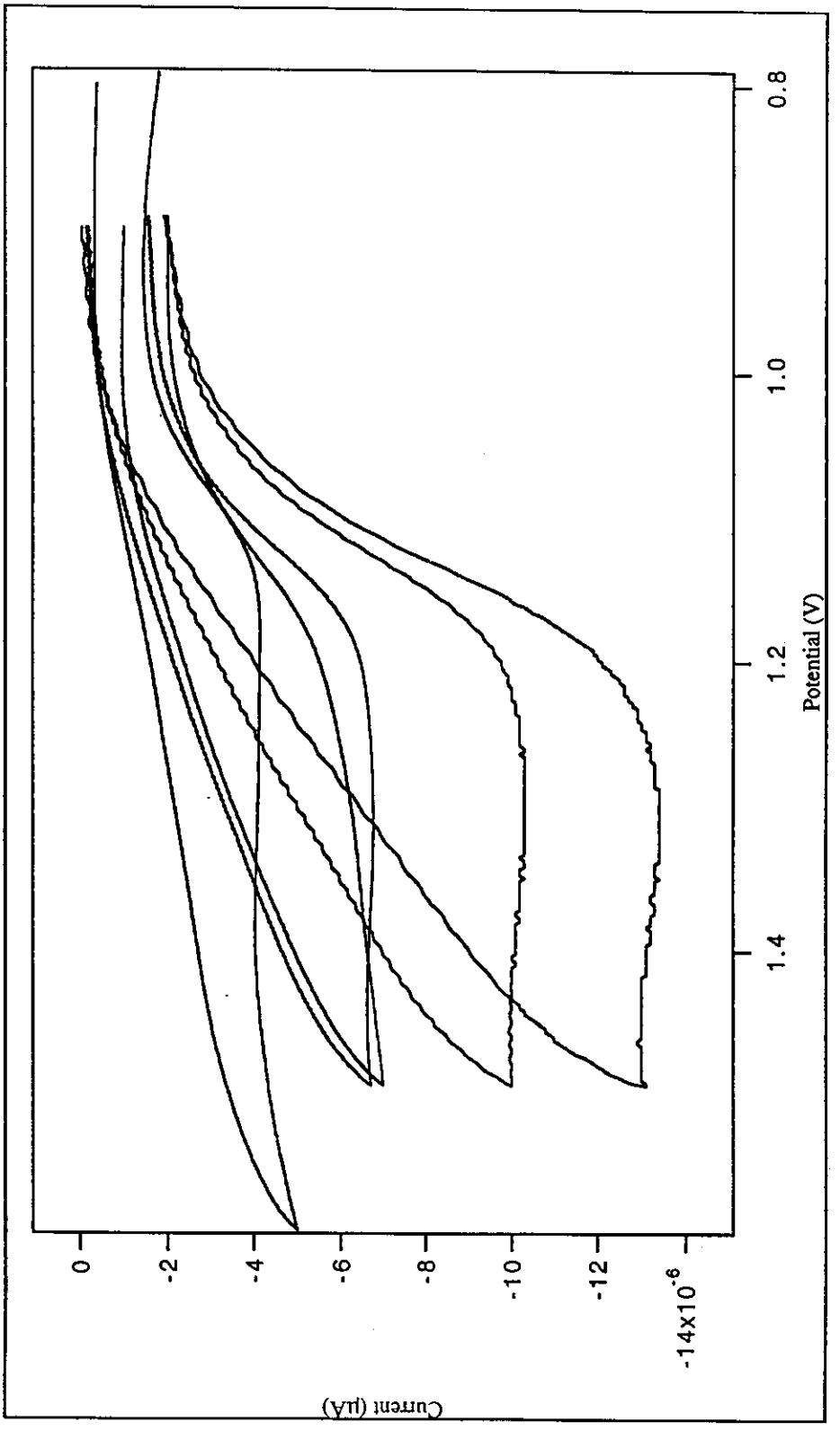

Figure 47 Cyclic voltammogram of quasi-reversible couples of $[Ru(tpy)(dmazpy)NO_2]PF_6$ Complexes scanned with various scan rates (50, 100, 1000 mV/s).

3.2.2.7. X-ray diffractometer

The most important method of structure determination is the X-ray crystallographic technique. Results from X-ray crystallography give the valuable data, such as the metal-ligand bond distances and angles, and the geometry of the complexes.

X-ray structure of $[Ru(tpy)(dmazpy)Cl]BF_4$

X-ray quality crystals of $[Ru(tpy)(dmazpy)Cl]BF_4$ were obtained by layering dichloromethane onto a methanol solution of the metal complex. A view of the molecular unit of $[Ru(tpy)(dmazpy)Cl]BF_4$ is shown in Figure 48, the crystallographic data are given in Table 29-31. Asymmetric unit of complex consists of the cation and a disordered BF_4^- anion. The structure of $[Ru(tpy)(dmazpy)Cl]BF_4$ is distorted octahedral. The dmazpy ligand is bound to ruthenium with the azo *trans* to the coordinated chlorine atom.

X-ray structure of $[Ru(tpy)(dmazpy)NO_2]BF_4$

Crystals of $[Ru(tpy)(dmazpy)NO_2]BF_4$ were grown by slowly evaporation of ethanol/acetone. A view of the molecular unit of $[Ru(tpy)(dmazpy)NO_2]BF_4$ is shown in Figure 49, and the crystallographic data are given in Table 32-34. The structure of $[Ru(tpy)(dmazpy)NO_2]BF_4$ is distorted octahedral. The ruthenium is coordinated to dmazpy ligand with the azo nitrogen (N3) *trans* to the coordinated NO_2^-.

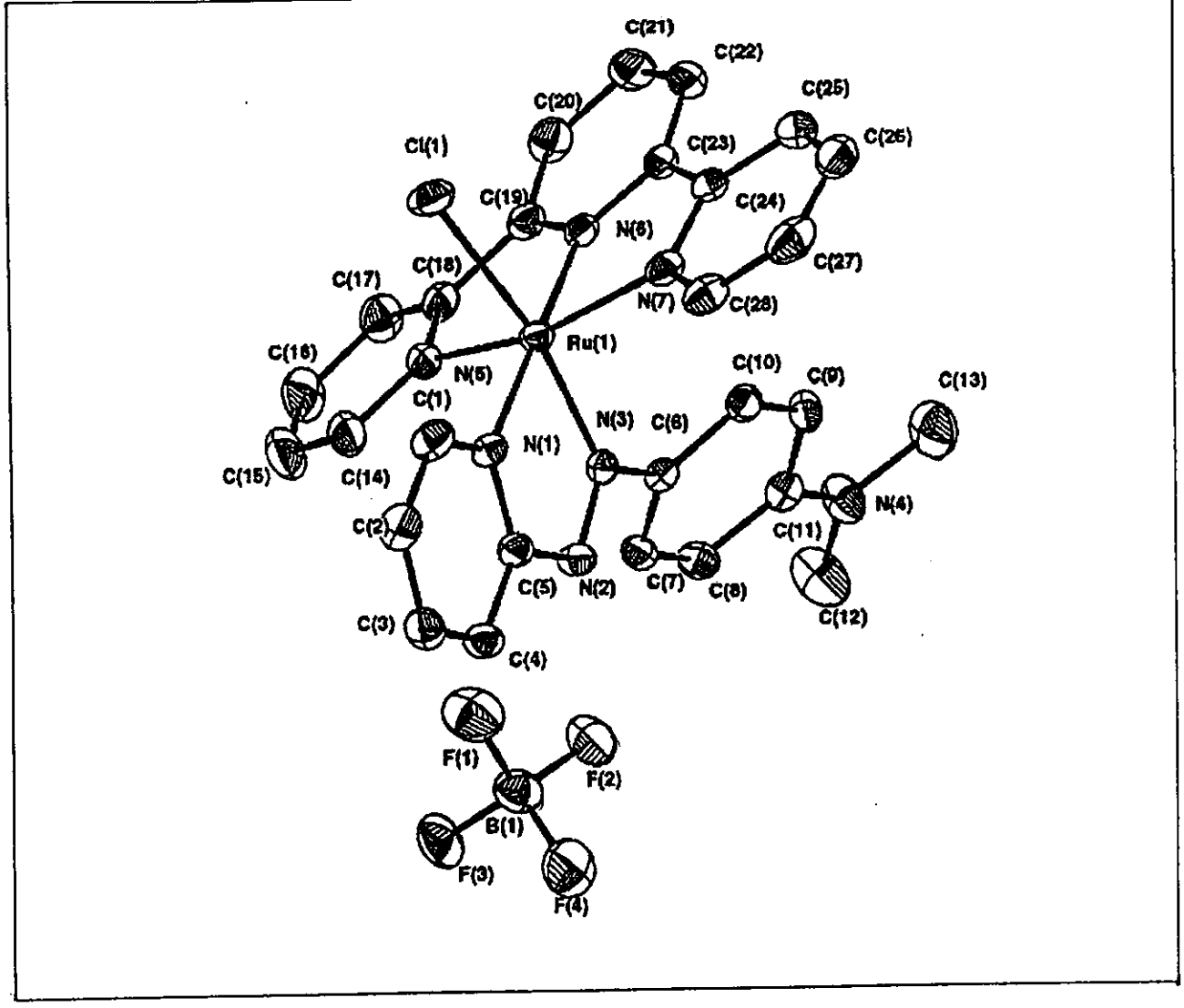

Figure 48 The structure of $[Ru(tpy)(dmazpy)Cl]BF_4$. (H-atom omitted)

Table 29 The crystallographic data for $[Ru(tpy)(dmazpy)Cl]BF_4$.

Empirical formula	$C_{28}H_{25}BClF_4N_7Ru$
Formula weight	682.88
Crystal system	monoclinic
Space group	P_{21}/n
Unit cell dimension	a = 13.4524(1) Å, $\alpha = 90°$
	b = 15.0244(1) Å, β = 95.8739(4)°
	c = 13.8899(2) Å, $\gamma = 90°$
Volume	2792.61(4) $Å^3$
Z	4
Temperature	173 (1) K
Wavelength	0 .7107 nm
Density (calculated)	1.624 mg/m^3
Absorption coefficient	0.717 nm^{-1}
Index ranges	$-17 < h < 17$, $-18 < k < 19$, $-18 < l < 18$
Goodness-of-fit on F^2	1.192
R indices (all data)	$R = 0.043$, $R_w = 0.052$

Table 30 Non-hydrogen interatomic distances of $[Ru(tpy)(dmazpy)Cl]BF_4$.

Atoms	Distance (Angstroms)
Ru((1))-Cl((1))	2.4100(6)
Ru((1))-N((1))	2.055(1)
Ru((1))-N((3))	1.976(1)
Ru((1))-N((5))	2.079(1)
Ru((1))-N((6))	1.976(1)
Ru((1))-N((7))	2.072(2)
N((1))-C((1))	1.349(3)
N((1))-C((5))	1.360(3)
N((2))-N((3))	1.306(2)
N((2))-C((5))	1.387(2)
N((3))-C((6))	1.427(2)
N((4))-C((11))	1.373(3)
N((4))-C((12))	1.442(4)
N((4))-C((13))	1.443(4)
N((5))-C((14))	1.340(3)
N((5))-C((18))	1.373(3)
N((6))-C((19))	1.346(3)
N((6))-C((23))	1.355(3)
N((7))-C((24))	1.379(3)
N((7))-C((28))	1.342(4)
C((1))-C((2))	1.370(4)
C((2))-C((3))	1.391(4)
C((3))-C((4))	1.370(4)

Table 30 (continued).

Atoms	Distance(Angstroms)
C((4))-C((5))	1.394(4)
C((6))-C((7))	1.389(4)
C((6))-C((10))	1.389(4)
C((7))-C((8))	1.374(4)
C((8))-C((11))	1.412(4)
C((9))-C((10))	1.384(4)
C((9))-C((11))	1.403(4)
C((14))-C((15))	1.387(4)
C((15))-C((16))	1.371(4)
C((16))-C((17))	1.384(4)
C((17))-C((18))	1.384(4)
C((18))-C((19))	1.480(4)
C((19))-C((20))	1.389(4)
C((20))-C((21))	1.386(4)
C((21))-C((22))	1.380(4)
C((22))-C((23))	1.388(4)
C((23))-C((24))	1.465(4)
C((24))-C((25))	1.381(4)
C((25))-C((26))	1.379(4)
C((26))-C((27))	1.382(4)
C((27))-C((28))	1.379(4)
F((1))-B((1))	1.389(3)
F((2))-B((1))	1.394(3)

Table 30 (continued).

Atoms	Distance(Angstroms)
F((3))-B((1))	1.384(4)
F((4))-B((1))	1.382(4)

Table 31 Non-hydrogen interbond angles of $[Ru(tpy)(dmazpy)Cl]BF_4$.

Atoms	Angles(degrees)
Cl((1))-Ru((1))-N((1))	94.07(4)
Cl((1))-Ru((1))-N((3))	169.24(5)
Cl((1))-Ru((1))-N((5))	90.67(4)
Cl((1))-Ru((1))-N((6))	87.97(5)
Cl((1))-Ru((1))-N((7))	87.82(5)
N((1))-Ru((1))-N((3))	76.63(6)
N((1))-Ru((1))-N((5))	99.24(6)
N((1))-Ru((1))-N((6))	177.36(6)
N((1))-Ru((1))-N((7))	102.17(8)
N((3))-Ru((1))-N((5))	85.59(6)
N((3))-Ru((1))-N((6))	101.18(6)
N((3))-Ru((1))-N((7))	99.33(6)
N((5))-Ru((1))-N((6))	79.04(6)
N((5))-Ru((1))-N((7))	158.59(8)
N((6))-Ru((1))-N((7))	79.56(8)
Ru((1))-N((1))-C((1))	129.7(1)
Ru((1))-N((1))-C((5))	112.4(1)
C((1))-N((1))-C((5))	117.8(2)
N((3))-N((2))-C((5))	111.7(2)
Ru((1))-N((3))-N((2))	120.6(1)
Ru((1))-N((3))-C((6))	125.6(1)
N((2))-N((3))-C((6))	112.7(2)
C((11))-N((4))-C((12))	121.3(2)

Table 31 (continued).

Atoms	Angles(degrees)
C((11))-N((4))-C((13))	120.4(3)
C((12))-N((4))-C((13))	118.3(2)
Ru((1))-N((5))-C((14))	127.9(1)
Ru((1))-N((5))-C((18))	113.6(1)
C((14))-N((5))-C((18))	118.1(2)
Ru((1))-N((6))-C((19))	119.3(1)
Ru((1))-N((6))-C((23))	118.3(1)
C((19))-N((6))-C((23))	122.0(2)
Ru((1))-N((7))-C((24))	113.2(2)
Ru((1))-N((7))-C((28))	128.2(2)
C((24))-N((7))-C((28))	118.6(2)
N((1))-C((1))-C((2))	122.5(2)
C((1))-C((2))-C((3))	119.4(3)
C((2))-C((3))-C((4))	119.3(3)
C((3))-C((4))-C((5))	118.7(2)
N((1))-C((5))-N((2))	117.6(2)
N((1))-C((5))-C((4))	122.3(2)
N((2))-C((5))-C((4))	120.1(2)
N((3))-C((6))-C((7))	121.0(2)
N((3))-C((6))-C((10))	119.7(2)
C((7))-C((6))-C((10))	119.3(2)
C((6))-C((7))-C((8))	120.5(2)
C((7))-C((8))-C((11))	121.2(3)

Table 31 (continued).

Atoms	Angles(degrees)
C((10))-C((9))-C((11))	120.6(3)
C((6))-C((10))-C((9))	120.7(3)
N((4))-C((11))-C((8))	121.4(3)
N((4))-C((11))-C((9))	120.9(3)
C((8))-C((11))-C((9))	117.7(3)
N((5))-C((14))-C((15))	122.4(2)
C((14))-C((15))-C((16))	119.4(3)
C((15))-C((16))-C((17))	119.2(3)
C((16))-C((17))-C((18))	119.4(3)
N((5))-C((18))-C((17))	121.5(2)
N((5))-C((18))-C((19))	114.6(2)
C((17))-C((18))-C((19))	123.9(2)
N((6))-C((19))-C((18))	112.9(2)
N((6))-C((19))-C((20))	120.1(2)
C((18))-C((19))-C((20))	127.0(3)
C((19))-C((20))-C((21))	118.6(3)
C((20))-C((21))-C((22))	120.6(3)
C((21))-C((22))-C((23))	119.2(3)
N((6))-C((23))-C((22))	119.5(2)
N((6))-C((23))-C((24))	113.4(2)
C((22))-C((23))-C((24))	127.1(2)
N((7))-C((24))-C((23))	115.2(2)
N((7))-C((24))-C((25))	121.0(2)

Table 31 (continued).

Atoms	Angles(degrees)
C((23))-C((24))-C((25))	123.7(2)
C((24))-C((25))-C((26))	119.6(3)
C((25))-C((26))-C((27))	119.1(3)
C((26))-C((27))-C((28))	119.6(3)
N((7))-C((28))-C((27))	122.1(2)
F((1))-B((1))-F((2))	109.6(2)
F((1))-B((1))-F((3))	109.2(2)
F((1))-B((1))-F((4))	110.0(3)
F((2))-B((1))-F((3))	109.5(3)
F((2))-B((1))-F((4))	109.0(2)
F((3))-B((1))-F((4))	109.5(2)

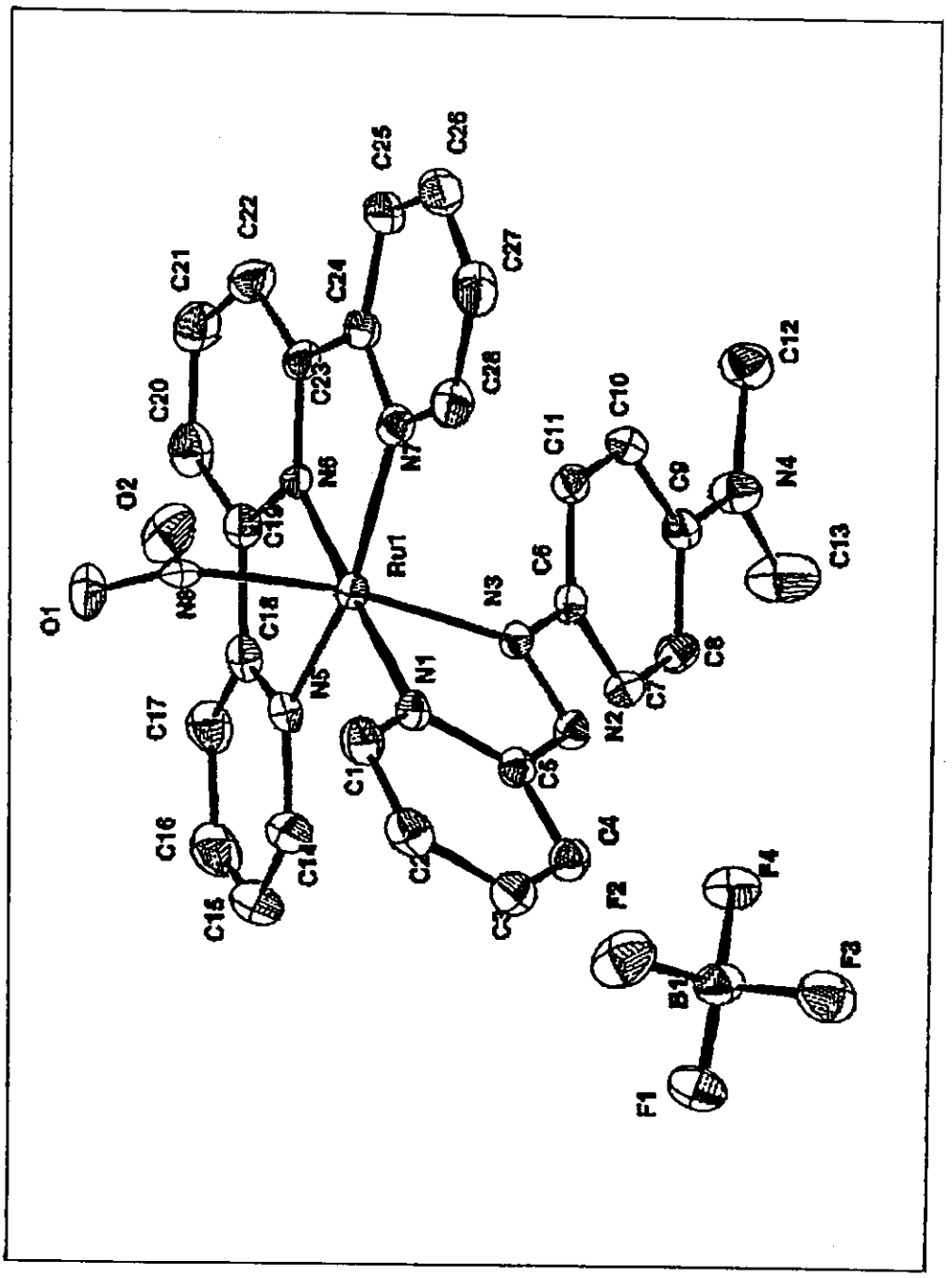

Figure 49 The structure of [Ru(tpy)(dmazpy)NO_2]BF_4 (H-atom omitted).

Table 32 The crystallographic data for $[Ru(tpy)(dmazpy)NO_2]BF_4$.

Empirical formula	$C_{28}H_{25}BF_4N_8O_2Ru$
Formula weight	693.44
Crystal system	monoclinic
Space group	P_{21}/n
Unit cell dimension	a = 13.4172(1) Å, $\alpha = 90°$
	b = 14.9860(1) Å, $\beta = 94.0188(4)°$
	c = 13.9057(2) Å, $\gamma = 90°$
Volume	2789.15(5) $Å^3$
Z	4
Temperature	123 (2) K
Wavelength	0.71073 nm
Density (calculated)	0.938 mg/m^3
Absorption coefficient	0.633 nm^{-1}
Index ranges	$-17 < h < 16, -19 < k < 19, -18 < l < 18$
Goodness-of-fit on F^2	1.045
R indices (all data)	$R = 0.0297, R_w = 0.0724$

Table 33 Non-hydrogen interatomic distances of $[Ru(tpy)(dmazpy)NO_2]BF_4$.

Atoms	Distances (Angstroms)
Ru(1)-N(1)	2.059(1)
Ru(1)-N(3)	2.025(2)
Ru(1)-N(5)	2.083(2)
Ru(1)-N(6)	1.981(1)
Ru(1)-N(7)	2.071(2)
Ru(1)-N(8)	2.059(2)
O(1)-N(8)	1.241(2)
O(2)-N(8)	1.253(2)
N(1)-C(1)	1.350(2)
N(1)-C(5)	1.363(2)
N(2)-N(3)	1.299(2)
N(2)-C(5)	1.389(3)
N(3)-C(6)	1.417(2)
N(4)-C(9)	1.370(3)
N(4)-C(12)	1.455(3)
N(4)-C(13)	1.447(3)
N(5)-C(14)	1.340(3)
N(5)-C(18)	1.372(2)
N(6)-C(19)	1.351(2)
N(6)-C(23)	1.351(2)
N(7)-C(24)	1.379(2)
N(7)-C(28)	1.345(2)
C(1)-C(2)	1.385(3)

Table 33 (continued).

Atoms	Distances (Angstroms)
C(2)-C(3)	1.388(3)
C(3)-C(4)	1.377(3)
C(4)-C(5)	1.392(3)
C(6)-C(7)	1.399(3)
C(6)-C(11)	1.394(3)
C(7)-C(8)	1.379(3)
C(8)-C(9)	1.415(3)
C(9)-C(10)	1.412(3)
C(10)-C(11)	1.377(3)
C(14)-C(15)	1.390(3)
C(15)-C(16)	1.383(3)
C(16)-C(17)	1.384(3)
C(17)-C(18)	1.387(3)
C(18)-C(19)	1.475(3)
C(19)-C(20)	1.395(3)
C(20)-C(21)	1.387(3)
C(21)-C(22)	1.381(3)
C(22)-C(23)	1.390(3)
C(23)-C(24)	1.469(3)
C(24)-C(25)	1.390(3)
C(25)-C(26)	1.380(3)
C(26)-C(27)	1.384(3)

Table 33 (continued).

Atoms	Distances (Angstroms)
C(27)-C(28)	1.385(3)
B(1)-F(1)	1.385(3)
B(1)-F(2)	1.390(3)
B(1)-F(3)	1.398(3)
B(1)-F(4)	1.402(3)

Table 34 Non-hydrogen interbond angles of $[Ru(tpy)(dmazpy)NO_2]BF_4$.

Atoms	Angels (degrees)
N(1)-Ru(1)-N(3)	76.21(6)
N(1)-Ru(1)-N(5)	99.16(6)
N(1)-Ru(1)-N(6)	177.39(7)
N(1)-Ru(1)-N(7)	102.36(6)
N(1)-Ru(1)-N(8)	95.29(6)
N(3)-Ru(1)-N(5)	84.98(6)
N(3)-Ru(1)-N(6)	101.57(6)
N(3)-Ru(1)-N(7)	99.11(6)
N(3)-Ru(1)-N(8)	170.01(6)
N(5)-Ru(1)-N(6)	79.19(6)
N(5)-Ru(1)-N(7)	158.46(6)
N(5)-Ru(1)-N(8)	91.30(6)
N(6)-Ru(1)-N(7)	79.26(6)
N(6)-Ru(1)-N(8)	86.79(6)
N(7)-Ru(1)-N(8)	87.74(6)
Ru(1)-N(1)-C(1)	129.4(1)
Ru(1)-N(1)-C(5)	112.7(1)
C(1)-N(1)-C(5)	117.8(2)
N(3)-N(2)-C(5)	112.3(1)
Ru(1)-N(3)-N(2)	119.5(1)
Ru(1)-N(3)-C(6)	126.1(1)
N(2)-N(3)-C(6)	113.1(1)

Table 34 (continued).

Atoms	Angels (degrees)
C(9)-N(4)-C(12)	120.7(2)
C(9)-N(4)-C(13)	121.1(2)
C(12)-N(4)-C(13)	118.2(2)
Ru(1)-N(5)-C(14)	127.8(1)
Ru(1)-N(5)-C(18)	113.3(1)
C(14)-N(5)-C(18)	118.6(2)
Ru(1)-N(6)-C(19)	118.9(1)
Ru(1)-N(6)-C(23)	118.8(1)
C(19)-N(6)-C(23)	121.9(2)
Ru(1)-N(7)-C(24)	113.4(1)
Ru(1)-N(7)-C(28)	128.4(1)
C(24)-N(7)-C(28)	118.2(2)
Ru(1)-N(8)-O(1)	121.1(1)
Ru(1)-N(8)-O(2)	120.3(1)
O(1)-N(8)-O(2)	118.6(2)
N(1)-C(1)-C(2)	122.3(2)
C(1)-C(2)-C(3)	119.4(2)
C(2)-C(3)-C(4)	119.3(2)
C(3)-C(4)-C(5)	118.8(2)
N(1)-C(5)-N(2)	118.0(2)
N(1)-C(5)-C(4)	122.5(2)
N(2)-C(5)-C(4)	119.6(2)

Table 34 (continued).

Atoms	Angels (degrees)
N(3)-C(6)-C(7)	121.2(2)
N(3)-C(6)-C(11)	119.9(2)
C(7)-C(6)-C(11)	118.9(2)
C(6)-C(7)-C(8)	120.7(2)
C(7)-C(8)-C(9)	120.8(2)
N(4)-C(9)-C(8)	121.2(2)
N(4)-C(9)-C(10)	120.9(2)
C(8)-C(9)-C(10)	117.9(2)
C(9)-C(10)-C(11)	120.7(2)
C(6)-C(11)-C(10)	121.1(2)
N(5)-C(14)-C(15)	122.1(2)
C(14)-C(15)-C(16)	119.6(2)
C(15)-C(16)-C(17)	118.6(2)
C(16)-C(17)-C(18)	119.8(2)
N(5)-C(18)-C(17)	121.3(2)
N(5)-C(18)-C(19)	115.2(2)
C(17)-C(18)-C(19)	123.5(2)
N(6)-C(19)-C(18)	112.9(2)
N(6)-C(19)-C(20)	119.7(2)
C(18)-C(19)-C(20)	127.4(2)
C(19)-C(20)-C(21)	118.8(2)
C(20)-C(21)-C(22)	120.7(2)

Table 34 (continued).

Atoms	Angels (degrees)
C(21)-C(22)-C(23)	118.8(2)
N(6)-C(23)-C(22)	120.1(2)
N(6)-C(23)-C(24)	113.0(2)
C(22)-C(23)-C(24)	126.9(2)
N(7)-C(24)-C(23)	115.3(2)
N(7)-C(24)-C(25)	121.3(2)
C(23)-C(24)-C(25)	123.5(2)
C(24)-C(25)-C(26)	119.5(2)
C(25)-C(26)-C(27)	119.4(2)
C(26)-C(27)-C(28)	119.1(2)
N(7)-C(28)-C(27)	122.6(2)